

UCLA

UCLA Electronic Theses and Dissertations

Title

SCA13 mutations reveal a causal relationship between excitability and neuronal degeneration in zebrafish Purkinje cells

Permalink

<https://escholarship.org/uc/item/8dk6w518>

Author

Hsieh, Jui-Yi

Publication Date

2015

Peer reviewed|Thesis/dissertation

UNIVERSITY OF CALIFORNIA

Los Angeles

SCA13 mutations reveal a causal relationship between excitability and neuronal degeneration in
zebrafish Purkinje cells

A dissertation submitted in partial satisfaction of the requirements for the degree Doctor of
Philosophy in Molecular, Cellular, and Integrative Physiology

by

Jui-Yi Hsieh

2015

ABSTRACT OF THE DISSERTATION

SCA13 mutations reveal a causal relationship between excitability and neuronal degeneration in zebrafish Purkinje cells

by

Jui-Yi Hsieh

Doctor of Philosophy in Molecular, Cellular, and Integrative Physiology

University of California, Los Angeles, 2015

Professor Diane M. Papazian, Chair

Abnormal cell excitability is commonly seen in neurodegenerative diseases. However, the roles of excitability in the pathogenic pathways are not fully understood. Through studying spinocerebellar ataxia type 13 (SCA13), we provide evidence in support of a direct causal link between altered excitability and neuronal degeneration. SCA13 is an autosomal dominant disease caused by mutations in the *KCNC3* gene encoding K_v3.3. K_v3.3 has been studied extensively, and plays crucial roles in regulating cell excitability. Three causative mutations have been identified: R3Ha, R4Hi and FLi. They have differential effects on the channel biophysics. Depending on the mutations, SCA13 emerges during either infancy or adulthood. R3Ha is a dominant negative mutation that causes the adult-onset form of SCA13, whereas the R4Hi and FLi mutations are gating modifiers that alter the voltage-dependence of channel activation and cause the infant-onset form of SCA13. R4Hi also shows a dominant-negative effect over wildtype subunits. We hypothesize that infant- and adult-onset SCA13 mutations change cell excitability in distinct ways, which in turn generate the two clinical forms of the disease. To test

this hypothesis, we developed a novel *in vivo* recording method in awake larval zebrafish. By employing this method, we characterized the electrical properties and functional maturation of cerebellar Purkinje cells, and investigated the impact of SCA13 mutations during early development. We found that while R3Ha shows frequency-dependent inhibition of excitability, R4Hi induces hyperexcitability and severe degeneration in developing Purkinje cells. Preliminary experiments suggest that this degeneration can be rescued by the addition of NS13001, a SK channel agonist that decreases excitability. Our findings argue strongly that the distinct biophysical properties of the SCA13 mutants generate different functional consequences in cell excitability, and that hyperexcitability is tightly related to the rapid morphological degeneration of Purkinje cells early in development. This degeneration is reminiscent of the early-onset atrophy of the cerebellum seen in children with infant-onset SCA13, suggesting that hyperexcitability may contribute to pathogenesis in this form of the disease. Our results suggest that there is a direct causal relationship between altered excitability and neuronal degeneration in SCA13 and potentially in other neurodegenerative diseases.

The dissertation of Jui-Yi Hsieh is approved.

Thomas Otis

Joanna Jen

Baljit Khakh

David Glanzman

Diane M. Papazian, Committee Chair

University of California, Los Angeles

2015

Table of Contents

List of Figures and Table	viii
Acknowledgments	x
Curriculum vitae.....	xii
Chapter 1	1
Introduction.....	1
Aims of this thesis	2
Altered excitability in neurodegenerative diseases	2
Spinocerebellar ataxia type 13 and the causative mutations in <i>KCNC3</i> gene	5
Cerebellar circuits are highly conserved through evolution.....	7
Zebrafish as a biological model to study SCA13.....	10
Chapter 2	15
Rapid development of Purkinje cell excitability and the functional maturation of the cerebellar circuit in zebrafish	15
Introduction.....	16
Materials and Methods.....	18
Animal maintenance	18
Generation of transgenic zebrafish	18
RNA in situ hybridization.....	19
<i>In situ</i> electrophysiology.....	21
Inferior olive stimulation	22
Visual stimulation experiments.....	22

Data analysis	23
Results	24
Rapid emergence of electrical excitability in zebrafish Purkinje cells	24
Rapid development and maturation of functional connectivity in the zebrafish cerebellar circuit	26
Sensory stimulation alters Purkinje cell activity starting at 4 dpf	28
DISCUSSION	32
Rapid functional development and highly conserved electrical properties in zebrafish cerebellum.....	32
Synapse elimination in the developing zebrafish cerebellum.....	33
Rapid development of afferent pathways conveying visual information to cerebellum in zebrafish.....	34
Advantages of zebrafish for functional mapping of afferent and efferent pathways to cerebellum and for investigating cerebellar control of motor behavior.....	36
Chapter 3	47
Hyperexcitability induced by infant-onset SCA13 mutation leads to rapid dendritic degeneration	47
Introduction.....	48
Materials and Methods.....	52
Animal Maintenance.....	52
RNA preparation and K _v 3.3 expression in <i>Xenopus</i> oocytes	53
Expressing exogenous K _v 3.3 in zebrafish cerebellar Purkinje cells	53
<i>In vivo</i> confocal imaging.....	54

Two-electrode voltage clamping experiments in <i>Xenopus</i> oocytes	54
<i>In situ</i> electrophysiology in zebrafish cerebellum	55
Sudden-darkness stimulation	56
Data analysis	56
Results	57
Adult-onset SCA13 mutation shows strong dominant-negative effect.....	57
Infant-onset SCA13 mutations modify channel gating.....	58
Overexpressing exogenous wild-type K _v 3.3 has no effect on Purkinje cell firing	60
Adult-onset zR3Ha mutation alters evoked responses but not spontaneous tonic firing.....	61
Infant-onset mutation zR4Hi induces hyperexcitability and cell degeneration	63
Mitigating hyperexcitability partially rescues morphological degeneration	65
Discussion	67
The frequency-dependent effects of adult-onset mutation zR3Ha	68
Gating modifying effect of zR4Hi leads to hyperexcitability.....	69
The emergence of hyperexcitability matches the onset of morphological degeneration.....	72
Chapter 4	82
Conclusion	82
Conserved electrical activity and maturation in zebrafish Purkinje cells.....	83
Altered cell excitability and neuronal degeneration	84
References	88

List of Figures and Table

FIGURE 1.1 THE TOPOLOGY OF ZEBRAFISH $K_v3.3$ CHANNEL SUBUNIT AND THE LOCATIONS OF SCA13 MUTATIONS.	12
FIGURE 1.2 ZEBRAFISH AND MAMMALIAN CEREBELLAR CIRCUITS ARE HIGHLY CONSERVED.	13
FIGURE 2.1. RAPID EMERGENCE AND MATURATION OF EXCITABILITY IN ZEBRAFISH PURKINJE CELLS.	38
FIGURE 2.2 EXPRESSION OF NAV1.6 AND $K_v3.3$ COINCIDES WITH THE EMERGENCE OF SPONTANEOUS TONIC FIRING IN PURKINJE CELLS.	40
FIGURE 2.3 DIRECT ELECTRICAL STIMULATION OF INFERIOR OLIVE INCREASES OCCURRENCE OF COMPLEX SPIKE-LIKE EVENTS.	42
FIGURE 2.4 DEVELOPMENT AND WINNOWING OF FUNCTIONAL CONNECTIONS BETWEEN CLIMBING FIBERS AND PURKINJE CELLS.	43
FIGURE 2.5 SUDDEN DARKNESS INCREASES THE FREQUENCY OF TONIC FIRING AND COMPLEX SPIKING.	44
FIGURE 2.6 COMPARISON OF PURKINJE CELL RESPONSES TO SUDDEN DARKNESS AT 4-7 DPF.	45
FIGURE 2.7 MATURATION OF AFFERENT PATHWAYS CONVEYING VISUAL INFORMATION TO CEREBELLUM.	46
FIGURE 3.1 zR3Ha SHOWS STRONG DOMINANT NEGATIVE EFFECTS.	74
FIGURE 3.2 zFLI FORMS FUNCTIONAL CHANNELS WITH ALTERED GATING PROPERTIES.	75
FIGURE 3.3 zR4Hi CAUSES DOMINANT NEGATIVE SUPPRESSION OF CURRENT AMPLITUDE AND ALTERS VOLTAGE-DEPENDENT GATING.	76
FIGURE 3.4 zR3Ha HAS NO EFFECT ON BASAL ACTION POTENTIAL FIRING IN PURKINJE CELLS.	77

FIGURE 3.5 zR3Hi INDUCES OSCILLATING FIRING PATTERN AFTER SUDDEN-DARKNESS STIMULATION.....	78
FIGURE 3.6 zR4Hi TRIGGERS RAPID DENDRITIC DEGENERATION AND CELL DEATH IN PURKINJE CELLS.....	79
FIGURE 3.7 zR4Hi INDUCES HYPEREXCITABILITY IN DEVELOPING PRKINJE CELLS.	80
FIG 3.8 SK CHANNEL AGONIST NS13001 REDUCES TONIC FIRING FREQUENCY AND PROVIDES PROTECTIVE EFFECT AGAINST zR4Hi-INDUCED DENDRITIC DEGENERATION.	81
TABLE 1.1 CORRESPONDING SCA13 MUTATIONS IN HUMAN AND ZEBRAFISH Kv3.3.....	14

Acknowledgments

I would like to take this opportunity to express my gratitude to Dr. Diane Papazian for her guidance, mentorship and support throughout my PhD study. Her insight in science and passion in pursuing the truth of nature has inspired me profoundly. I would also like to thank my thesis committee members: Drs. Thomas Otis, Baljit Khakh, Joanna Jen, and David Glanzman. Their scientific comments and advice has enlightened me and has expedited the progress of the projects significantly.

The content of Chapter 2 of this thesis has been previously published in Hsieh et al., 2014, and is presented here in a modified format. Dr. Diane Papazian, Dr. Fadi Issa, Dr. Ji-Jun Wan, and Brittany Ulrich coauthored in this study. Dr. Papazian was the principle investigator and oversaw the entire project. Dr. Fadi Issa and Brittany Ulrich conducted the confocal imaging experiments, and Dr. Ji-Jun Wan provided technical support and inspiration in the development of a novel *in vivo* electrophysiology method allowing recordings in awake zebrafish. In Chapter 3, I included data collected by Dr. Meng-Chin Lin and Brittany Ulrich. They performed the two-electrode voltage clamp and confocal imaging experiments, respectively. Their hard work and generosity is highly appreciated. I thank them for letting me include their data in this thesis. Drs. Paul Mathews, Ray Luo, Meera Pratap, Ka-Hung Lee are also appreciated for their intellectual inputs to the projects and technical support to data analysis.

Figure 1.2 in this thesis is a reprint from Hashimoto and Hibi (2012), Development and evolution of cerebellar neural circuits. *Development, Growth & Differentiation*, 54: 373–389. doi: 10.1111/j.1440-169X.2012.01348.x. It is very kind of John Wiley and Son publisher to grant the permission of using this figure in my thesis.

I would like to thank my family for being supportive and understanding throughout my PhD journey. Studying in a foreign country has been a sweet and bitter experience, and they have accompanied me and helped me through all the highs and lows. Although they are almost eight thousand miles away, I could not have accomplished my study here without their warm encouragement.

Jui-Yi Hsieh

EDUCATION

- National Taiwan University** Sep 2004 – July 2006
- *Master of Science in Physiology*
- National Taiwan University** Sep 2000 – July 2004
- *Bachelor of Science in Life Science*

RESEARCH EXPERIENCE

Department of Physiology, University of California, Los Angeles

Graduate Student Researcher to Dr. Diane Papazian Sep 2009 – present

Focus: The etiology of human spinocerebellar ataxia type 13 (SCA13), a disease that manifests itself in both neurodegenerative and neurodevelopmental forms

- Characterized biophysical properties of causative K_v3.3 mutations in *Xenopus* oocytes
- Conducted dynamic-clamping on hippocampal neurons expressing exogenous K_v3.3
- Examined the transportation of K_v3.3 subunits to plasma membrane by Western blotting
- Established lab specific protocols for stereotaxic surgery and AAV2/5 microinjection in rats, and protocols for *in utero* and *in vivo* brain electroporation in mice
- Created a library of K_v3.3 clones for AAV production and for *in vivo* expression in zfish
- Built two patch-clamping/optogenetic rigs and performed electrophysiology in slices
- Developed a novel method for *in vivo* electrophysiology in Purkinje cells in awake zfish that allows simultaneous optogenetics, Ca²⁺ imaging, and sensory stimulation
- Performed *in vivo* loose-patch recordings and confocal imaging in awake zfish and described the consequences of SCA13 mutations on cerebellar maturation and function

Oregon Health Science University, the Vollum Institute

Visiting scholar to Dr. Paul Brehm's Laboratory Oct 2012

- Learned *in vivo* electrophysiology and Ca²⁺ imaging in Zebrafish spinal cord
- Performed whole-cell recordings on primary motor neurons in the spinal cord and paired-recordings in motor neuron and muscle cell

Department of Physiology, University of California, Los Angeles

Research Assistant to Dr. Diane Papazian Dec 2008 – Aug 2009

Focus: The biophysics of voltage sensors in Shaker potassium channels

- Created a library of Shaker clones and prepared RNA for expression in *Xenopus* oocytes
- Characterized the biophysics of Shaker mutants by two-electrode voltage clamp
- Advanced the understandings of voltage-sensor motion during channel gating

Graduate Institute of Physiology, National Taiwan University

Graduate Student Researcher to Dr. Chung-Chin Kuo Aug 2004 – Oct 2006

Focus: The interaction between anticonvulsants and Na_v1.2

- Created a library of Na_v1.2 clones and prepared RNA for expression in *Xenopus* oocytes
- Investigated the working mechanisms of various anticonvulsants and local anesthetics (carbamazepine, lamotrigine, lidocaine and phenytoin) on Na_v1.2 by electrophysiology
- Proposed a novel structure-function model that details the drug-channel interaction and explains the difference in affinity/efficacy between drugs

Graduate Institute of Zoology, National Taiwan University

Undergraduate Student Researcher to Dr. Chien-Yuan Pan Sep 2002 – July 2004

Focus: The effects of polyphenols from green tea extracts on epinephrine and norepinephrine release

- Performed primary chromaffin cell culture from bovine adrenal glands
- Studied the effects of polyphenols on various types of Ca_v channels and on Ca^{2+} -induced- Ca^{2+} -release by whole-cell electrophysiology and pharmacological approaches
- Proposed a mechanism describing the effects of polyphenols on adrenal gland secretion

TECHNIQUES AND SKILLS

- **Electrophysiology**
 - Patch-clamping: loose-patch, perforated-patch, and whole-cell patch
 - In cultured cells, mouse/rat brain slices, and Zebrafish (*in vivo*)
 - With simultaneous Ca^{2+} imaging and optogenetical manipulation *in vivo*
 - Paired patch-clamp recordings at neuromuscular junction *in vivo*
 - Two-electrode voltage clamping in *Xenopus* oocytes
- **Stereotaxic survival surgery and adeno-associated virus microinjection**
- **Confocal imaging and calcium imaging** (GCaMP-HS and GCaMP5) *in vivo*
- **Primary cell culture and cell line culture**
- **DNA transfection, virus infection, and *in utero/in vivo* brain electroporation**
- **Standard molecular biology and biochemistry techniques**
- **Analysis computer software:** Pulse, Clampfit, Igor, and OriginLab

AWARDS AND SCHOLARSHIPS

- Graduate Student Fellowship 2013
 - Awarded for outstanding academic performance and achievement
- Jennifer S. Buchwald Graduate Fellowship in Physiology 2009 – 2010
- National Health Research Institute Scholarship 2004 – 2006
- First Prize, Hsieh Te-kuei and Feng Sung-yen Scientific Poster Contest 2004
- Presidential Award, Department of Life Science, National Taiwan University 2004
 - Awarded for academic performance ranked in top 5% of class

PUBLICATIONS

- **Hsieh, J.-Y.**, Ulrich, B., Issa, F. A., Wan, J. & Papazian, D. M. Rapid development of Purkinje cell excitability, functional cerebellar circuit, and afferent sensory input to cerebellum in zebrafish. *Front. Neural Circuits* 8, 1–12 (2014).
- Lin, M.C., **Hsieh, J.-Y.**, Mock, A. F. & Papazian, D. M. R1 in the Shaker S4 occupies the gating charge transfer center in the resting state. *J. Gen. Physiol.* 138, 155–63 (2011).
- Mock, A.F., Richardson, J.L., **Hsieh, J.-Y.**, Rinetti, G. & Papazian, D. M. Functional effects of spinocerebellar ataxia type 13 mutations are conserved in zebrafish Kv3.3 channels. *BMC Neurosci.* 11, 99 (2010).
- Yang, Y.-C., **Hsieh, J.-Y.** & Kuo, C.-C. The external pore loop interacts with S6 and S3-S4 linker in domain 4 to assume an essential role in gating control and anticonvulsant action in the Na^+ channel. *J. Gen. Physiol.* 134, 95–113 (2009).

Chapter 1

Introduction

Aims of this thesis

The aims of this thesis are to understand how the differential biophysical properties of $K_v3.3$ mutants in spinocerebellar ataxia type 13 (SCA13) generate distinct clinical phenotypes, and to establish a causal relationship between excitability and neuronal degeneration that may be generalized to other diseases.

In the first chapter, I briefly summarize the current understanding regarding the roles of excitability in neurodegenerative diseases and the properties of causative mutations in SCA13. I also describe the general rationale of using zebrafish as a biological model to study neurological diseases, and several technical advantages it provides for the experimental designs in this thesis.

By employing the zebrafish system, we focused on investigating: 1) the electrical maturation of cerebellar Purkinje cells, 2) the functional maturation of cerebellar circuits and 3) the consequences of SCA13 mutations in developing cerebellum. I addressed the first two aspects in Chapter 2 by using a novel *in vivo* recording method developed in our lab. Findings in this chapter establish the foundation for further studies using zebrafish cerebellum. In Chapter 3, I first describe the conservation of functional effects of SCA13 mutations between human and zebrafish $K_v3.3$ using two-electrode voltage clamp in *Xenopus* oocytes, and then demonstrate how the distinct biophysical properties of SCA13 mutations leads to differential consequences in cell function *in vivo* during cerebellar development.

Altered excitability in neurodegenerative diseases

Altered excitability is a common phenotype in neurodegenerative diseases, including amyotrophic lateral sclerosis (ALS), Huntington's disease and several types of spinocerebellar ataxia (SCA) caused by polyglutamine repeat expansions (Bae et al., 2013; Chopra and

Shakkottai, 2014). However, the role of excitability during disease progression is not fully understood, and the causal relationship between altered excitability and neuronal death has not been established.

In the ALS, the importance of hyperexcitability in the etiology has been widely recognized, although there is an unsettled debate whether it contributes directly to the pathogenesis of the disease or whether it is merely a transient phenotype during the progression of the disease (Bae et al., 2013). A popular “dying forward” mechanism proposed over two decades ago suggests a central role of hyperexcitability mediated glutamate excitotoxicity in the degeneration of motor neurons (Eisen et al 1992). This idea has been supported by a significant number of studies over the years (reviewed by Kiernan, 2009). Recently, a study by Wainger et al (2014) further supports the “dying forward” hypothesis by showing that development of hyperexcitability is intrinsic to the diseased motor neurons, and blocking hyperexcitability through pharmacological means improves motor neuron viability and alleviates ER stress. ER stress activates the unfolded protein response, which is thought to contribute to pathogenesis in ALS. Reducing the level of ER stress has been shown to improve the viability of the motor neurons in ALS (Kiskinis et al., 2014). Nonetheless, despite the supporting evidence, a direct link tying hyperexcitability and neuronal degeneration has not been established. This is partly because hyperexcitability develops only in the early stages of ALS and disappears in the advanced phase, and because ALS can be caused mutations found in over 20 genes that involve a wide range of cell functions (Sreedharan and Brown, 2013). The heterogeneous nature of ALS makes it very difficult to study the exact contribution of every single factor.

Abnormal neuronal firing is also reported in many polyglutamine diseases, including, Huntington’s disease and several types of SCA (SCA1-3, SCA6, SCA7, SCA17, and

dentatorubral-pallidoluysian atrophy). The onset and the degree of severity are often correlated with the number of polyglutamine repeats in the target proteins. Interestingly, many studies on different polyglutamine diseases have reported that the alteration in excitability precedes the development of pathology (reviewed by Chopra and Shakkottai, 2014). This observation supports the idea that altered excitability may be an early event in pathogenesis in these diseases. For instance, a recent study by Hansen et al (2013) showed that there is a progressive reduction in the firing of cerebellar Purkinje cells before the emergence of any morphological changes or motor defect in SCA2 mice. Furthermore, evidence has been presented by Kasumu et al (2012) showing that reverting the bursting firing pattern seen in diseased Purkinje cells to a more normal tonic firing pattern using pharmacological agents significantly improves motor functions and the viability of Purkinje cells in SCA2 mice. This suggests that rectifying the altered firing pattern provides a protective effect against disease-induced neuronal degeneration. However, the mechanisms by which polyglutamine expansions cause changes in excitability and how those changes in excitability contribute to neuronal death remain unknown. It is possible that changed neuronal activity is merely a side effect of the main pathogenetic pathway. Some polyglutamine diseases cause a decrease in neuronal excitability while others cause an increase in neuronal activity (reviewed by Chopra and Shakkottai, 2014), which may reflect the fact that expression of proteins with polyglutamine repeat expansions can alter a variety of downstream cell functions. Thus, despite the prevalence of altered excitability in polyglutamine diseases, the roles of it during pathogenesis remain unclear. Further study is needed to establish a direct causal relationship between the excitability and neuronal degeneration.

Taken together, while altered excitability is commonly seen in neurodegenerative diseases and may have important roles during the disease progression, whether it contributes

directly to the etiology of these diseases is an open question under investigation. In most neurodegenerative diseases, it is difficult to evaluate the role of altered excitability in pathogenesis for several reasons, including: 1) putative disease-causing mutations occur in multiple genes that involve a variety of cell functions, 2) causative mutations happen in genes with unknown function, and 3) the effects of causative mutations on neuronal function are unclear. Spinocerebellar ataxia type 13 (SCA13) provides a promising opportunity to investigate whether altered excitability alone is sufficient to trigger neurodegeneration. It is a disease caused by mutations in a single gene that encodes a well-studied ion channel, $K_v3.3$ (see below), and the causative mutations show very clear and defined effects on the channel function as described in previous studies and in Chapter 3 of this thesis (Waters et al., 2006; Figuorea et al 2010, Minassian et al 2012). These two features of SCA13 eliminate the complications seen in other diseases, and studying the etiology of SCA13 may provide valuable insights regarding the causal relationship between changes in excitability and neuronal degeneration. This knowledge may greatly advance our understanding of the roles of excitability in neurodegenerative diseases and potentially inspire new therapeutic strategies.

Spinocerebellar ataxia type 13 and the causative mutations in *KCNC3* gene

Human spinocerebellar ataxia type 13 (SCA13) is an autosomal dominant disease that exists in two clinical forms differing in whether onset occurs in infancy or adulthood. The infant-onset form shows pathological phenotypes in early childhood before the cerebellum is fully mature. This form of SCA13 is associated with motor delay, persistent motor deficits, and severe and early-onset atrophy of the cerebellum. On the other hand, the symptoms of the adult-onset form include progressive cerebellar degeneration and progressive ataxia and do not emerge until

the late 20s or early 30s (Herman-Bert et al. 2000; Waters et al. 2006; Figueroa et al. 2010; Figueroa et al., 2011). Genetic studies have identified three causative mutations in the human *KCNC3* gene, which encodes the voltage-gated potassium channel type 3.3 (K_v3.3). They are R420H, R423H and F448L (Figure 1.1; Table 1.1) (Waters et al 2006; Figueroa et al., 2010). R420H causes adult-onset SCA13, whereas R423H and F484L cause the infant-onset form. There is a very strong genotype to phenotype correlation between the mutations and the clinical forms regardless of the genetic background. This suggests strongly that the existence of two clinical forms is not due to variations in the genetic background but to the type of mutation in the *KCNC3* gene.

Compared to other types of voltage-gated potassium channels that reduce excitability, K_v3.3 has unique biophysical properties that facilitate high-frequency repetitive firing in neurons. These properties include depolarized voltage-dependence in channel activation and rapid gating kinetics (Rudy, 1999; Rudy and McBain, 2001). K_v3.3 is expressed in multiple types of neurons throughout mammalian cerebellar cortex, including Purkinje cells (Goldman-Wohl et al., 1994). Its function is crucial for regulating electrical firing in Purkinje cells, and losing K_v3.3 activity leads to alterations in action potential shape and failure in spike generation (Mckay and Turner, 2004; Mckay and Turner, 2005). It also has been reported that knockout mice lacking K_v3.3 show motor deficits that can be rescued by restoring K_v3.3 function. (Hurlock et al 2008; also reviewed by Joho and Hurlock, 2009).

Previous studies on SCA13 mutations showed that infant- and adult-onset mutations have distinct effects on K_v3.3 channel function. The adult-onset SCA13 mutation, R420H, is a non-functional subunit that has a strong dominant-negative effect on wild-type subunits. When the two types of subunits are co-expressed in the *Xenopus* oocytes, R420H significantly suppresses

wild-type current amplitude (Waters et al., 2006). In contrast, F448L, an infant-onset mutation, forms functional channels and, when co-expressed with wild-type subunits, shows a dominant gain-of-function effect that shifts the voltage-dependence of channel opening to more negative potentials (Waters et al., 2006; Minassain et al., 2012). R423H also causes the infant-onset form of SCA13. It is a non-functional subunit that exhibits both dominant negative and dominant gating-modifying effects on wild-type subunits (Figuroa et al., 2010; Minassian et al., 2012).

It has been proposed that the divergence of clinical phenotypes is caused by the differential effects of SCA13 mutations on K_v3.3 biophysics and cell excitability (Waters et al., 2006; Minassian et al., 2012). To test this idea, I investigated the biophysical properties of K_v3.3 subunits carrying SCA13 mutations and characterized their impact on neuronal function in the developing cerebellum *in vivo*. We found a clear link between altered biophysical properties, cell excitability, and neuronal degeneration. These findings are described in Chapter 3 of this thesis.

Cerebellar circuits are highly conserved through evolution

The cerebellum controls fine motions by integrating sensory and predictive inputs and motor feedback information. It also plays roles in modulating cognitive and emotional functions (Ito, 2008; Koziol et al., 2014). Cerebellar organization, circuit, cell types, and development have been studied extensively in the past decades, and it has been shown that all these aspects are well conserved through evolution from teleosts to mammals with some minor differences (Fig 1.2) (Hibi and Shimizu, 2012; Hashimoto and Hibi, 2012).

A variety of neuronal types have been identified in the teleost cerebellum. Similar to the mammalian cerebellum, most of them are GABAergic neurons, including Purkinje cells (PCs), Golgi cells and stellate cells. Basket cells, a group of GABAergic interneurons found in

mammalian cerebellum, have not yet been found in fish cerebellum. Glutamatergic neurons in the teleost fish cerebellum include granule cells (GCs), eurydendroid cells (ECs) and unipolar brush cells (Hibi and Shimizu, 2012; Hashimoto and Hibi, 2012).

Among all the cell types, GCs and PCs are the most important neurons that control information flow. In mammalian cerebellar cortex, GCs receive all the entering information from mossy fibers (MFs). MFs carry sensory and predictive information from various parts of the brain to cerebellum (Fig 1.2). This context information is then relayed to PCs through parallel fibers (PFs), the long projecting axons of GCs. Purkinje cells integrate inputs from multiple GCs and send the processed signals to neurons in the deep cerebellar nuclei (DCN). In mammals, Purkinje cells are the sole output neurons in the cerebellar cortex. In addition to the PF inputs, PCs also receive synaptic inputs from climbing fibers (CFs) that originate from inferior olive in the posterior hindbrain (Fig 1.2). In mature mammalian cerebellum, there is a one-to-one innervation pattern between CFs and PCs. CFs are afferent fibers that carry the error correcting signals to cerebellum. These signals represent the discrepancy between predicted motion and actual motor outputs. When CF inputs coincide with the context information from PFs, PF-PC synaptic activity is suppressed via long-term depression, which is believed to be critical to motor learning (Ito, 2002a, 2002b, 2006).

The anatomical organization of neurons in the cerebellum of zebrafish and other teleosts is similar to that of the mammalian cerebellum. While the latter has 10 lobes, the zebrafish cerebellum has only 3, namely the valvula cerebelli (Va), the corpus cerebelli (CCe), and the vestibulo-lateral lobe. Each lobe in mammalian cerebellum has a three-layer structure, including the molecular layer, the Purkinje cell layer, and the granule cell layer (Fig 1.2). In zebrafish however, only the CCe shares this structure and orientation. Although the Va has the same three-

layer structure, the orientation is inverted. The vestibulo-lateral lobe contains only the granule cell layer (Butler and Hodos, 1996; Wullimann et al., 1996; Altman and Bayer 1997; Bae et al., 2009). The molecular layer, which is the most superficial, contains PFs, stellate cells, and the dendrites of PCs. In this layer, PFs form glutamatergic synapses with distal PC dendrites while the proximal dendrites of PCs are innervated by CFs. The second layer is the Purkinje cell layer which contains the cell bodies of PCs. The granule cell layer is the deepest of the three. It accommodates GCs, Golgi cells, unipolar brush cells and eurydendroid cells. It is also the place where GCs, Golgi cells, and mossy fibers interact with one another. Eurydendroid cells are anatomically equivalent to the DCN neurons in mammalian brain (Ikenaga et al., 2006; Heap et al 2013), although it is unclear whether they serve the same function. Eurydendroid cells receive inputs from both PCs and parallel fibers. The former are located in the granule cell layer while the latter are located in the molecular layer.

Despite detailed anatomical studies, little is known about the electrical excitability and firing patterns of cerebellar neurons in zebrafish. The lack of functional knowledge limits the use of zebrafish as a biological model for mechanistic studies on neurodegenerative diseases. To develop zebrafish as a promising model system for studying mammalian diseases such as SCA13, it is important to investigate whether the function of the cerebellum, including the excitability of cerebellar neurons and the activity of their neuronal connections, has been conserved in evolution. Thus, in Chapter 2, we characterized the electrical properties of developing Purkinje cells and the functional maturation of climbing fibers inputs. We found that zebrafish Purkinje cells show highly conserved firing patterns compared to their mammalian counterparts, that there are functional connections between PFs and PCs, and that the maturation

of zebrafish CF inputs exhibits a winnowing process similar to that found in the mammalian cerebellum (see above and Chapter 2).

Zebrafish as a biological model to study SCA13

In this thesis, I investigated whether changes in excitability can result in neuronal degeneration by testing the hypothesis that infant- and adult-onset SCA13 mutations alter $K_v3.3$ properties in distinct ways and thereby confer differential effects on cell excitability which may underlie the divergence of the two clinical forms. To achieve this goal, we employed zebrafish as a biological model to study SCA13.

As described above, zebrafish and mammalian cerebella are highly conserved in terms of gross structure, neuronal types, and local circuits. Through aligning their sequences, we reported that zebrafish and human $K_v3.3$ share amino acid identity up to 82% (Mock et al., 2010) and that $K_v3.3$ is highly expressed in zebrafish Purkinje cells (Hsieh et al., 2014). In addition, we have demonstrated that zebrafish Purkinje cells show conserved electrical properties compared to mammalian Purkinje cells (Chapter 2). These similarities between the zebrafish and mammalian cerebella provide a solid and logical foundation for our experiments.

Zebrafish has gained increasing popularity in the field of neurodevelopmental research in past years. It offers many technical advantages when compared to mammalian models, including ease of genetic manipulation, rapid development outside the mother's body, and optical transparency during early development. These features enable experimental designs that can be more difficult to achieve in mammalian models. For instance, the common way to introduce mutations to mammalian neurons *in vivo* is either through virus infection or through creating transgenic lines. The technical and financial hurdles of both are relatively high. In contrast, in the

zebrafish system, the introduction of mutant proteins to neurons can easily be done by DNA microinjection (see methods in Chapter 3) into single cell staged embryos. This is because zebrafish embryos are fertilized and develop completely outside the mother's body. External development also allows us to investigate the onset and progression of SCA13 at very early stages of cerebellar development using optical approaches and *in vivo* electrophysiology in living animals. It would be much more difficult to do the same experiment in a mammalian system.

In addition to lower technical hurdles, zebrafish offers another advantage to study neurodegenerative diseases. Zebrafish grow and develop much more rapidly than mammals. This allows us to follow and study the entire progression of neuronal degeneration in SCA13 within a reasonable time frame. The development of the mouse cerebellum starts around embryonic day 10 and is not complete until postnatal day 20. In contrast, the zebrafish cerebellum matures within one week post-fertilization (Bae et al., 2009). The structure emerges rapidly between 2 and 3 days-postfertilization (dpf), and becomes anatomically mature between 5 and 6 dpf (Bae et al., 2009; Tanabe et al., 2010; and Hibi and Shimizu 2012). Functional connections between neurons are established within the same developmental window, including those between mossy fibers and GCs, those between PFs and PCs, and those between CFs and PCs. Taking advantage of this rapid development, zebrafish serves as a promising model to characterize cerebellar maturation and to investigate disease mechanisms in SCA13.

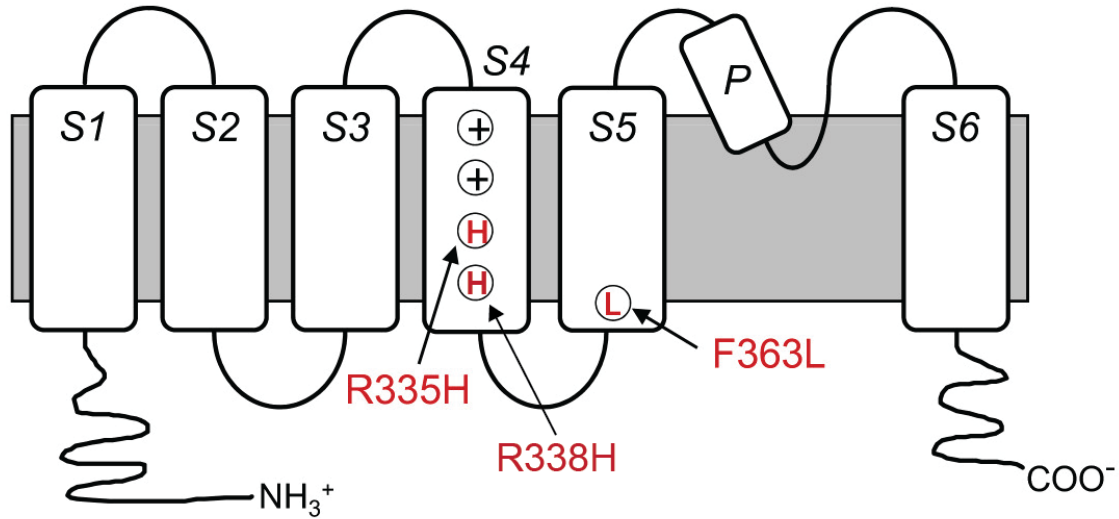


Figure 1.1 The topology of zebrafish Kv3.3 channel subunit and the locations of SCA13 mutations.

Schematic illustration of one zebrafish Kv3.3 subunit is shown. Transmembrane segments are labeled S1 to S6. P marks the pore region. Both amino and carboxyl terminuses are on the intracellular side. SCA13 mutations were labeled in red. R335H leads to adult-onset form of SCA13, and R338H and F363L generate the infant-onset form. The corresponding mutations in the human Kv3.3 are listed in Table 1.1.

Figure modified and adapted from Mock et al., 2010.

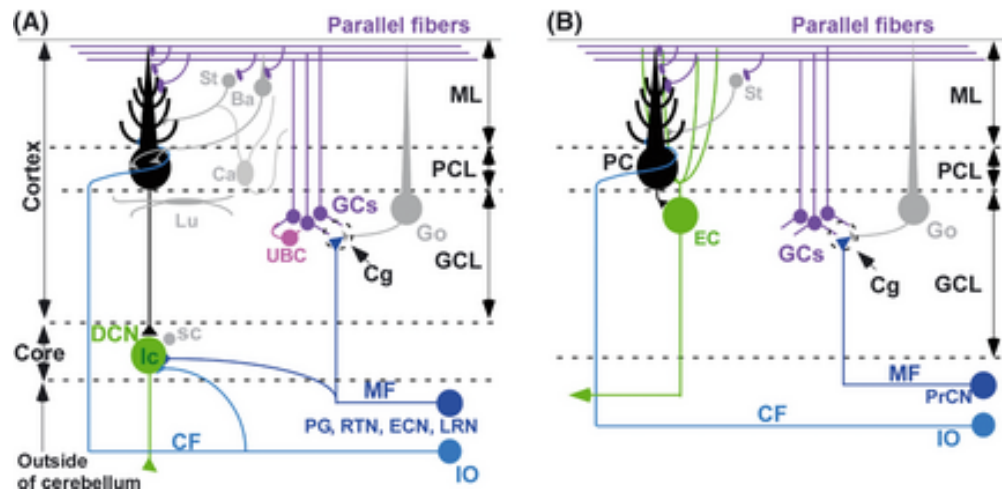


Figure 1.2 Zebrafish and mammalian cerebellar circuits are highly conserved.

Schematic representation of cerebellar neurons and neural circuits in the mouse (A) and zebrafish (B) cerebellum. Ba, basket cell; Ca, candelabrum cell; CF, climbing fiber; Cg, cerebellar glomeruli; DCN, deep cerebellar nuclei (lc, large cell; sc, small cell); EC, eurydendroid cell; ECN, external cuneate nuclei; GCs, granule cells; GCL, granule cell layer; Go, Golgi cell; IO, inferior olive nuclei; Lu, Lugaro cell; LRN, lateral reticular nuclei; MF, mossy fiber; ML, molecular layer; PC, Purkinje cell; PCL, Purkinje cell layer; PG, pontine gray nuclei; PrCN, precerebellar nuclei (except IO); RTN, reticulotegmental nuclei; St, stellate cells; UBC, unipolar brush cell.

This figure is a reprint of Figure 1 from:

Hashimoto, M. and Hibi, M. (2012), Development and evolution of cerebellar neural circuits.

Development, Growth & Differentiation, 54: 373–389. doi: 10.1111/j.1440-169X.2012.01348.x

Permission has been granted by John Wiley and Son through Copyright clearance center (RightsLink) website.

Table 1.1 Corresponding SCA13 mutations in human and zebrafish Kv3.3

SCA13 form	Human <i>KCNC3</i>		Zebrafish <i>kcnc3a</i>	
	Mutation	label	Mutation	label
adult-onset	R420H	hR3Ha	R335H	zR3Ha
infant-onset	R423H	hR4Hi	R338H	zR4Hi
infant-onset	F448L	hFLi	F363L	zFLi

*h:human, z:zebrafish, a:adult-onset, i:infant-onset

Chapter 2

Rapid development of Purkinje cell excitability and the functional maturation of the cerebellar circuit in zebrafish

The content of Chapter 2 was published previously and is presented here in a modified format: Hsieh J-Y, Ulrich B, Issa FA, Wan J and Papazian DM (2014) Rapid development of Purkinje cell excitability, functional cerebellar circuit, and afferent sensory input to cerebellum in zebrafish. *Front. Neural Circuits* **8**:147. doi: 10.3389/fncir.2014.00147

Introduction

The zebrafish, a lower vertebrate, has great potential for optogenetic mapping of brain circuits because of its transparency, rapid development, and ease of genetic manipulation (Arrenberg & Driever, 2013). The power of optogenetic mapping is increased significantly by the ability to record electrophysiologically in live animals from neurons that integrate converging input information and generate output signals for efferent pathways. One such neuron is the cerebellar Purkinje cell, the sole output neuron of the cerebellar cortex. Little is known about the electrical activity of cerebellar neurons in zebrafish. We have now used patch clamp electrophysiology in situ in live zebrafish to investigate the electrical properties of Purkinje cells, the functional maturation of the cerebellar circuit, and the emergence of sensory input to the cerebellum during brain development.

The embryological origins and anatomical organization of cerebellar neurons are highly conserved in zebrafish and mammals (Hashimoto and Hibi, 2012). Advantageously for brain mapping, the cerebellum is smaller, simpler, and develops much more rapidly in zebrafish than in mammals. The zebrafish cerebellum has 3 lobes, the corpus cerebelli (CCe), the valvula cerebelli (Va), and the vestibulolateral lobe. CCe and Va have tri-lamellar structures comprising the granule cell, Purkinje cell, and molecular layers. These layers have the same orientation in CCe as in the mammalian cerebellum, but are inverted in Va (Bae et al., 2009; Hashimoto and Hibi, 2012). In contrast, the vestibulolateral lobe contains only the granule cell layer (Hashimoto and Hibi, 2012). Thus, the CCe lobe of the zebrafish cerebellum has the strongest similarity to the mammalian cerebellum. In mammals, Purkinje cell compartments have been defined by stripes of aldolase-C (zebrin-II) expression (Ji and Hawkes, 1994). In contrast, it has been shown that zebrin-II is expressed specifically and exclusively in all zebrafish Purkinje cells (Bae et al.,

2009). Anatomical evidence suggests that zebrafish Purkinje cells, like their mammalian counterparts, receive two types of direct excitatory inputs, parallel fibers and climbing fibers, which are the axons of cerebellar granule cells and neurons of the inferior olive, respectively (Bae et al., 2009; Hashimoto and Hibi, 2012). In mammals, parallel fibers convey sensory and predictive information that is carried into the cerebellum by mossy fibers from precerebellar nuclei, whereas climbing fibers provide error correction signals that help to optimize motor control (D'Angelo et al., 2011). The interaction between parallel fiber and climbing fiber inputs to Purkinje cells is crucial for motor learning (Ito, 2002a; 2002b; 2006). The function of parallel and climbing fiber inputs in zebrafish has not yet been investigated. Zebrafish Purkinje cells target eurydendroid cells, which are equivalent to deep cerebellar nuclei neurons in mammals (Hibi and Shimizu, 2012). Similar to deep cerebellar nuclei neurons, eurydendroid cells project to the hindbrain, tectum, and thalamus (Heap et al., 2013).

We found that zebrafish Purkinje cells, which are born at 3 days post-fertilization (dpf) (Bae et al., 2009), are electrically excitable by 4 dpf. A mature pattern of spontaneous tonic firing interspersed with complex spiking is established over the next 48 hours. The electrical properties and the expression of ion channels that control firing are highly conserved compared to mammalian Purkinje cells. By 4 dpf, Purkinje neurons receive visual input conveyed by mossy fibers to parallel fibers, with visual input via climbing fibers developing by the next day. Rapid development of a functional cerebellum is likely to be an essential survival advantage in zebrafish, which develop entirely outside the body of the mother where they must avoid predators and find food starting early in life. A notable advantage of zebrafish is that electrophysiological analysis of Purkinje cells is technically easy in a minimally-disturbed, live animal preparation with intact brain, sensory input, and motor output. This facilitates

experiments that would be technically challenging and significantly more invasive in mammals. Our results indicate that the zebrafish cerebellum is an excellent system in which to combine optogenetic mapping and electrophysiological analysis, to evaluate emerging optical methods for functional brain mapping, and to investigate cerebellar control of motor behavior and motor learning.

Materials and Methods

Animal maintenance

Zebrafish (*Danio rerio*) were housed in the University of California, Los Angeles (UCLA) Zebrafish Core Facility at 28°C using a 14 h/10 h light/dark cycle. Adults were bred to obtain embryos. Animals were raised until 9 dpf in a 28°C incubator using the same light/dark cycle. Starting at 5 dpf, larvae were fed brine shrimp powder twice daily. Animal procedures were approved by the Chancellor's Animal Research Committee at UCLA.

Generation of transgenic zebrafish

Previously, a zebrafish transgenic line, rk22Tg:*Tg(aldoca:gap43-Venus)*, which expresses a membrane-bound form of the Venus yellow fluorescent protein specifically in cerebellar Purkinje cells under the control of the zebrafish *aldolase Ca (aldoca)* promoter, was generated in the AB wild type strain by Tanabe et al. (2010). Aldolase C (zebrin-II) is a specific Purkinje cell marker in zebrafish and mammals (Brochu et al., 1990; Tanabe et al., 2010). Membrane tethering of Venus is conferred by a palmitoylation site in the first 20 amino acids of zebrafish gap43, which have been fused to the Venus N-terminus. Using a plasmid containing

the *aldoca:gap43-Venus* insert in the pT2K vector (kind gift of Dr. Masahiko Hibi), we generated an equivalent transgenic line, la118Tg:*Tg(aldoca:gap43-Venus)*, in the unpigmented Tüpfel long fin nacre (TLN) strain using Tol2-mediated transgenesis (Kawakami et al., 2004; Schoonheim et al., 2010; Tanabe et al., 2010; zfin.org/ZDB-GENO-080307-1). Plasmid DNA and *in vitro* transcribed transposase mRNA were mixed and co-injected into single-celled embryos (Kawakami et al., 2004). Injected fish were raised to sexual maturity and bred. Germline transgenic animals were identified in the F1 generation by *gap43-Venus* expression in Purkinje cells.

RNA in situ hybridization

In situ hybridization was used to investigate Purkinje cell-specific expression of Kv3.3 and Nav1.6. Probes derived from the zebrafish *kcnc3a* (Kv3.3a) or *scn8aa* (Nav1.6a) genes were separately mixed with an *aldoca* (zebrin-II) probe, which was used to identify differentiated Purkinje cells (Tsai et al., 2001; Bae et al., 2009; Mock et al., 2010; Tanabe et al., 2010). Whole mount, double fluorescent *in situ* hybridization was performed as described by Brend and Holley (2009) at 3, 4, 5, and 6 dpf using TLN zebrafish. Animals were euthanized by immersion in 0.2% MS222 and then fixed overnight (~15 h) in 4% paraformaldehyde at 4°C. Yolk sacs were removed by dissection. Larvae were permeabilized by digesting with 200 µg/mL proteinase K for 25 min at room temperature. Zebrafish were incubated overnight at 68°C in 50 µL prehybridization buffer containing 1 µL *aldoca* probe and 1 µL *kcnc3a* or 1µL *scn8aa* probe. Fluorescein-labeled *kcnc3a* and *scn8aa* probes were visualized using the TSA Plus Fluorescein Kit (PerkinElmer) with an incubation time of 45 min at room temperature. Digoxigenin-labeled *aldoca* probes were visualized using the TSA Plus Cy5 Solution (PerkinElmer) with an

incubation time of 30 min at room temperature. Specimens were mounted dorsal side up in 75% glycerol. Images were acquired using an Olympus Fluoview FV300 laser scanning confocal microscope with an Olympus 40X/1.3 oil immersion objective. Signals from antisense and sense probes were imaged using the same laser settings.

Gene-specific probes for *aldoca* and *scn8aa* were made using primers from the last coding exon and the 3' untranslated region of each gene (Thisse & Thisse, 2008). To generate antisense and sense probes for the zebrafish *aldoca* gene (NM_001029952), genomic DNA was amplified by PCR using the forward primer 5'-ATTAGGTGACACTATAGAAGGGAAGTACACGGTTTGTGGTGA-3' and the reverse primer 5'-TAATACGACTCACTATAGGGCACATCTCACAGTTTTATTGCAGCAC-3'. The 698 bp product was transcribed using the Digoxigenin RNA Labeling Kit (Roche Diagnostics) by T7 RNA polymerase to make the antisense probe and SP6 RNA polymerase to make the sense probe. Probes to *scn8aa* (NM_131628) were amplified from zebrafish genomic DNA using the forward primer 5'-ATTAGGTGACACTATAGAAGACAGTAAGGGCAAAAAGGGCAA-3' and the reverse primer 5'-TAATACGACTCACTATAGGGAATGGGCTGAACGTTTTCCC-3'. The 703 bp product was transcribed using the RNA Labeling Kit with Fluorescein NTP Labeling Mix (Roche Diagnostics) by T7 RNA polymerase to make the antisense probe and by SP6 RNA polymerase to make the sense probe. Probes for *knc3a* (NM_001195240.1) were made using a clone containing the first 1363 bp of the cDNA sequence in the pCRII vector (Mock et al., 2010). To generate the antisense probe, the clone was linearized by digestion with HindIII (New England BioLabs) and transcribed by T7 RNA polymerase using the RNA Labeling Kit with Fluorescein NTP Labeling Mix (Roche Diagnostics). For the sense probe, the

clone was linearized with XhoI (New England BioLabs) and transcribed by SP6 RNA polymerase.

***In situ* electrophysiology**

Larval zebrafish between 4 and 14 dpf were anesthetized with medical grade 0.02% MS222 (Western Chemical) for ~10 seconds, then glued dorsal side up onto coverslips in a recording chamber. The chamber was filled with external solution containing (in mM): 134 NaCl, 2.9 KCl, 2.1 CaCl₂, 1.2 MgCl₂, 10 HEPES, and 10 glucose, pH 7.5. Curare (10 μM) was added to paralyze the animals. Skin around the head and the skull were gently removed using fine forceps. Electrophysiological recordings were performed in awake animals starting 5-10 min after the dissection and were stable for up to one hour. All data shown in this study were acquired within 45 minutes after the dissection. To avoid possible circadian variation in the results, all recordings were made between noon and 6 pm local time. At the end of the experiment, zebrafish were euthanized by immersion in 0.2% MS222.

Data were acquired in the cell-attached, loose patch configuration using a HEKA EPC10 patch clamp amplifier and Pulse software (HEKA Elektronik). Borosilicate pipettes (7 to 10 MΩ, World Precision 1B150F-4) were filled with external solution. Purkinje cells were visualized under an upright Olympus BX51WI microscope using a 40X/0.80 water-immersion lens. Recordings were made from cells in the corpus cerebelli (CCe). Patch pipettes approached Purkinje cells from the rostral side at an angle of 30° relative to the horizontal plane. Seal resistances ranged from 20 MΩ to 2 GΩ. Experiments were performed at room temperature (22-25°C) with the ambient and microscope lights turned off. Electrical activity was recorded in voltage clamp mode at 0 mV. Data were acquired at 20-50 kHz and filtered at 3 kHz. Only

recordings with consistent spike amplitudes and non-overlapping spike waveforms were analyzed.

Inferior olive stimulation

Inferior olive neurons were stimulated using a theta pipette (~5 μm tip opening) filled with external solution. Depending on the age of the animal, the tip of the theta pipette was placed 250 to 300 μm anterior to the end of brainstem at a depth of 125 to 150 μm from the dorsal surface. These coordinates were chosen based on a previous anatomical study by Bae et al. (2009) and the results of our preliminary experiments. To identify an appropriate stimulus amplitude, 2 ms pulses ranging from 20 to 200 μA were delivered to the inferior olive using a stimulus isolator (A.M.P.I.). A stimulus of 50 μA evoked maximal complex spiking in Purkinje cells by the criterion that there was no apparent difference in the response when larger stimuli were applied. Therefore, a 2 ms 50 μA stimulus was used in all experiments. Data were analyzed only from Purkinje cells that showed complex spiking in the absence of direct olivary stimulation. Otherwise, if stimulation failed to elicit complex spikes, we could not distinguish the scenario in which there was no climbing fiber-Purkinje cell connection from the scenario in which inferior olive neurons were damaged by the placement of the theta pipette.

Visual stimulation experiments

A 1 W, 6500K white LED light source (Thorlabs) was installed on the microscope to illuminate the preparation through the halogen light pathway. A white LED was chosen to avoid possible color-dependent variations in Purkinje cell responses. Animals were light adapted for 2 min before the LED was turned off. In all experiments, light adaptation was performed using the

minimum LED intensity that evoked consistent Purkinje cell responses. The power of the LED was controlled by the HEKA EPC10 amplifier. Switching the LED on and off was time-locked with electrophysiological recordings. Purkinje cell activity was recorded for 10 s before and 10-60 s after the LED was turned off. To avoid over-stimulating the visual system, recordings were made from one Purkinje cell per animal in most cases. Occasionally, recordings were made from two Purkinje cells in the same animal. Each Purkinje cell was subjected to 1-4 trials, with an inter-trial interval of at least 2 min. No signs of habituation or desensitization were noted when multiple trials were performed on the same cell.

Data analysis

Electrophysiological data were imported into Igor 6.2 (WaveMetrics) and analyzed with Clampfit 10.2 and 10.4 (Molecular Devices). The regularity of spontaneous tonic firing was quantified by determining the coefficient of variation of adjacent intervals (CV2) defined as $\frac{2}{n} \sum_{i=1}^n \frac{|I_{i+1} - I_i|}{I_{i+1} + I_i}$, where I is interspike interval in ms. CV2 is preferable to the conventional coefficient of variation (CV, standard deviation/mean) for data recorded on a short time scale (Walter et al., 2006; Wulff et al., 2009). Data are provided as mean \pm SEM. Statistical significance was assessed using Student's t-test or ANOVA followed by either Tukey's or Holm-Bonferroni post hoc tests. Spearman's rank method was used for correlation analysis. Excel 2011 (Microsoft) and Origin 8 (OriginLab) were used to perform statistical testing. Adobe Illustrator (Adobe) was used to prepare figures.

Results

Rapid emergence of electrical excitability in zebrafish Purkinje cells

During brain development in zebrafish, *ptfla*-expressing precursor cells located in the ventricular zone give rise to cerebellar Purkinje cells which are born, differentiate, migrate, and begin to extend neurites at 3 dpf (Bae et al., 2009; Kani et al., 2010; Tanabe et al., 2010). The primary dendrite and axon form at 4 dpf, and fine branches and spines become visible shortly thereafter. Starting at 4 dpf, we used patch clamp electrophysiology to investigate the development of electrical excitability in Purkinje cells. Experiments were performed at room temperature (22-25°C) using a transgenic zebrafish line made in the unpigmented Tüpfel longfin nacre (TLN) strain that expresses a membrane-bound form of Venus, a yellow fluorescent protein, specifically in Purkinje cells under the control of the zebrafish *aldoca* promoter (Fig 2.1A) (Schoonheim et al., 2010; Tanabe et al., 2010). After removing the overlying skin and skull, recordings were made using loose patch electrodes in live, awake animals in situ in the intact brain (Fig 2.1B). Recordings were made primarily from Purkinje cells located in the medial region of each cerebellar hemisphere.

At 4 dpf, Purkinje cells were already electrically excitable, with spontaneous, irregular firing of action potentials at an average frequency of ~5 Hz at room temperature (Fig 2.1C). By 5 dpf, the average tonic firing frequency had increased significantly to ~9 Hz, a value that did not change significantly on subsequent days (Fig 2.1D-G). For comparison, the tonic firing rate in mammalian Purkinje cells in acute cerebellar slices is ~12 Hz at room temperature (23-26°C) (Wulff et al., 2009).

The regularity of tonic firing was assessed by measuring the coefficient of variation of adjacent intervals (CV2). Firing regularity increased significantly between 4 and 6 dpf, as

indicated by a decrease in CV2 from ~ 0.8 at 4 dpf to ~ 0.5 at 6 dpf (Fig 2.1H). In contrast, CV2 did not differ significantly from 6-9 dpf (Fig 2.1H). These values are higher than that reported for rodent Purkinje cells in cerebellar slices (~ 0.2) (Wulff et al., 2009). However, the numbers are not directly comparable because the animals in our experiments were awake and could have been responding to uncontrolled sensory stimuli, which would be expected to increase the variability of tonic firing. Consistent with this interpretation, CV2 for tonic firing is $\sim 0.4-0.6$ in awake mice, and the coefficient of variation of the interspike interval (CV, standard deviation/mean) is $\sim 0.5-1$ in awake cats (Armstrong & Rawson, 1979; Wulff et al., 2009; Zhou et al., 2014).

In addition to tonic spiking, by 5 dpf a majority of cells occasionally fired action potentials with more complex waveforms, consisting of a large initial spike followed by a longer lasting but lower amplitude depolarization (Fig 2.1D, expanded trace). These electrical events strongly resemble complex spikes observed in mammalian Purkinje cells, which are initiated by synaptic input from inferior olive neurons via climbing fibers (see below) (D'Angelo et al., 2011). The pattern of regular, spontaneous firing of simple spikes interspersed with occasional complex spike-like events was also observed at 6 and 7 dpf (Fig 2.1E,F) and was stable through 14 dpf, the last time point that was investigated (data not shown). Our results indicate that the excitability of zebrafish Purkinje cells develops within 24-48 hours after the cells are born resulting in a stable firing pattern that strongly resembles the electrical activity of mammalian Purkinje cells.

In mammalian Purkinje cells, spontaneous tonic firing arises from the interplay of resurgent Na^+ currents, mediated in large part by Nav1.6, and rapidly activating and deactivating K^+ currents conducted by members of the Kv3 family, particularly Kv3.3 and Kv3.4 (Raman et

al., 1997; Khaliq et al., 2003; Martina et al., 2003; Akemann & Knöpfel, 2006). We used in situ hybridization to investigate whether Nav1.6 and Kv3.3 are expressed in zebrafish Purkinje cells during the development of spontaneous tonic firing (Brend & Holley, 2009). Differentiated Purkinje cells were identified using a probe directed against the *aldoca* (zebrin-II) gene (Tanabe et al., 2010). Expression of Nav1.6, Kv3.3, and zebrin-II was not detected in TLN animals at 3 dpf, when Purkinje cells are born (Fig 2.2A-F). However, expression of both channel types and zebrin-II was detected by antisense probes starting at 4 dpf (Fig 2.2A-F). The intensity of staining for Nav1.6 increased noticeably between 4 and 5 dpf (Fig 2.2A,B). These results show that the time course of Kv3.3 and Nav1.6 expression is strongly correlated with the emergence of excitability and the development of regular tonic firing, suggesting that the ion channels that underlie spontaneous pacemaking activity are conserved in zebrafish and mammalian Purkinje cells.

Rapid development and maturation of functional connectivity in the zebrafish cerebellar circuit

To test the hypothesis that complex spike-like events indeed reflect the postsynaptic response of Purkinje cells to climbing fiber input, we investigated whether direct stimulation of the inferior olive increased the frequency of these events. At 5 dpf, brief supra-threshold stimuli were applied to the inferior olive using a theta pipette (Fig 2.1B). In the immediate post-stimulus period, the frequency of action potentials with complex waveforms in Purkinje cells increased dramatically (Fig 2.3). These results indicate that olivary neurons make functional climbing fiber synapses onto Purkinje cells by 5 dpf, and that activation of these synapses elicits complex spikes that strongly resemble those recorded in mammalian Purkinje cells.

To investigate the development of functional climbing fiber synapses, we determined the prevalence of complex spiking as a function of developmental age in the absence of olivary neuron stimulation. At 4 dpf, complex spikes were detected in ~35% of Purkinje cells (7/19 cells). This value was not increased by direct stimulation of olivary neurons (not shown). In contrast, complex spiking occurred in ~65-70% of cells at 5-6 dpf (20/29 & 20/31 cells at 5 & 6 dpf, respectively), and in ~85% of cells at 7 dpf (19/22 cells). In cells that exhibited complex spiking, the frequency of complex spikes was low at 4 dpf, suggesting that active climbing fiber connections were just beginning to form (Fig 2.4A). Complex spike frequency increased dramatically at 5 dpf, attaining a maximum value of 0.40, before subsiding to an intermediate frequency of 0.24 at 6 dpf that did not differ significantly from that measured on subsequent days.

During the development of the mammalian cerebellum in the early postnatal period, individual Purkinje cells are initially innervated by multiple climbing fibers. Over the next 2 weeks, these inputs are winnowed by activity-dependent competition until each Purkinje cell is innervated by a single 'winner' climbing fiber (Crepel, 1982; Bosman & Konnerth, 2009; Hashimoto & Kano, 2013). The finding that the frequency of complex spiking reaches a maximum at 5 dpf and subsequently declines to a stable level raises the possibility that zebrafish Purkinje cells are innervated by multiple climbing fibers at 5 dpf and that these are winnowed to a single input between 5-7 dpf. To test this hypothesis, the inferior olive was directly stimulated to activate all available climbing fibers. Electrical stimulation increased complex spike frequency dramatically between 5 and 8 dpf compared to the unstimulated values (Fig 2.4A). Therefore, with or without direct stimulation, the highest frequency of complex spiking was observed at 5 dpf (Fig 2.4A).

Before activity-dependent winnowing is complete in mammals, individual Purkinje cells are innervated by climbing fiber inputs of differing strengths (reviewed by Hashimoto & Kano, 2013). The winner climbing fiber corresponds to the strongest input. Therefore, winnowing should be accompanied by an overall increase in the time course of the Purkinje cell response because strong synaptic inputs result in a more rapid approach to threshold than weaker inputs. To investigate whether zebrafish Purkinje cells are innervated by climbing fibers of different strengths at 5 dpf, we determined the average number of complex spikes occurring in sequential 200 ms bins following the stimulus at 5-8 dpf (Fig 2.4B). We found that the temporal distribution of postsynaptic responses changed as a function of developmental age. There was a greater number of complex spikes occurring at later times post stimulus at 5 dpf than on subsequent days (Fig 2.4B). Taken together, the data suggest that climbing fibers begin to make functional connections with Purkinje cells starting at ~4 dpf, that Purkinje cells are innervated by multiple climbing fibers of varying strengths at 5 dpf, and that winnowing of redundant climbing fiber inputs occurs between 5-7 dpf and is completed by ~7 dpf.

Sensory stimulation alters Purkinje cell activity starting at 4 dpf

A significant advantage of zebrafish is that the activity of cerebellar Purkinje cells can be recorded in situ in living, awake animals using a minimally-disturbed preparation with intact sensory systems, and afferent and efferent pathways. We took advantage of this to investigate the development of functional sensory input to the zebrafish cerebellum and its consequences for electrical activity in Purkinje cells. We chose visual stimulation because the visual system is functional at this stage of development, reproducible visual stimuli can be readily applied, and vision is highly relevant to zebrafish behavior because it guides prey capture (feeding) and

contributes to the avoidance of predators (Fleisch & Neuhauss, 2006; Westphal & O'Malley, 2013; Chhetri et al 2014). Zebrafish were adapted to a white LED light for 2 min. The visual system was then stimulated by turning the light off while recording simultaneously from Purkinje cells. Fig 2. 5A shows the response of an individual Purkinje cell at 7 dpf to sudden darkness. Turning off the LED increased the instantaneous tonic firing frequency, from ~15 Hz prior to the stimulus to ~60 Hz in the first 150 ms after the stimulus (Fig 2.5B). Increases in tonic firing frequency are likely mediated by mossy fiber pathways that convey visual information to granule cells, leading to activation of parallel fiber synapses onto Purkinje cells (D'Angelo et al., 2011). Most Purkinje cells responded to the stimulus by increasing the rate of firing (Fig 2.5C). However, in rare instances, the firing frequency was unaltered or even decreased (Fig 2.5C, trials 28 and 9 respectively). This could reflect lack of visual input to the cell or an alternative wiring pattern, respectively. In addition to the increase in tonic firing frequency, the lights off stimulus transiently increased the frequency of complex spiking in the majority of Purkinje cells (Fig 2.5C). The similarity of the responses in most Purkinje cells may reflect the fact that the bulk of our recordings were made in a restricted region of the cerebellum.

To investigate the development of functional sensory input pathways to the cerebellum, we repeated the lights off stimulation experiment at different days post-fertilization. The average frequency of tonic firing after the stimulus was calculated for each 100 ms interval and normalized to the average frequency prior to the stimulus (Fig 2.6A). Strikingly, even at 4 dpf, turning the LED off dramatically increased the frequency of tonic spiking in the post-stimulus period. After an initial, dramatic increase in frequency, the firing rate remained elevated by ~1.5-fold over the pre-stimulus value for tens of seconds. These results indicate that functional sensory input conveyed via parallel fibers emerges within 24 h of the birth of Purkinje cells.

Similarly, at 5, 6, and 7 dpf, turning the LED off transiently and dramatically increased the frequency of tonic firing. As at 4 dpf, this was followed by a persistent, ~1.4- to 2.3-fold elevation in firing rate that subsided to the baseline level over ~20-30 sec.

To investigate when climbing fibers become responsive to visual input, the number of complex spikes per 250 ms intervals before and after the stimulus was plotted on peristimulus time histograms (Fig 2.6B). No increase in complex spiking was observed at 4 dpf (not shown), when functional climbing fiber connections are rare and complex spike frequency is low (see Fig 2.4A). In contrast, at 5, 6, and 7 dpf, the number of complex spikes was significantly elevated for ~1 s following the stimulus, indicating that visual input activated olivary neurons, which provide error correction signals to Purkinje cells (D'Angelo et al., 2011).

In response to sudden darkness, the tonic firing rate remained elevated for tens of seconds after the increase in complex spiking had subsided (Fig 2.6). This suggests that parallel fiber inputs, which innervate inhibitory interneurons in the molecular layer in addition to Purkinje cells (D'Angelo et al., 2011), maintain a net excitatory drive to Purkinje cells that is not directly evoked by sudden darkness. Therefore, additional afferent pathways and/or feedback loops are likely to contribute to the prolonged alteration in tonic firing frequency. Alternatively, climbing fiber input may result in a persistent mode switch in tonically-firing Purkinje cells (Loewenstein et al., 2005; Schonewille et al., 2006). However, this would not explain the results obtained at 4 dpf when visual stimulation did not evoke complex spikes.

The initial phase of the response to sudden darkness is presumably mediated by the pathway that connects retinal photoreceptors to Purkinje cells with the fewest synapses. To characterize the development and maturation of this pathway, we determined whether the initial response to sudden darkness varied as a function of developmental age. We identified the first

peak in instantaneous tonic firing frequency in the immediate post-stimulus period (see Fig 2.5B, inset). Interestingly, this initial peak firing rate did not differ significantly between 4 and 7 dpf (Fig 2.7A). When normalized to the pre-stimulus frequency, the most dramatic increase in instantaneous firing frequency was observed at 4 dpf (10-fold) compared to subsequent days (4-fold), at least in part because the basal firing rate is significantly lower at 4 dpf compared to subsequent days (Fig 2.7B; see Fig 2.1F). We also measured the time that elapsed between the stimulus and the initial peak in tonic firing frequency, and found that the latency of the response, which was ~300 ms at 4 dpf, declined to ~200 ms at 5 dpf (Fig 2.7C). This suggests that the circuit reacts more promptly as it matures, which may reflect refinement of the afferent pathway circuitry.

As noted above (Fig 2.6B), complex spiking increased significantly in the post-stimulus period starting at 5 dpf. Similarly to the increase in the tonic firing frequency (Fig 2.7A), the increased frequency of complex spiking, averaged over the first 500 ms post-stimulus, did not differ significantly between 5 and 7 dpf (Fig 2.7D). Compared to the pre-stimulus value, complex spike frequency increased in the post-stimulus period by 8-fold at 5 dpf and ~14 fold at 6 and 7 dpf, reflecting the higher frequency of complex spiking at 5 dpf compared to subsequent days (see Fig 2.4A). The latency to the first complex spike post-stimulus did not differ significantly between 5 and 7 dpf (Fig 2.7E). These results indicate that climbing fibers respond to afferent visual input within 48 h of the birth of Purkinje cells and that the response is stable on subsequent days.

DISCUSSION

Rapid functional development and highly conserved electrical properties in zebrafish cerebellum

A functional cerebellar circuit receiving afferent sensory information develops rapidly in zebrafish. Purkinje cells, which are born at 3 dpf, spontaneously fire action potentials by 4 dpf. The firing rate is modulated by visual input, likely conveyed by mossy fibers to cerebellar granule cells, which make parallel fiber synapses onto Purkinje cells (Bae et al., 2009; D'Angelo et al., 2011). Within 48 h of their birth, Purkinje cells display spontaneous tonic firing interspersed with complex spikes, which correspond to the post-synaptic response to climbing fiber activation (D'Angelo et al., 2011). Soon after they form, climbing fiber inputs respond to visual stimulation. The development of regular tonic firing in zebrafish is correlated with the time course of expression of the voltage-gated Nav1.6 and Kv3.3 channels, which underlie spontaneous pacemaking in mammalian Purkinje cells (Raman et al., 1997; Khaliq et al., 2003; Martina et al., 2003; Akemann & Knöpfel, 2006). In addition, Kv3.3 channels control the complex spike waveform (Hurlock et al., 2008; Zagha et al., 2008; Veys et al., 2013). Our results suggest that the electrical properties of mammalian and zebrafish Purkinje cells are highly conserved.

The rapid emergence of Purkinje cell excitability and cerebellar circuit activity is temporally correlated with the anatomical development of the zebrafish cerebellum (Bae et al., 2009, Tanabe et al., 2010). In zebrafish, the tri-lamellar structure of the cerebellar cortex forms by 5 dpf. The rapid time course makes zebrafish advantageous for *in vivo* studies of cerebellar development and function. In contrast, in rats, cerebellar cortical layers are not evident and

Purkinje cells are not functionally mature until ~2-3 postnatal weeks, which corresponds to ~5-6 weeks post-fertilization (Altman & Bayer, 1997; McKay & Turner, 2005).

Synapse elimination in the developing zebrafish cerebellum

Our data suggest that zebrafish Purkinje cells, like mammalian Purkinje cells, are initially innervated by multiple climbing fibers that are winnowed until only the strongest input remains (Crepel, 1982; Bae et al., 2009; Hashimoto & Kano, 2013). The frequency of complex spikes evoked by electrical stimulation of the inferior olive was significantly higher at 5 dpf than at 7 dpf. We suggest that Purkinje cells are innervated by multiple climbing fibers at 5 dpf and that these inputs are winnowed to a single input by ~7 dpf. However, our data do not rule out an alternative, non-mutually exclusive hypothesis, that an age-dependent decrease in the excitability of olivary neurons underlies the decline in complex spike frequency after 5 dpf. Nevertheless, our results indicate that reduced climbing fiber excitability is unlikely to be solely responsible. First, the number of complex spikes evoked in the first 200 ms after electrically stimulating the inferior olive did not differ significantly between 5 and 8 dpf. In contrast, a significantly higher number of complex spikes was evoked between 200 and 400 ms post-stimulus at 5 dpf compared to subsequent days (see Fig 2.4B). This suggests that strong and weak climbing fiber inputs co-exist on Purkinje cells at 5 dpf. Strong inputs should elicit rapid responses. In contrast, the response to weaker inputs would be delayed because weaker stimuli result in a slower approach to threshold in the postsynaptic cell. The selective loss of delayed complex spiking after 5 dpf is consistent with the specific elimination of weaker climbing fiber inputs. In contrast, if the decrease in complex spike frequency were primarily due to reduced excitability of olivary neurons, a reduction in the rate of complex spiking should manifest itself equally between 0-200

and 200-400 ms post-stimulus. Second, whereas the frequency of complex spiking evoked by direct electrical stimulation was greater at 5 dpf than on subsequent days, this was not the case when complex spiking was evoked by sudden darkness (see Fig 2.7D). After sudden darkness, there was no significant difference in complex spike frequency at 5, 6, or 7 dpf. The most plausible interpretation of these results is that direct electrical stimulation of olivary neurons activated both strong and weak climbing fiber inputs at 5 dpf, whereas sudden darkness, a more physiological stimulus, activated only the strong inputs. Consistent with this, the increase in complex spike frequency in response to the visual stimulus was not as great as that seen in response to direct electrical stimulation of the inferior olive (compare Figs. 2.4A and 2.7D).

Rapid development of afferent pathways conveying visual information to cerebellum in zebrafish

The zebrafish visual system is fully functional by 80 hours post-fertilization (~3.3 dpf) as indicated by the presence of an active optokinetic response (Chhetri et al., 2014). We used sudden darkness as a stimulus to investigate the functional development of pathways that convey visual information to the cerebellum and to determine the effect of visual input on electrical activity in Purkinje cells. At 4 dpf, sudden darkness robustly increased the frequency of spontaneous firing, indicating that functional connections had already been made by mossy fibers onto granule cells and by granule cells onto Purkinje cells, even though Purkinje cells had not yet established a mature pattern of activity. Purkinje cells responded to sudden darkness more rapidly at 5 dpf than at 4 dpf, indicating that one or more circuit components continued to mature and undergo synaptic refinement. During this period, active synaptogenesis occurs between retinal ganglion cells and their targets in the optic tectum (Niell et al., 2004; Meyer &

Smith, 2006). In addition, synapses between Purkinje cells and their presynaptic partners mature anatomically as dendritic spines form (Bae et al., 2009; Tanabe et al., 2010).

In contrast, sudden darkness did not evoke complex spiking at 4 dpf. Our data indicate that functional connectivity between climbing fibers and Purkinje cells started to emerge at 4 dpf, although the fraction of cells firing complex spikes and complex spike frequency were low. Therefore, an effect of sudden darkness on complex spiking rate might have gone undetected at 4 dpf. Alternatively, functional afferent connections conveying visual information to the inferior olive may not have developed by 4 dpf. On subsequent days, sudden darkness increased the complex spike frequency in most Purkinje cells. Interestingly, the increased rate of complex spiking lasted less than 1 second, whereas tonic firing frequency remained elevated over baseline for tens of seconds. This persistent increase is unlikely to be a direct response to sudden darkness. Rather, it may reflect feedback from other brain regions such as the thalamus, which receives input from both the visual system and eurydendroid cells, which convey efferent information from the cerebellum (Burrill & Easter, 1994; Heap et al., 2013).

Although we recorded dramatic changes in Purkinje cell activity in response to sudden darkness, we are unable to interpret the results in behavioral terms because the animals were paralyzed during electrophysiological experiments. Indeed, we cannot rule out the possibility that details of the Purkinje cell response, such as its time course, were affected by the inability of paralyzed animals to mount a behavioral response. The response of freely-behaving zebrafish at 6-7 dpf to large decreases in light intensity has been characterized by Burgess and Granato (2005). Darkness elicits large angle turns (O-bends) with novel kinematics and a latency of 200-300 ms that are distinct from the escape response (Burgess & Granato, 2005). Whether the cerebellum is involved in this behavior is unknown.

The rapid development of the cerebellum and its afferent and efferent pathways likely confers an essential survival advantage for zebrafish, which develop outside the body of the mother and must escape predators and hunt for food starting early in life (Westphal & O'Malley 2013). However, little is known about the role of the cerebellum in controlling behavior in zebrafish. Interestingly, the functional maturation of the cerebellum between 4 and 7 dpf coincides with the time zebrafish must begin to actively hunt for food, since the yolk sac is depleted at 4-5 dpf (Westphal & O'Malley 2013). Finding food involves prey capture, a complex, visually-guided behavior that may require cerebellar input. The emergence of this behavior is temporally well-correlated with the development of a functional cerebellum responsive to visual input. Zebrafish are incapable of capturing prey at 3 dpf, but can successfully capture *Paramecia* at 5 dpf (Westphal & O'Malley 2013). Further work will be required to determine whether this behavior is under cerebellar control.

Advantages of zebrafish for functional mapping of afferent and efferent pathways to cerebellum and for investigating cerebellar control of motor behavior

Our data indicate that zebrafish is an excellent model system in which to combine optogenetics and electrophysiological recording to map functional afferent and efferent connections to the cerebellum and to investigate cerebellar control of behavior. The electrical activity of Purkinje cells can be readily recorded in situ in live zebrafish with intact sensory modalities and motor output. Such experiments would be technically challenging and significantly more invasive in mice. As new genetically-encoded sensors of Ca^{2+} or voltage emerge, it will be feasible to correlate optical signals with the underlying electrical events recorded electrophysiologically at high temporal resolution in vivo. Such experiments are

essential for interpreting optical measures of neuronal function during brain mapping experiments. In addition, our results set the stage for genetically manipulating the electrical activity of Purkinje cells in verifiable ways and determining the behavioral consequences.

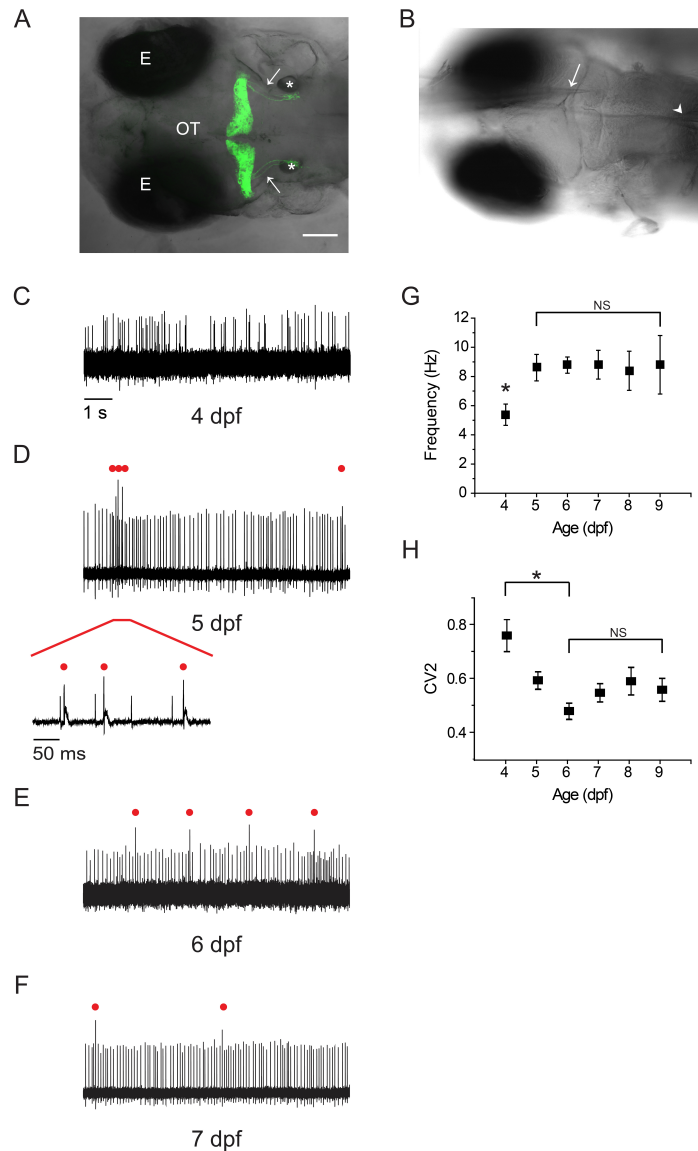


Figure 2.1. Rapid emergence and maturation of excitability in zebrafish Purkinje cells.

(A) Dorsal view of *la118Tg:Tg(aldoca:gap43-Venus)* transgenic zebrafish at 5 dpf shows that membrane-bound Venus is specifically and exclusively expressed in cerebellar Purkinje cells (Tanabe et al., 2010). Anterior is to the left. A z-projection of 168 1 μ m confocal images has been superimposed on the corresponding bright field image. Images were acquired with an Olympus Fluoview FV300 laser scanning confocal microscope. Labels: E, eye; OT, optic tectum; *, otic vesicle; arrows, cerebellovestibular axon tracts. Scale bar, 100 μ m. (B) The recording configuration is shown. A transgenic zebrafish at 5 dpf has been fixed in the recording chamber. A loose-patch electrode (arrow) was inserted from the anterior side and advanced to contact the cell body of a Purkinje cell. In some experiments, a theta pipette (arrowhead) was placed in the inferior olive to stimulate climbing fibers. (C-F) Shown are representative loose-patch recordings acquired at (C) 4 dpf, (D) 5 dpf, (E) 6 dpf, and (F) 7 dpf. In (D), red bar marks

portion of trace that is shown on an expanded time scale below the main trace. In D, E, and F, complex spike-like events are indicated by red dots. (G) The average simple spike firing frequency has been plotted versus age (n=7-31 cells from 6-24 animals). The frequency at 4 dpf, 5.4 Hz, was significantly different from the frequency on all subsequent days, which averaged ~9 Hz (*, ANOVA: 4-9 dpf, $F(5,113)=2.41$, $p=0.04$, followed by Tukey's post-hoc test: 4 and 5 dpf, $p<0.05$). Values obtained between 5 and 9 dpf did not differ significantly (NS, ANOVA: 4-9 dpf, $F(5,113)=2.41$, $p=0.04$, $p<0.05$, followed by Holm-Bonferroni post-hoc test: 5-9 dpf, $p\geq 0.05$). (H) The regularity of spontaneous tonic firing was quantified by determining the coefficient of variation of adjacent intervals (CV2), which has been plotted against age (n=7-31 cells from 6-24 animals). CV2 declined significantly from 4 dpf (CV2=0.76) to 6 dpf (CV2=0.48); CV2 did not differ significantly from 6-9 dpf (ANOVA: 4-9 dpf, $F(5,113)=5.83$, $p=7.96E-5$, followed by Holm-Bonferroni post-hoc test: 4-6 dpf, $p<0.05$ [*] and 6-9 dpf, $p\geq 0.05$ [NS]).

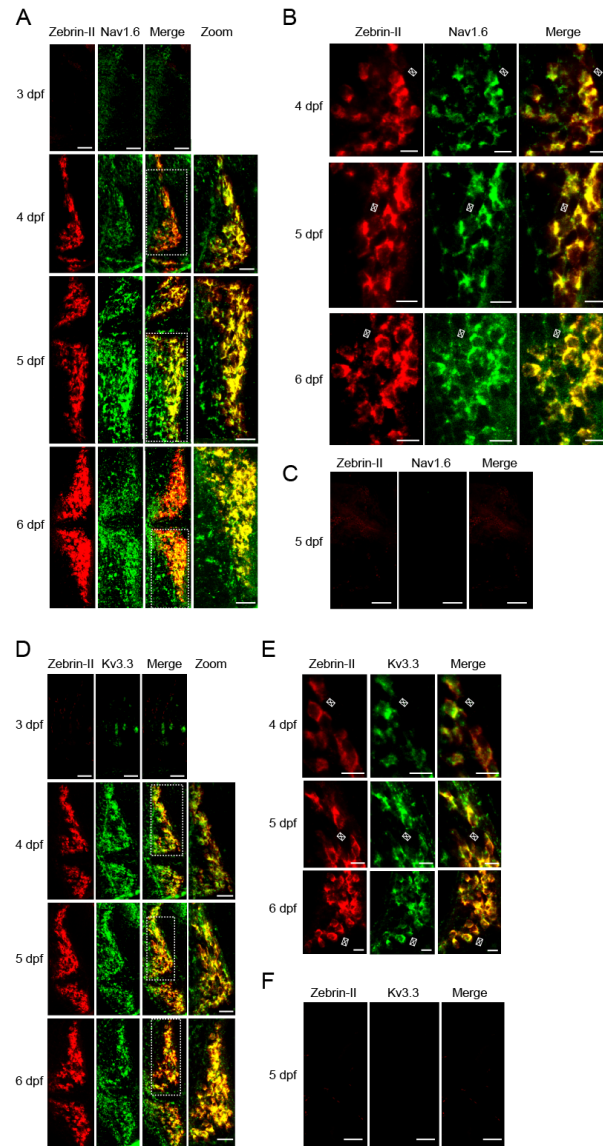


Figure 2.2 Expression of Nav1.6 and Kv3.3 coincides with the emergence of spontaneous tonic firing in Purkinje cells.

(A) Whole mount double fluorescent in situ hybridization was performed on TLN zebrafish at 3, 4, 5, and 6 dpf using digoxigenin-labeled aldoca (Zebirin-II, red) and fluorescein-labeled scn8aa (Nav1.6, green) antisense probes (Thisse & Thisse, 2008; Brend & Holley, 2009). Projected confocal image stacks for aldoca, scn8aa, and merged images are shown in the 3 left-most panels, respectively. Dashed white boxes in merged images denote regions of one cerebellar hemisphere that have been enlarged and shown in the right-most panel (zoom). Here and in subsequent parts of the figure, dorsal views are shown. Anterior is to the left. Scale bars: 40 μ m. (B) Enlarged single optical sections from the projections in Fig 2. 2A at 4, 5, and 6 dpf are shown. Arrowheads identify individual Purkinje cell bodies. Scale bars: 10 μ m. (C) Whole mount double fluorescent in situ hybridization was performed on TLN zebrafish at 5 dpf using

digoxigenin-labeled *aldoca* (Zeb1rin-II, red, left panel) and fluorescein-labeled *scn8aa* (Nav1.6, green, center panel) sense probes (Thisse & Thisse, 2008; Brend & Holley, 2009). Merged image is shown in right panel. Scale bar: 40 μm . (D) Whole mount double fluorescent in situ hybridization was performed on TLN zebrafish at 3, 4, 5, and 6 dpf using digoxigenin-labeled *aldoca* (Zeb1rin-II, red) and fluorescein-labeled *kcnc3a* (Kv3.3, green) antisense probes (Thisse & Thisse, 2008; Brend & Holley, 2009). Projected confocal image stacks for *aldoca*, *kcnc3a*, and merged images are shown in the 3 left-most panels, respectively. Dashed white boxes in merged images denote regions of one cerebellar hemisphere that have been enlarged and shown in the right-most panel (zoom). Scale bars: 40 μm . (E) Enlarged single optical sections from the projections in Fig 2. 2D at 4, 5, and 6 dpf are shown. Arrowheads identify individual Purkinje cell bodies. Scale bars: 10 μm . (F) Whole mount double fluorescent in situ hybridization was performed on TLN zebrafish at 5 dpf using digoxigenin-labeled *aldoca* (Zeb1rin-II, red, left panel) and fluorescein-labeled *kcnc3a* (Kv3.3, green, center panel) sense probes (Thisse & Thisse, 2008; Brend & Holley, 2009). Merged image is shown in right panel. Scale bar: 40 μm .

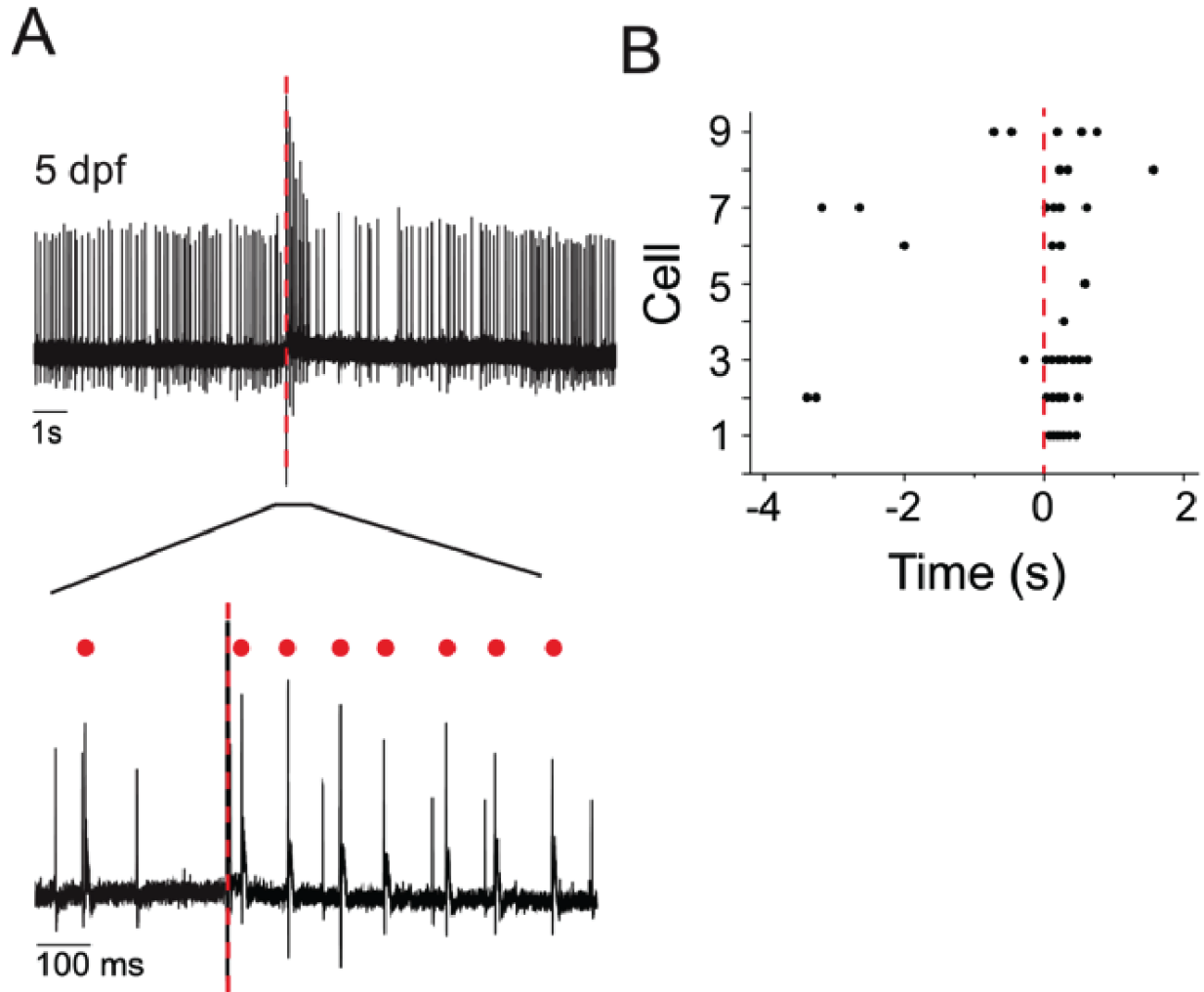


Figure 2.3 Direct electrical stimulation of inferior olive increases occurrence of complex spike-like events.

(A) Upper: The inferior olive was stimulated using a theta pipette (see Fig 2.1B) at the time indicated by the red dashed line. Shown is a representative recording of Purkinje cell activity obtained at 5 dpf. Lower: The portion of the upper trace marked by a bar is shown on an expanded time scale. Red dots indicate complex spikes. (B) Peristimulus raster plot shows the occurrence of complex spikes before and after stimulation of the inferior olive at time 0 (red dashed line). Results were obtained from 9 Purkinje cells from 4 animals at 5 dpf. The trace shown in part A corresponds to cell #3.

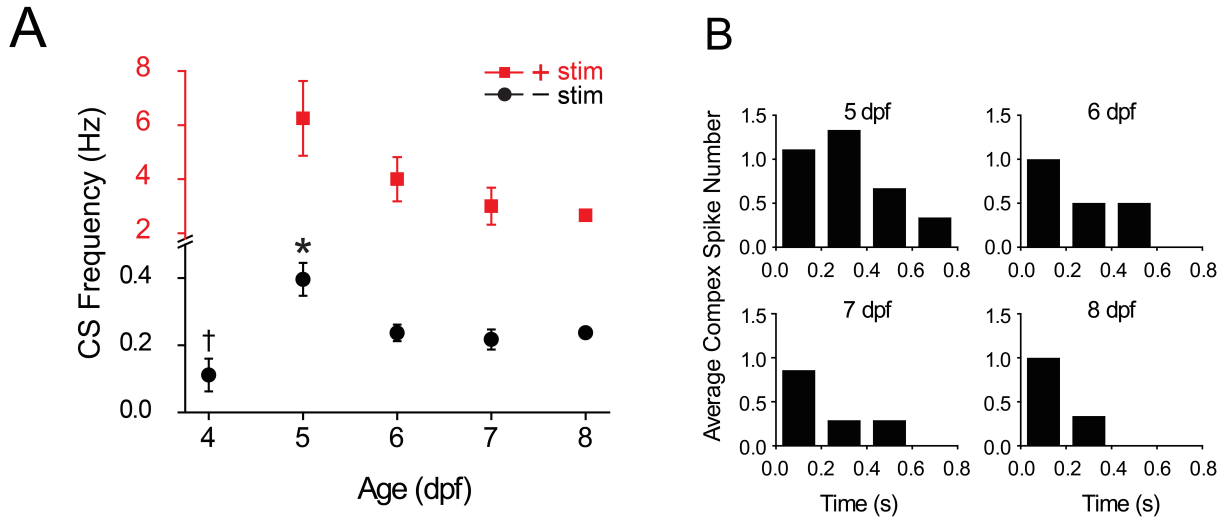


Figure 2.4 Development and winnowing of functional connections between climbing fibers and Purkinje cells.

(A) The average frequency of complex spiking in Purkinje cells in the absence (black circles) and presence (red squares) of direct electrical stimulation of the inferior olive has been plotted versus age. Note change in vertical scale for data obtained in the absence (black) and presence (red) of stimulation. In the absence of stimulation, complex spike frequency was averaged over 10 s recordings; the frequency at 5 dpf (0.4 Hz) was significantly higher than on all subsequent days (*, ANOVA: 4-8 dpf, $F(4,67)=6.17$, $p=2.75E-4$, followed by Tukey's post-hoc test: $p<0.05$; $n=6-20$ cells, 5-17 animals). The frequency at 4 dpf (0.11 Hz) was significantly lower than that measured at 6 dpf (0.24 Hz) (†, ANOVA: 4-8 dpf, $F(4,67)=6.17$, $p=2.75E-4$, followed by Tukey's post-hoc test: $p<0.05$; $n=7$ and 20 cells, 6 and 14 animals at 4 and 6 dpf, respectively). Complex spike frequency did not vary significantly between 6 and 8 dpf (ANOVA: 4-8 dpf, $F(4,67)=6.17$, $p=2.75E-4$ followed by Holm-Bonferroni post-hoc test: 6-8 dpf, $p\geq 0.05$; $n=6-20$ cells, 5-14 animals). In the presence of stimulation, the frequency of complex spiking was averaged over the first 500 ms after the stimulus. Evoked complex spike frequency decreased from 6.3 Hz at 5 dpf ($n=9$ cells, 4 animals) to 2.7 Hz at 8 dpf ($n=3$ cells, 3 animals) (Spearman's rank correlation, $r=-1$). Electrical stimulation increased complex spike frequency by ~16-fold at 5-6 dpf and by ~12-fold at 7-8 dpf. (B) Complex spiking was evoked by direct electrical stimulation of the inferior olive at 5-8 dpf. The average number of complex spikes per 200 ms bin after the stimulus has been plotted ($n=3-9$ cells, 3-4 animals). Cells that did not fire complex spikes in the absence of stimulation were excluded from the analysis.

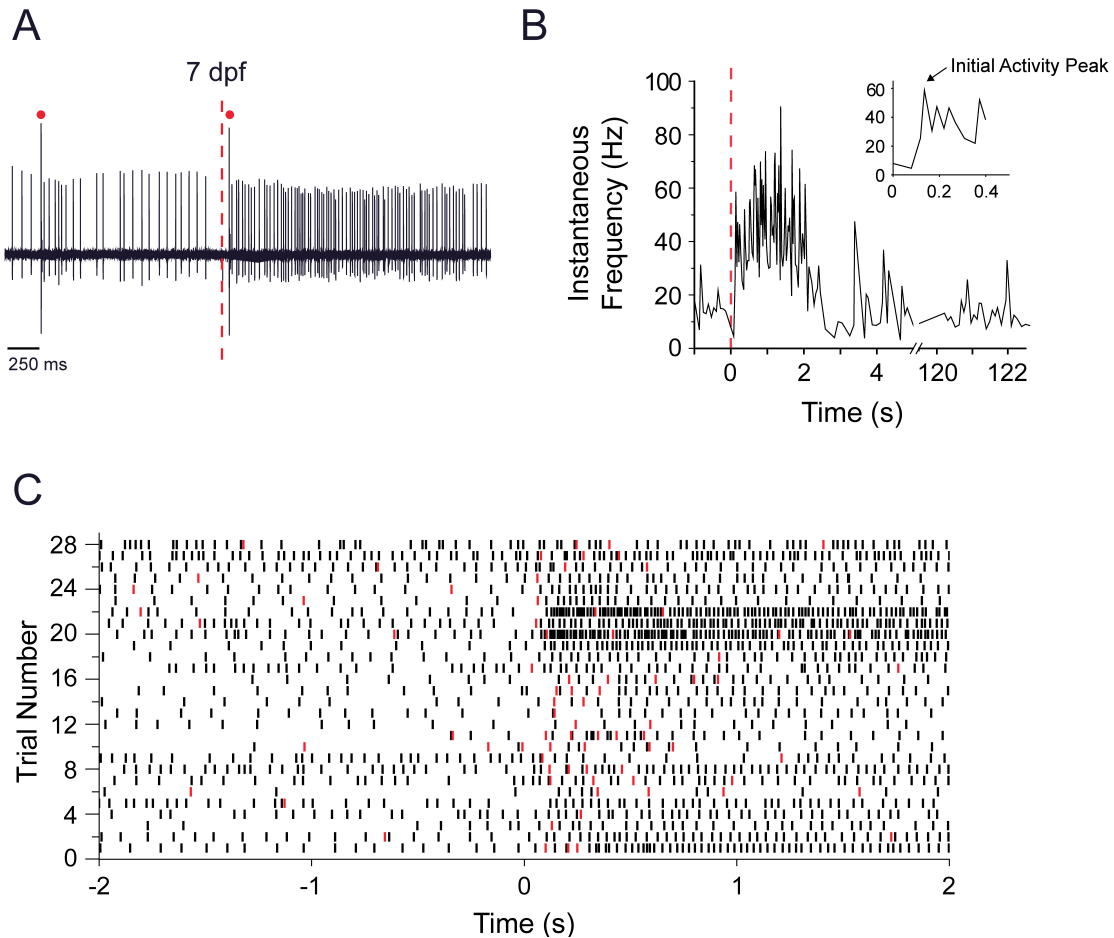


Figure 2.5 Sudden darkness increases the frequency of tonic firing and complex spiking.

(A) Purkinje cell firing at 7 dpf was recorded before and after turning off the LED at the time indicated by the red dashed line. A representative trace is shown. Red dots indicate complex spikes. (B) The instantaneous tonic firing frequency in the cell shown in part A was measured before and after the LED was turned off at time 0 (dashed red line). The frequency, which fluctuated around 15 Hz in the light, increased significantly to ~60 Hz during the first 150 ms after turning the LED off and remained elevated at ~40-60 Hz for several seconds. Inset shows the instantaneous firing frequency during the first 500 ms of darkness on an expanded time scale. The arrow indicates the initial peak in firing frequency after the stimulus, which corresponds to the direct response of the Purkinje cell to sudden darkness (see Fig 2. 7). (C) Peristimulus raster plot shows the timing of simple action potentials (black symbols) and complex spikes (red symbols) before and after the LED was turned off at time 0. Data were obtained from 28 trials in 11 Purkinje cells from 9 animals at 7 dpf. The trace shown in part A corresponds to trial #23. At 7 dpf, the spontaneous tonic firing frequency in the absence of stimulation ranged from 4.5-19.5 Hz (mean \pm SEM: 8.8 ± 0.98 Hz, $n=22$ cells from 20 animals). After sudden darkness, the peak tonic firing frequency ranged from 19.4-100.7 Hz (mean \pm SEM: 40.4 ± 7.4 Hz, $n=11$ cells, 9 animals).

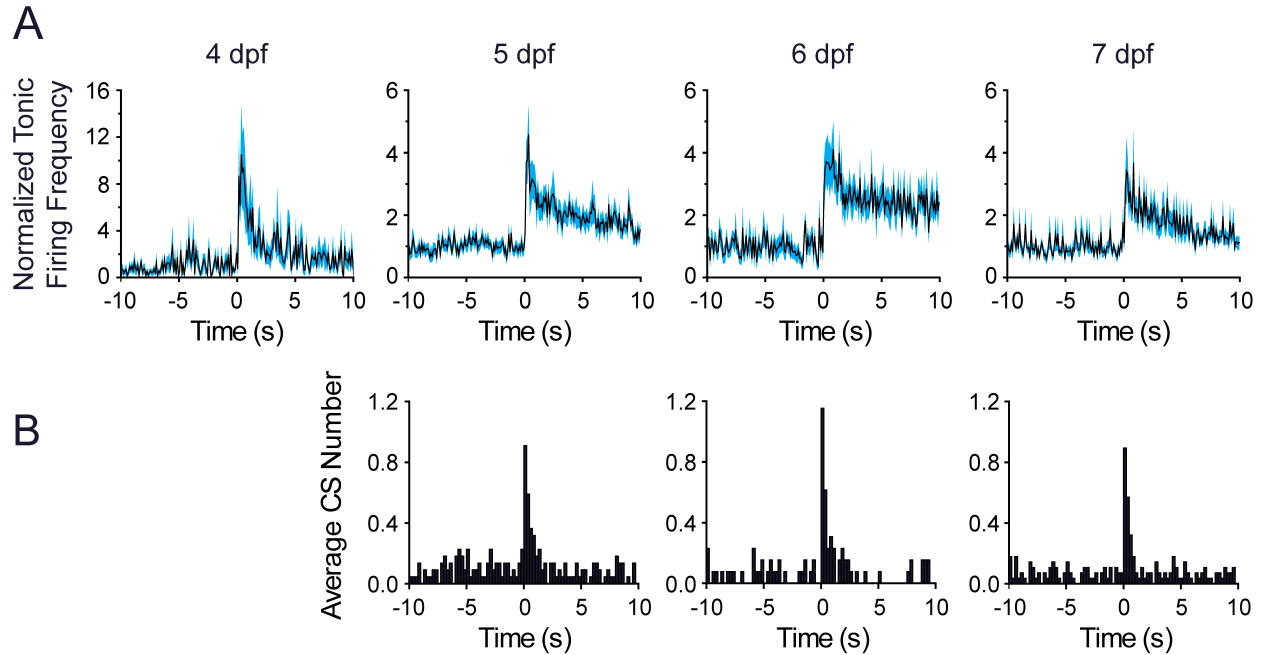


Figure 2.6 Comparison of Purkinje cell responses to sudden darkness at 4-7 dpf.

(A) After turning the LED off at time 0, the frequency of tonic firing was calculated for each 100 ms interval and normalized to the average frequency calculated over the 10 s period prior to the stimulus (solid lines, $n=6-14$ cells, 5-11 animals). The cyan-shaded areas represent the SEM. Please note compressed vertical scale at 4 dpf. (B) The bar graphs show the average number of complex spikes recorded in each 250 ms interval, calculated by dividing the total number of complex spikes in all cells by the number of cells ($n=13-28$ trials from 8-11 cells, 5-9 animals). The LED was turned off at time 0. Note that sudden darkness did not evoke complex spikes at 4 dpf.

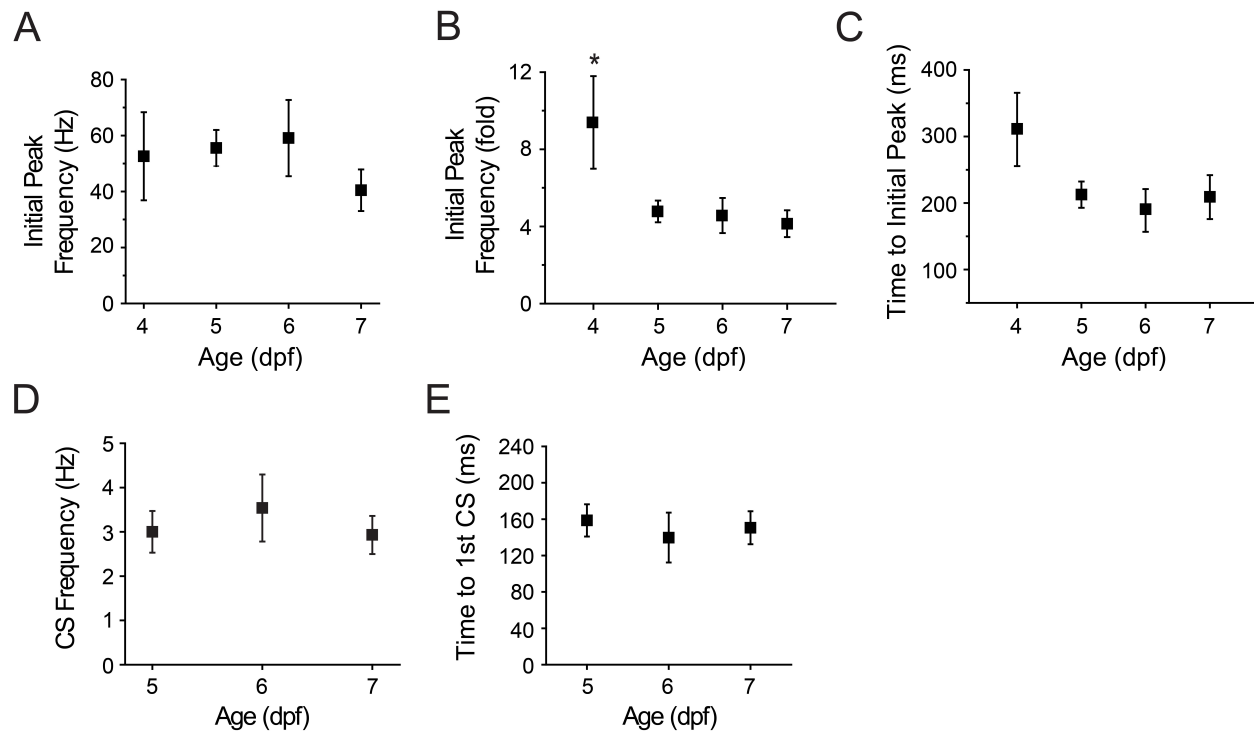


Figure 2.7 Maturation of afferent pathways conveying visual information to cerebellum.

(A) The graph shows the initial peak in instantaneous simple spike frequency after turning off the LED at different ages (see Fig 2. 5B, inset). Values obtained at 4-7 dpf did not differ significantly (ANOVA: 4-7 dpf, $F(3,35)=0.75$, $p=0.53$, $n=6-14$ cells, 5-11 animals). (B) Initial peak simple spike frequencies evoked by sudden darkness in part A were normalized to the average simple spike frequency measured before turning off the LED and plotted versus age. The fold-change in initial peak frequency was significantly higher at 4 dpf than on subsequent days (*, ANOVA: 4-7 dpf, $F(3,35)=4.36$, $p=0.01$, followed by Tukey's post-hoc test: $p<0.05$, $n=6-14$ cells, 5-11 animals). (C) The latency between turning off the LED and the initial peak in simple spike frequency has been plotted versus age. The latency decreased from 311 ± 55 ms at 4 dpf to 212 ± 19 ms at 5 dpf, 189 ± 32 ms at 6 dpf and 209 ± 33 ms at 7 dpf ($n=6, 14, 9$ and 11 cells at 4, 5, 6 and 7 dpf, respectively, 5-11 animals) (Spearman's rank correlation, $r=-0.8$). (D) The graph shows the complex spike frequency measured in the first 500 ms after turning off the LED at 5-7 dpf ($n=13-28$ trials from 8-10 cells, 5-9 animals). Values did not differ significantly. (E) The graph shows the latency between turning off the LED and the first complex spike at 5-7 dpf. Values did not differ significantly ($n=9-24$ trials from 8-10 cells, 5-9 animals). Trials in which sudden darkness did not evoke complex spikes within 500 ms post-stimulation were excluded from the analysis.

Chapter 3

Hyperexcitability induced by infant-onset SCA13 mutation leads to rapid dendritic degeneration

Introduction

Spinocerebellar ataxia type 13 (SCA13) is an autosomal dominant disease caused by mutations in the *KCNC3* gene (Waters et al., 2006). Three causative mutations have been identified in human *KCNC3*: R420H, R423H and F448L (Table 1.1 and Fig 1.1). Depending on the mutation, SCA13 emerges either during infancy or adulthood. There is a very strong genotype to phenotype correlation between the mutations and the types of SCA13, and thus the distinct clinical forms do not result from different genetic background. The infant-onset form of SCA13 is caused by either R423H or F448L, and results in motor delay, persistent motor deficits, and maldevelopment of cerebellum. The adult-onset form, caused by R420H, leads to progressive cerebellar degeneration and progressive ataxia (Waters et al., 2006; Figueroa et al., 2010).

The *KCNC3* gene encodes the voltage-gated potassium channel 3.3 ($K_v3.3$). $K_v3.3$ is expressed throughout the brain but within very specific neuronal subpopulations (Chang et al., 2007). It has rather positive-shifted voltage-dependence and fast gating kinetics compared to delayed rectifier potassium channels (Rudy et al., 1999; Rudy and McBain, 2001). These unique and specialized biophysical properties facilitate the recovery of Na_v inactivation, and promote sustained high frequency spiking in neurons, including cerebellar Purkinje cells (Raman and Bean, 1997; Khaliq et al., 2003; Akemann and Knopfel, 2006). Purkinje cells are the sole output neurons in the mammalian cerebellar cortex, and play significant roles in integrating sensory information and in regulating motor outputs (reviewed by Ito, 2002a, 2002b and 2006). They are spontaneously active neurons that generate action potentials without external inputs. Upon synaptic activation from climbing fibers, Purkinje cells generate a second type of action potential called complex spikes. Complex spikes have a more complex waveform compared to the

spontaneous simple spikes. The interaction between simple spikes and complex spikes shapes Purkinje cell output, which in turn modulates motor function. Previous studies have shown that both types of spikes require proper $K_v3.3$ function, and that mice lacking $K_v3.3$ show deficits not only at cellular level but also at behavioral level (Hurlock et al., 2008).

Given the importance of $K_v3.3$ in regulating cell excitability and in controlling the pattern of action potential firing, we hypothesize that $K_v3.3$ mutations cause cell degeneration in SCA13 by altering electrical properties of the cell. Abnormal cell excitability is not uncommon in neurodegenerative diseases (Bae et al 2013; Chopra and Shakkottai, 2014). However, it is inconclusive whether its presence is the up-stream cause of degeneration or merely a downstream side effect. The idea that altered cell excitability can be the sole original cause has not been established. Two characteristics of SCA13 make the disease ideal to test the idea: 1) SCA13 is caused by mutations in a single gene that encodes an ion channel critical to excitability, and 2) SCA13 has little to no correlation to genetic backgrounds (Waters et al., 2006; Figueroa et al., 2010). These features provide advantages in establishing the causal relationship between cell excitability and neuronal degeneration.

Zebrafish has gained much popularity in the field of neurodevelopmental research in the past years. Several aspects make this model advantageous, including ease in genetic manipulation, rapid development outside the mother's body, and optical transparency during early development. These features allow experimental designs that are often very difficult or impractical in mammalian systems, such as *in vivo* imaging and electrophysiology in developing animals. It has been shown that zebrafish and mammalian cerebella are highly conserved in terms of neuronal types and anatomy (Hashimoto and Hibi, 2012), and we recently reported that the functional properties of zebrafish Purkinje cells are very similar to their mammalian

counterparts, including electrical activities, maturation process and types of ion channels on plasma membrane (Hsieh et al., 2014). Furthermore, Mock et al (2010) showed that zebrafish K_v3 has up to 82% identity in amino acid sequence to human ortholog, and they share the same biophysical and pharmacological properties: positively shifted gating, fast activation and deactivation and high TEA sensitivity.

Here, we characterized the biophysical properties of SCA13 mutations in zebrafish $K_v3.3$. R335H (zR3Ha), R338H (zR4Hi) and F363L (zFLi) are the three corresponding SCA13 mutations to those in the human $K_v3.3$ (R420H, R423H and F448L respectively; Table 1.1). Previous studies have shown that R420H (hR3Ha) is a dominant negative mutation that cannot form functional channels on its own (Waters et al., 2006). R423H (hR4Hi) shares similar characteristic, although a report has shown that when overexpressed at extreme level it generates a small amount of ionic current in *Xenopus* oocytes (Figuroa et al., 2010; Minassian et al 2012). In contrast, F448L (hFLi) mutant subunits form functional homotetramers showing negatively shifted voltage-dependence in gating. Minassian et al (2012) reported that this gating modification is a dominant phenotype as the hFLi-wildtype heterotetramers had shifted voltage-dependence in channel opening. They also showed that hR4Hi-wildtype heterotetramers shared the same shift, but not hR3Ha-wildtype. We expressed the zebrafish SCA13 mutations in *Xenopus* oocytes and tested if the biophysical properties are conserved compared to their human counterparts. We found that zR3Ha and zR4Hi are dominant negative mutations as their human counterparts, and zFLi and zR4Hi shifted the voltage-dependence of wildtype subunits in comparable amplitude as previously reported. We concluded that biophysical effects of SCA13 mutations are conserved in zebrafish $K_v3.3$.

In the light of these findings, we employed a formerly described zebrafish model to further investigate the functional consequences of SCA13 mutations in Purkinje cells *in vivo* during cerebellar development (Hsieh et al., 2014; see also Chapter 2). We particularly focused on the comparison between zR3Ha and zR4Hi. Both of them are nonfunctional subunits that show strong dominant negative effects on wildtype current level. Yet, the former leads to adult-onset SCA13 and the latter results in infant-onset form. The only major difference between the two is that zR4Hi, in addition to being a dominant negative mutation, is also a gating modifier when co-expressed with wildtype subunits. zR3Ha and zR4Hi were expressed in zebrafish Purkinje cells *in vivo* through DNA microinjection. We performed electrophysiological recordings from mutant-expressing cells in awake animal at various time points in the first week post-fertilization, and described the progression of functional effects caused by these mutations. We found that zR3Ha had little impact on the spontaneous firing behaviors during Purkinje cell maturation. However, it affected significantly the response of cells to changes in synaptic input caused by sudden darkness. In normal Purkinje cells, sudden darkness elicited an immediate increase in firing frequency that decayed smoothly over ten of seconds. In contrast, zR3Ha-expressing cells failed to sustain elevated firing after sudden darkness and showed intermittent silent periods during the recovery phase. This is reminiscent of results reported by Issa et al (2011), who found that hR3Ha compromised the high frequency firing behavior of primary motor neurons in zebrafish. When the membrane was depolarized, control motor neurons showed sustained high frequency firing throughout the entire depolarizing period. In contrast, mutant-expressing neurons were unable to sustain action potentials after an initial burst of spikes. In addition, when the cells were excited by current injection or by synaptic activation induced by a sudden light change, hR3Ha-expressing cells showed significantly lower firing frequency

compared to normal motor neurons. In other words, the hR3Ha decreased excitability in these neurons. Taken together with our results, these observations suggest that the functional impact of the adult-onset zR3Ha mutation is revealed only when the cells fire at higher frequencies.

On the other hand, zR4Hi, the infant-onset SCA13 mutation showed drastic effects on spontaneous tonic firing. It caused hyperexcitability and dendritic degeneration in developing Purkinje cells. The emergence and progression of the abnormal electrical activity was temporally well correlated with the onset of morphological deterioration. In addition, pharmacologically suppressing hyperexcitability by agonizing small conductance Ca^{2+} -activated potassium channels (SK channels) either partially rescued or delayed the degeneration. These findings strongly suggested that there is a causal relationship between altered excitability and cell degeneration, and that changing excitability alone is sufficient to trigger pathways that lead to neuronal degeneration. We concluded that SCA13 is a great example to study the causal relationship between excitability and neuronal death, and that zebrafish is a promising model to investigate the etiology of SCA13.

Materials and Methods

Animal Maintenance

An unpigmented zebrafish strain, Tüpfel long fin nacre (TLN), and a previously described transgenic line, la118Tg:Tg(aldoca:gap43-Venus), were housed in the University of California, Los Angeles (UCLA) Zebrafish Core Facility at 28°C using a 14 h/10 h light/dark cycle. The TLN fish was used for imaging experiments, and the aldoca:gap43-Venus line was used for electrophysiology experiments. This transgenic line was previously generated in our lab (Hsieh et al., 2014) and showed Purkinje-cell specific expression of gap43-Venus, a membrane

tethered yellow fluorescent protein. Adults were bred to obtain embryos. Starting at 5 days post-fertilization, larvae were fed brine shrimp powder twice daily. Animal procedures were approved by the Chancellor's Animal Research Committee at UCLA.

RNA preparation and K_v3.3 expression in *Xenopus* oocytes

Zebrafish *kcnc3a* cDNA was previously cloned into the Bluescript vector (Waters et al., 2006). SCA13 mutations (zR3Ha, zR4Hi, and zFLi) were introduced using the QuikChange mutagenesis kit. Plasmid DNAs were then linearized and transcribed by mMessage mMachine T7 Ultra kit (Ambion). *In vitro* transcribed RNAs were injected into *Xenopus* oocytes using standard methods (Timpe et al., 1988; Papazian et al., 1991). The procedure of surgery to harvest oocytes from *Xenopus laevis* was approved by the Chancellor's Animal Research Committee at UCLA. Injected oocytes were kept at 18°C for 1-2 days before electrophysiological experiments.

Expressing exogenous K_v3.3 in zebrafish cerebellar Purkinje cells

Wildtype and mutant K_v3.3 DNA (aldoca-K_v3.3-P2A-mCherry) were subcloned into pMiniTol2 vector (Addgene) by Brandon Brown using the In-Fusion cloning kit (Clontech). The *aldolase* Ca promoter (aldoca) was used to drive cell-type specific expression in cerebellar Purkinje cells (Brochu et al., 1990; Tanabe et al., 2010). The 2A viral sequence generates two separate proteins from one message and has been shown effective in many biological model systems, including zebrafish (Ryan et al., 1991; reviewed by Szymczak and Vignali, 2005; de Felipe et al., 2006; Kim et al., 2011). We employed the P2A sequence here to separate K_v3.3 and mCherry during protein translation. This experimental design is more advantageous than the common fusion protein method in that it allows the fluorescent marker to label cell morphology

independently, and thus eliminates the potential bias caused by the distribution pattern of $K_v3.3$ in cells. To characterize the impact of exogenous $K_v3.3$ on cell morphology and electrical activity, plasmid DNA containing either wildtype or mutant $K_v3.3$ was injected into single-cell staged zebrafish embryos. The expression was screened between 3.5 and 5 days post-fertilization (dpf). Electrophysiological recording and confocal imaging were only performed between 3.5 and 8 dpf.

***In vivo* confocal imaging**

pMiniTol2 plasmid DNA containing either WT-EGFP or zR4Hi-P2A-mCherry was expressed in zebrafish cerebellar Purkinje cells under the control of *aldoca* promoter. The progression of morphological development and degeneration was characterized by confocal imaging between 4 and 6 dpf. Zebrafish were embedded in 1% agarose with a dorsal side up orientation. Optical slices (1 micron) were acquired using an Olympus Fluoview FV300 laser scanning confocal microscope. Each fish was imaged on several consecutive days to follow the morphological changes from the same group of cells.

Two-electrode voltage clamping experiments in *Xenopus* oocytes

Ionic currents were recorded at room temperature (20-22°C) using a Warner OC-725C two-electrode voltage clamp. Electrodes were filled with 3 M KCl and had resistances of 0.3-1.0 MΩ. During electrophysiological recording, oocytes were bathed in 85 mM NaCl, 4 mM KCl, 1.8 mM CaCl₂, 10 mM HEPES, pH 7.2. To quantify the voltage-dependence of channel activation, tail currents were recorded. In these experiments, 85 mM NaCl plus 4 mM KCl was replaced by 89 mM RbCl. Rb⁺ increases tail current amplitude by slowing channel deactivation,

which makes the measurement easier (Swenson & Armstrong, 1981). Tail current amplitudes were then normalized by the maximum value obtained in the experiment and plotted versus voltage. Data were fitted with a single Boltzmann function, and voltage-dependence of the channel was determined by the midpoint potential ($V_{1/2}$) and slope factor of the function. Pulse protocols were generated and data were acquired using pClamp software (Axon Instruments). Data were sampled at 10 kHz and filtered at 2 kHz. Linear capacitive and leak currents were subtracted using a P/-4 protocol (Bezanilla and Armstrong, 1977).

***In situ* electrophysiology in zebrafish cerebellum**

Larval zebrafish between 3.5 and 8 dpf were anesthetized with medical grade 0.02% MS222 (Western Chemical) for ~10 s, then glued dorsal side up onto coverslips in a recording chamber. The chamber was filled with external solution containing (in mM): 134 NaCl, 2.9 KCl, 2.1 CaCl₂, 1.2 MgCl₂, 10 HEPES, and 10 glucose, pH 7.5. Curare (10 μ M) was added to paralyze the animals. Skin around the head and the skull were gently removed using fine forceps. Electrophysiological recordings were performed in awake animals starting 5–10 minutes after the dissection and were stable for up to 1 hour. All data shown in this study were acquired within 45 minutes after the dissection. At the end of the experiment, zebrafish were euthanized by immersion in 0.2% MS222. Data were acquired in loose patch configuration using a HEKA EPC10 patch clamp amplifier and Pulse software (HEKA Elektronik). Borosilicate pipettes (7–12 M Ω , World Precision 1B150F-4) were filled with external solution. Purkinje cells were visualized under an upright Olympus BX51WI microscope using a 40 \times /0.80 water-immersion lens. Recordings were made from cells in the corpus cerebelli lobe (CCe) of the zebrafish cerebellum. Patch pipettes were advanced toward Purkinje cells using a motorized

micromanipulator from the rostral side at an angle of 30° relative to the horizontal plane. Seal resistances ranged from 20 MΩ to 200 MΩ. Experiments were performed at room temperature (22–25°C) with the ambient and microscope lights turned off. Electrical activity was recorded in voltage clamp mode at 0 mV. Data were acquired at 20 kHz and filtered at 3 kHz.

Sudden-darkness stimulation

A 1W, 6500K white LED light source (Thorlabs) was installed on the microscope to illuminate the preparation through the halogen light pathway. A white LED was chosen to avoid possible color-dependent variations in Purkinje cell responses. Animals were light adapted for 2 min before the LED was turned off. In all experiments, light adaptation was performed using the minimum LED intensity that evoked consistent Purkinje cell responses. The power of the LED was controlled by the HEKA EPC10 amplifier. Switching the LED on and off was time-locked with electrophysiological recordings. Purkinje cell activity was recorded for 10 s before and 40 s after the LED was turned off. To avoid over stimulating the visual system, recordings were made from one Purkinje cell per animal. Each Purkinje cell was subjected to 1–4 trials, with an inter-trial interval of at least 2 minutes.

Data analysis

Electrophysiological data were analyzed with Clampfit 10.2 and 10.4 (Molecular Devices). Data acquired by HEKA EPC10 amplifier were imported into Igor 6.2 (WaveMetrics) and converted to Clampfit compatible format for analysis. The regularity of spontaneous tonic firing was quantified by determining the coefficient of variation of adjacent intervals (CV2)

defined as $\frac{2}{n} \sum_1^n \frac{|I_{i+1} - I_i|}{I_{i+1} + I_i}$, where I is interspike interval in ms. CV2 is preferable to the conventional coefficient of variation (CV, standard deviation/mean) for data recorded on a short time scale (Walter et al., 2006; Wulff et al., 2009). Data are provided as mean \pm SEM. Statistical significance was assessed using Student's t-test or ANOVA. Excel 2011 (Microsoft) and Origin 8 (OriginLab) were used to perform statistical testing. Adobe Illustrator (Adobe) was used to prepare figures.

Results

Adult-onset SCA13 mutation shows strong dominant-negative effect

It was previously shown that the adult-onset SCA13 mutation, hR3Ha cannot form functional channels in *Xenopus* oocytes when expressed on its own, but is able to reduce current amplitude when co-expressed with wild-type subunits (Waters et al., 2006). In a separate study by Minassian et al (2012), strong evidence showed that incorporation of one mutant subunit in a channel tetramer does not affect its function, but the existence of two or more subunits completely abolishes it.

We tested whether these functional effects are conserved in the zebrafish mutant subunit, zR3Ha, the corresponding mutation to hR3Ha in human $K_v3.3$. Wild-type and zR3Ha RNA were expressed in *Xenopus* oocytes. Representative current traces obtained after expressing wild-type or mutant $K_v3.3$ are shown in Fig 3.1A and B. Similar to its human $K_v3.3$ counterpart, zR3Ha RNA did not generate functional channels (Fig 3.1B). However, when co-expressed with wild-type RNA, it decreased the wild-type current amplitude in a dose-dependent manner (Fig 3.1C-D). This argues strongly that the wild-type and the mutant subunits can co-assemble and form

heterotetramers. It is important to note that the ratio represents the relative RNA amount injected and not the stoichiometry of channel tetramers.

To investigate the stoichiometry of the effect of zR3Ha on channel function, we compared the amplitude of current reduction to that predicted by the binomial distribution at various ratios. The binomial distribution predicts the fraction of every tetrameric subunit combination. We assumed that the wild-type and mutant subunits can co-assemble randomly with no discrimination and that the incorporation of mutant subunits does not affect single channel conductance. Another assumption is that the relationship between RNA and protein levels is the same for mutant and wild type proteins, which may not be the case if the proteins differ in stability. Under these assumptions, our experimental data are most compatible with the predication of the binomial distribution for the hypothesis that the presence of 2 or more mutant subunits abolishes channel activity (Fig 3.1D). In this scenario, a heterotetramer channel with 3:1 wild-type to zR3Ha stoichiometric ratio is functional, but channels with more than one mutant subunit are not. This is consistent with that reported by Minassian et al (2012) showing the incorporation of one hR3Ha subunit in a channel does not abolish its activity. We conclude that the biophysical properties and functional consequences of hR3Ha are conserved in zR3Ha.

Infant-onset SCA13 mutations modify channel gating

In humans, both hFLi and hR4Hi lead to the infant-onset form of SCA13. hFLi is a dominant gain-of-function mutation that negatively shifts the voltage-dependence of channel activation (Waters et al., 2006; Figueroa et al., 2010; Minassian et al., 2012). hR4Hi, similar to hR3Ha that causes adult-onset SCA13, is a dominant negative mutation that reduces wild-type current amplitude when co-expressed in *Xenopus* oocytes. Neither hR4Hi nor hR3Ha can form

functional channels (Waters et al., 2006; Figueroa et al., 2010). Although both arginine-to-histidine mutations mediate dominant negative suppression of current amplitude, hR4Hi dominantly alters the voltage-dependence of channel opening while hR3Ha shows no effects on channel gating (Minassian et al., 2012). In human $K_v3.3$, both infant-onset SCA13 mutations, hFLi and hR4Hi, negatively shift the voltage-dependence of the channel activation.

To see if this negative shift is conserved in the zebrafish $K_v3.3$ mutations, we investigated the properties of zFLi and zR4Hi in *Xenopus* oocytes. These mutations correspond to hFLi and hR4Hi in human $K_v3.3$ respectively (Table 1.1). Representative traces recorded from oocytes expressing zFLi RNA are shown in Fig 3.2A. The currents were elicited by stepping from a holding potential at -90 mV to various test voltages that ranged between -60 and +60 mV. We analyzed the activation of zFLi channels, and found a -7.6 mV shift in voltage dependence compared to wild-type homotetrameric channels (Fig 3.2B). This value is comparable to the shift caused by hFLi mutation (Waters et al., 2006).

In contrast to zFLi subunits that form functional homotetrameric channels, zR4Hi mutant subunits failed to form functional channels efficiently when expressed alone. We observed no activity when the amount of RNA injected is equivalent to that of wild type (data not shown), but upon injecting RNA in 20-fold excess, a small current is evident. This suggests that at extremely high (non-physiological) subunit concentrations, zR4Hi can form functional channels, but this is an extremely inefficient process. This characteristic is similar to their corresponding mutation in human $K_v3.3$ (Fig 3.3A; Figueroa et al., 2010; Minassian et al., 2012). When co-expressed with wild-type subunits, zR4Hi significantly reduced wild-type current amplitude (Fig 3.3B-C) by ~70% at a 1:1 ratio. The amplitude of this reduction fits the prediction that it takes 2 or more zR4Hi subunits in a channel to abolish the channel function (Fig 3.1D, blue bars at 1:1 ratio).

Minassian et al (2012) reported the same observation in the human R4H mutation, hR4Hi. Our results suggest that zR3Ha and zR4Hi mutations affect channel function with the same stoichiometry, and this phenomenon is conserved between zebrafish and human K_v3.3 subunits.

We analyzed the voltage-dependence of the reduced wild-type current, and found that it was negatively shifted by -6 mV when the expression ratio was at 1:1, wild-type to zR4Hi (Fig 3.3D). The level of the shift is similar to that caused by hR4Hi (Minassian et al., 2012). Our results suggest that the functional effects of infant-onset SCA13 mutations are conserved between human and zebrafish K_v3.3.

Overexpressing exogenous wild-type K_v3.3 has no effect on Purkinje cell firing

To see if exogenous K_v3.3 conductance has a non-specific effect on the Purkinje cell activity, we overexpressed wild-type K_v3.3 subunits in Purkinje cells through DNA microinjection. A representative trace from a Purkinje cell at 5 dpf shows spontaneous tonic firing at ~6 Hz with several complex spikes (Fig. 3.4A). We analyzed the average frequency and regularity (CV2) of tonic firing and complex spiking frequency in Purkinje cells at 5 dpf. None of the three was significantly affected by the expression of exogenous wild-type K_v3.3 compared to the Purkinje cells in uninjected animals (Fig 3.4B-D). Our results show that overexpressing wild-type K_v3.3 does not significantly alter the firing of cerebellar Purkinje cells, strongly suggesting that any functional consequences in cells expressing mutant subunits is due to the mutations per se.

Adult-onset zR3Ha mutation alters evoked responses but not spontaneous tonic firing

The *aldoca*-zR3Ha-P2A-mCherry plasmid was injected into single-celled zebrafish embryos. The *aldoca* promoter drove specific expression in cerebellar Purkinje cells starting around 3 days post-fertilization (dpf). Fluorescence-guided loose-patch electrophysiology was performed in awake zebrafish between 4 and 8 dpf using a previously described method (Hsieh et al., 2014; see also Chapter 2). A representative trace recorded in a Purkinje cell at 5 dpf is shown in Fig 3.4A. zR3Ha-expressing Purkinje cells generated both simple spikes and complex spikes similar to those recorded from uninjected animals (Fig 2.1). The tonic firing frequency and regularity did not change significantly in the presence of zR3Ha, nor did the complex spike frequency (Fig 3.4B-D). Similar results were observed throughout the first week of development (Fig 3.4E). We conclude that zR3Ha has little effect on the spontaneous tonic firing of cerebellar Purkinje cells when their firing frequency is at basal level.

A previous study by Issa et al (2011) showed that exogenous hR3Ha (equivalent to zR3Ha in zebrafish) reduced the excitability of primary motor neurons in zebrafish *in situ*. The maximum firing frequency was reduced and the capacity to sustain firing was significantly impaired. Interestingly, the degree by which hR3Ha decreases motor neuron excitability depends on the firing frequency. The effect is larger when the cell is firing at high frequency and less dramatic when the cell is firing at a low rate. The impact of hR3Ha becomes statistically significant when the firing frequency exceeds ~20 Hz (Issa et al., 2011). This raises the possibility that zR3Ha shows no effect on basal activities in zebrafish Purkinje cells because these cells fire at a relatively low rate (~9 Hz) under our recording conditions. If so, effects of the mutation on excitability might be revealed if the cells are driven to fire at a high frequency.

To test this hypothesis, we employed a previously described “sudden-darkness” protocol to stimulate Purkinje cells *in vivo* in awake zebrafish (Hsieh et al., 2014). In control Purkinje cells between 5 and 7 dpf, this protocol consistently elicited a ~4-fold increase in simple spike frequency within 300 ms post-stimulation that gradually decayed over tens of seconds (Fig 2.6). Here, we compared the responses of control and zR3Ha-expressing Purkinje cells to sudden darkness at 5 dpf (Fig 3.5). Both control and zR3Ha-expressing cells showed an increase in simple spike frequency after the light was turned off. The increase in firing frequency was similar (4.6- and 4-fold for control and zR3Ha-expressing cells respectively). Interestingly, while the initial frequency elevation was minimally affected by zR3Ha, the mutation induced an oscillating firing pattern during the decay phase, which was not seen in the control Purkinje cells. During the oscillation, the firing frequency decreased temporarily and then rebounded. The fact that this pattern is seen in the averaged data from multiple trials and cells suggest this phenotype is an authentic response of the cells, and not merely a result of experimental variation. The oscillations occurred approximately every 5 seconds. In addition, while the spike frequency of control cells stayed stable around baseline after the decay phase, the frequency of zR3Ha-expressing cells fell lower than baseline several times especially during the inter-burst intervals. This drop in frequency sometimes fell close to 0. These intermittent silent periods suggest that zR3Ha-expressing cells fail to sustain the action potentials during prolonged high frequency firing. This phenomenon is reminiscent of that reported by Issa et al (2011) in which hR3Ha impaired sustained high frequency firing in primary motor neurons. Taken together, while zR3Ha had limited effects on spontaneous tonic firing and basal complex-spike frequency, it reduced excitability when the cells were stimulated to fire at high frequency. These results

indicate that the dominant-negative zR3Ha mutant exerts its functional impact on cell excitability in a frequency-dependent manner.

Infant-onset mutation zR4Hi induces hyperexcitability and cell degeneration

To investigate the functional effects of infant-onset mutations *in vivo*, we expressed zR4Hi and mCherry in developing Purkinje cells using plasmid DNA containing aldoca-zR4Hi-P2A-mCherry through DNA microinjection. Aldoca promoter drives Purkinje-cell specific expression and the 2A viral sequence allows the separation of zR4Hi and mCherry during protein translation. This approach is more advantageous than the fusion protein method in that mCherry can freely diffuse in the cell and label the morphology more accurately without being biased by the distribution of zR4Hi subunits. In these experiments, we excluded zFLi, because it can form functional channels without co-assembling with wild type subunits, resulting in channels with significantly left-shifted channel activation compared to zFLi/wild-type heterotetrameric channels. As a result, overexpressing zFLi is likely to silence neuronal firing. In contrast, in human SCA13, mutant and wild type subunits are present in equal dosage, promoting the formation of heterotetrameric channels and limiting the number of mutant homotetramers. zR4Hi does not have this complication since it is a non-functional subunit that must co-assemble with wild-type subunits to exert its effect, limiting the size of the left-shift in activation to a modest ~6 mV (Fig 3.3D). Thus, we only focused on zR4Hi in this part of the study and investigated its functional effect *in vivo*.

Purkinje cells expressing zR4Hi subunits showed morphological degeneration starting at ~4 dpf, and lost their dendritic arbors between 5 and 6 dpf (Fig 3.6). In several instances, the cells identified at 4 dpf disappeared completely by 5 or 6 dpf. The disappearance is likely due to

cell death and not to loss of mCherry expression because the expression driven by aldoca promoter is constitutively on after 3 dpf. This degeneration was not seen in control Purkinje cells or in cells expressing the adult-onset zR3Ha mutation or in cells expressing exogenous wild-type subunits.

Furthermore, we observed that abnormal firing preceded the emergence of morphological degeneration. Purkinje cells expressing zR4Hi subunits showed spontaneous tonic firing at 3.75 dpf. The firing pattern was regular, and the majority of cells were firing at 1-2 Hz. This frequency is similar to that control cells from uninjected animals at 3.75 dpf (Fig 3.7 A-B). Starting at 4 dpf, zR4Hi cells showed high frequency spiking, and this elevated firing activity turned into intermittent episodes of high frequency bursting in the following 6 hours by 4.25 dpf (Fig 3.7A). The frequency in the burst went up to ~50 Hz, which is about 9-fold higher than the average rate (5.4 Hz) from control cells at this age (Fig 2.1). We also recorded the activity of zR4Hi cells at 5 and 7 dpf. However, only two cells showed action potentials and all the rest were completely silent (Data not shown). This indicates that the period of hyperexcitability is followed by hypoexcitability and silence that is temporally correlated with morphological degeneration. None of the cells recorded after 4.25 dpf showed extensive dendritic arbors.

We followed the progression of this abnormal electrical activity, from normal to a hyperexcitable phase to silence, every 6 hours starting at 3.5 dpf. While both control and zR4Hi-expressing cells showed increases in frequency over time, the progression of the latter was much more dramatic. The average firing rate of zR4Hi cells was 0.3 Hz at 3.5 dpf and 20.8 Hz at 4.25 dpf (Fig 3.7C). In contrast to this 60-fold change, the frequency increased only 6-fold in control cells (from uninjected animals) over the same time span, from 0.7 Hz at 3.5 dpf to 5 Hz at 4.25 dpf. Furthermore, we noticed that the frequencies recorded from control cells were fairly

consistent. The variation between cells and animals was limited, and the frequencies were distributed in a narrow range. In contrast, the distribution of firing frequencies in zR4Hi cells was significantly wider, ranging from 2.5 to 64 Hz at 4.25 dpf (Fig 3.7C). Compared to control Purkinje cells, zR4Hi-expressing cells showed significantly elevated excitability starting 3.75 - 4 dpf.

Interestingly, the timing of this divergence in firing between non- and zR4Hi-expressing cells coincided nicely with the expression of endogenous wild-type $K_v3.3$ in Purkinje cells (Fig 2.2D and E). This observation is consistent with the idea that zR4Hi subunits need to co-assemble with wild-type subunits to produce dominant negative suppression of current amplitude and to modify gating. Without the presence of wild-type subunits, zR4Hi subunits would be unlikely to affect cell excitability because they form nonfunctional homotetrameric channels. In addition, we also noticed that the onset of abnormal firing in zR4Hi cells (~3.75 dpf) preceded the emergence of morphological deterioration starting at 4 dpf. This suggests that zR4Hi-induced hyperexcitability is upstream to cell degeneration in the pathogenetic pathway.

Mitigating hyperexcitability partially rescues morphological degeneration

To investigate whether hyperexcitability triggers cell degeneration, we counteracted zR4Hi-induced hyperexcitability by pharmacologically activating small conductance Ca^{2+} -activated potassium channels (SK channels). SK channels play important roles in regulating tonic firing in Purkinje cells. Blocking SK channel activity by apamin leads to high frequency firing followed by bursting and silence in Purkinje cells (Womack and Khodakhah, 2003). In contrast, Kasumu et al (2012) showed that agonizing SK channel activity by NS309 significantly reduced tonic firing frequency in Purkinje cells. They also demonstrated that applying NS13001

(another SK channel agonist) improved motor performance in mice with spinocerebellar ataxia type 2. These results suggest that reverting altered excitability in diseased Purkinje cells is sufficient to provide beneficial effects to the phenotype at both the cellular and behavioral levels.

Here, we hypothesize that the SK channel agonist, NS13001, provides protective effects against hyperexcitability-triggered morphological degeneration. We first tested if NS13001 can reduce the frequency of tonic firing in control Purkinje cells in zebrafish. NS13001 was added acutely to the external solution during electrophysiological recordings. Zebrafish at 6 dpf were used in these experiments because our previous study showed that the electrical properties of Purkinje cells are stable and mature at this age (see Chapter 2). We found that 10 μ M NS13001 significantly reduced spontaneous tonic firing frequency by \sim 50% (Fig 3.8A and B). A further reduction was observed when the drug concentration was increased to 20 μ M. Our results suggest that NS13001 can reduce excitability in zebrafish Purkinje cells as in mammalian Purkinje cells.

To see if reducing excitability has protective effects on zR4Hi-induced degeneration, we added 20 μ M NS13001 to the water starting at 3 dpf when Purkinje cells were born. Zebrafish expressing zR4Hi in Purkinje cells were identified and kept in water containing NS13001 through the first week of post-fertilization. The water was changed daily and the SK agonist NS13001 was replenished daily. It is important to note that the efficacy of 20 μ M NS13001 in water is unlikely to be the same as that during electrophysiological recordings. In electrophysiological experiments, the drug has more direct access to the Purkinje cells because the skin around the head and the skull were removed. In contrast, the NS13001 in the water had to enter the circulation system of the zebrafish before it could reach cerebellar Purkinje cells.

In preliminary experiments, we found that adding 20 μ M NS13001 in the water starting at 3 dpf seems to have a protective effect against morphological degeneration in zR4Hi cells during development. Instead of dendritic retraction, the dendrites kept growing in the presence of NS13001 up to 6 dpf (Fig 3.8C), a time most zR4Hi-expressing cells would either have lost their dendrites or have disappeared (Fig 3.6). Nonetheless, NS13001 did not completely prevent or revert the degeneration. We noticed that not all NS13001 treated zR4Hi cells showed dendrites at 6 dpf, and that the rescued dendrites showed fewer branches than that of a normal Purkinje cell at 6 dpf (Fig 3.6 and 3.8C). These preliminary results suggest that suppressing hyperexcitability has beneficial effects on the morphology in zR4Hi-expressing cells.

Discussion

All three causative SCA13 mutations identified are found in *KCNC3* gene that encodes $K_v3.3$ (Waters et al., 2006; Figueroa et al., 2010). $K_v3.3$ has significant roles in regulating the excitability of cerebellar Purkinje cells (reviewed by Joho and Hurlock, 2009). Here, we characterized the biophysical properties of all three mutations in *Xenopus* oocytes, and investigated their effects on excitability in developing Purkinje cells in zebrafish. We found that while the adult-onset mutation exhibits pure dominant negative effect, both of the infant-onset mutations modify activation gating by negatively shifting the voltage dependence of channel opening. The ability to alter gating differentiates the infant-onset mutations from the adult-onset mutation. We also found that infant-onset mutation zR4Hi triggers hyperexcitability and dendritic degeneration while the adult-onset mutation causes hypoexcitability in Purkinje cells when they are driven to fire at high frequencies. The distinct outcomes in excitability are most likely conferred by their differential impact on channel gating. Our findings depict a clear

scheme showing the functional impact of SCA13 mutations, from altered biophysical properties to cellular excitability to neuronal viability. The preliminary experiments on NS13001 rescuing neuronal morphology suggests that hyperexcitability triggers rapid degeneration of Purkinje cells expressing the zR4Hi mutation.

The frequency-dependent effects of adult-onset mutation zR3Ha

Both our results and a previous report by Issa et al (2011) showed that R3Ha decreased neuronal excitability *in vivo*. This phenotype is likely due to the dominant negative nature of R3Ha over endogenous wild-type subunits. Indeed, under whole-cell voltage clamp, Issa et al showed that exogenous hR3Ha subunits significantly reduce outward currents during depolarization in primary motor neurons. Consistent with their finding, our results from two-electrode voltage clamp experiments in *Xenopus* oocytes showed that zR3Ha subunits strongly decrease wild-type current amplitude when co-expressed. Given the importance of $K_v3.3$ activity in facilitating the recovery of Na_v from inactivation during repetitive firing (reviewed by Joho and Hurlock, 2009), it is not surprise that the dominant negative zR3Ha mutation would lead to a decrease in neuronal excitability. In the presence of zR3Ha, the efficacy of endogenous $K_v3.3$ recovering Na_v is compromised, which results in accumulation of Na_v inactivation and in spiking failure. This interpretation is consistent with the finding that zR3Ha suppresses excitability more dramatically when neurons are driven to fire at higher frequencies. From this aspect, the degree of severity of zR3Ha affecting cell function is dependent on how actively the cells are firing. At low frequency, the accumulation of Na_v inactivation is relatively insignificant to the generation of action potential, and the demand for $K_v3.3$ function is low. Under this condition, the effect of zR3Ha is less obvious. However, when the activity level is high, a greater level of $K_v3.3$ function

is required to recover Na_v and to sustain fast repetitive spiking. In this scenario, zR3Ha will have significant functional impact because of its strong dominant negative effect. Thus, the higher the firing frequency is, the more severe the mutant effect will be.

Interestingly, the way zR3Ha compromised cell excitability is reminiscent of that of antiepileptic drugs and local anesthetics, such as carbamazepine, phenytoin, and lidocaine. They are use-dependent drugs that exert functional effects by locking Na_v in the inactivated state and preventing recovery. The accumulation of inactivation then decreases excitability and silences the cell. Although the fundamental mechanisms are different, zR3Ha is behaving like an intrinsic use-dependent drug that has minimal impact at a basal level of activity but has an increasing impact as the level of activity increases. This frequency-dependent nature of zR3Ha efficacy may explain why it has little effect on spontaneous tonic firing, but shows significant impact on the sudden-darkness evoked responses in Purkinje cells.

Gating modifying effect of zR4Hi leads to hyperexcitability

zR3Ha and zR4Hi are located close to one another in the primary sequence of the Kv3.3 protein (Fig 1.1), and both of them show strong dominant negative effect over wild-type subunits. Yet, they result in distinct clinical forms of SCA13. zR3Ha leads to the adult-onset form and zR4Hi causes the infant-onset form. By studying their biophysical properties, we found that while zR3Ha gave a pure dominant negative effect, zR4Hi showed both dominant negative and gating modifying effects. This makes them an ideal pair for investigating the effect of altered gating on the excitability and viability of Purkinje cells.

We presented strong evidence showing that the pure dominant negative mutation, zR3Ha leads to hypoexcitability *in vivo* in Purkinje cells. This is accomplished by its ability to reduce

endogenous $K_v3.3$ activity during high frequency repetitive firing. In contrast, zR4Hi induces significant hyperactivity in Purkinje cell, a mutation dual-wielding dominant negative and gating modification effects. The distinct consequences of the two dominant negative mutations on excitability may directly reflect their differential ability to alter channel gating. While zR3Ha has no effect on the opening of channels, zR4Hi negatively shifts the voltage-dependence of activation when co-assembled with wild-type subunits.

Intuitively speaking, a negatively shifted activation is likely to decrease excitability because Na_v now has to overcome a larger outflowing potassium flux during the generation of action potentials. However, in the vicinity of action potential threshold, the shift caused by zR4Hi increases channel activation by a negligible amount (between -40 and -30 mV in Fig 3.3D). Thus, the shift is unlikely to cause any suppression over the initiation of action potentials. In fact the shift caused by zR4Hi can promote repetitive spiking because $K_v3.3$ conductance is significantly increased at voltages more positive than -20 mV (Fig 3.3D). This increase facilitates cell repolarization and potentially elevates the firing rate. Thus, rather than decreases cell excitability, a modest left shift in activation caused by the presence of zR4Hi mutant subunits can increase it. Although more quantitative experimental design and analysis are needed to address more detailed conclusions, it is plausible that the gating modification conferred by zR4Hi pushes the Purkinje cells onto a distinct path than those expressing zR3Ha.

Interestingly, a previous study by Irie et al (2014) showed that R424H (the corresponding mutation to zR4Hi and hR4Hi in rat $K_v3.3$) causes hypoexcitability in cultured mouse Purkinje cells. At first glance, their results contradict our *in vivo* observation with zR4Hi. Our findings suggest that zR4Hi causes hyperexcitability rather than hypoexcitability in cerebellar Purkinje cells. However, there are differences between the experimental designs that may confer the

contradictory conclusions. First, they used lentivirus to express mutant subunits in the cultured Purkinje cells. They reported an 8.3-fold ratio between the expression of exogenous mutant subunit and the endogenous wild-type subunit. At this ratio, the binomial distribution predicts that over 99.5% of the channel tetramers will have two or more mutant subunits. These channel tetramers are not functional. Thus, the endogenous $K_v3.3$ activity is almost completely compromised by the dominant negative effect of the mutation. In addition, the gating modifying effect of the mutation is likely to be obscured at this extreme expression ratio because only ~0.4% of the channel tetramers will have the 3:1 stoichiometry between wildtype and mutant $K_v3.3$ subunits. Heterotetramers with this stoichiometry are functional channels with altered activation gating. For comparison, in human SCA13, the expression ratio between wild-type and mutant subunits is 1:1, at which the fraction of channels with the same stoichiometry is 25%. Thus, under their experimental conditions, the apparent phenotype of zR4Hi will look like that of zR3Ha, a pure dominant-negative mutation that causes hypoexcitability.

Furthermore, Irie et al (2014) reported a chronic elevation of intracellular Ca^{2+} concentration and significant dendritic degeneration in cultured Purkinje cells expressing mutant $K_v3.3$ subunits. This degeneration could be rescued by the application of ω -agatoxin IVA that blocks P/Q type voltage-gated calcium channel. While this strong evidence suggests the important roles of Ca^{2+} in the process of mutant induced degeneration, it is contradictory to their conclusion that R4Hi induces hypoexcitability. Hypoexcitability is not likely to cause elevated intracellular Ca^{2+} level, nor is it likely to increase P/Q calcium channel activity. In contrast, hyperexcitability can elevate intracellular Ca^{2+} concentration and increase the activity of P/Q channels. The fact that blocking P/Q channels provides protective effects against degeneration suggests a role of hyperexcitability rather than hypoexcitability.

We showed that the progression of altered excitability in zR4Hi-expressing Purkinje cells happened rapidly within 6 to 12 hours (Fig 3.7), from normal firing to high frequency firing to silence. Irie et al followed the changes in excitability every 3 to 4 day after viral infection. With this temporal resolution, it is not impossible that they only captured the very late phase of the progression, the silent phase. Indeed, they reported that ~40% of the mutant-expressing Purkinje cells were not spontaneously active. Taken together, we believe that the distinct conclusion addressed in the two studies is a direct result of different experimental designs.

The emergence of hyperexcitability matches the onset of morphological degeneration

We showed that zR4Hi induced hyperexcitability in developing Purkinje cells. The divergence between zR4Hi-expressing and normal cells occurred between 3.75 and 4 dpf. The timing matches the onset of endogenous Kv3.3 expression (Fig 2.6) and the emergence of excitability in normal Purkinje cells. In other words, once the cells became electrically active, zR4Hi started to affect their function. The progressive impact of zR4Hi increases the tonic firing frequency starting at 3.75-4 dpf, induces a bursting firing pattern at 4.25 dpf, and silences the cells by 5.25 dpf. Interestingly, this rapid progression is accompanied by severe dendritic degeneration starting at 4 dpf, just 6 hours after the emergence of zR4Hi-induced hyperexcitability. Within 2 days by 6 dpf, all the zR4Hi-expressing cells have either significantly lost their dendrites or completely disappeared. The onset and progression of abnormal electrical activity was temporally correlated with morphological deterioration. The fact that changes in excitability seems to precede that of morphology argues strongly for a causal relationship of the two. In addition, when the zR4Hi-induced hyperexcitability was pharmacologically suppressed by SK channel agonist NS13001, the morphological degeneration was partially rescued. Our

findings suggest that zR4Hi-induced hyperexcitability triggers morphological degeneration and likely cell death in developing Purkinje cells.

Although we have demonstrated strong evidence arguing the causal relationship between altered excitability and neuronal degeneration, the underlying mechanism tying the two remains unknown. One possible link is through aberrant Ca^{2+} activity. This is a commonly proposed mechanism in many neurodegenerative diseases (Bezprozvanny, 2009; D'Amelio and Rossini, 2012; Berridge, 2013; Chopra and Shakkottai, 2014; Zaltieri et al., 2015). Indeed, as Irie et al (2014) reported, intracellular Ca^{2+} level is significantly altered by the expression of R4Hi in Purkinje cells, and inhibiting voltage-gated Ca^{2+} channel activity provides beneficial effect against cell degeneration. Further investigation is needed to uncover the roles of Ca^{2+} during neuronal degeneration and in the SCA13 etiology.

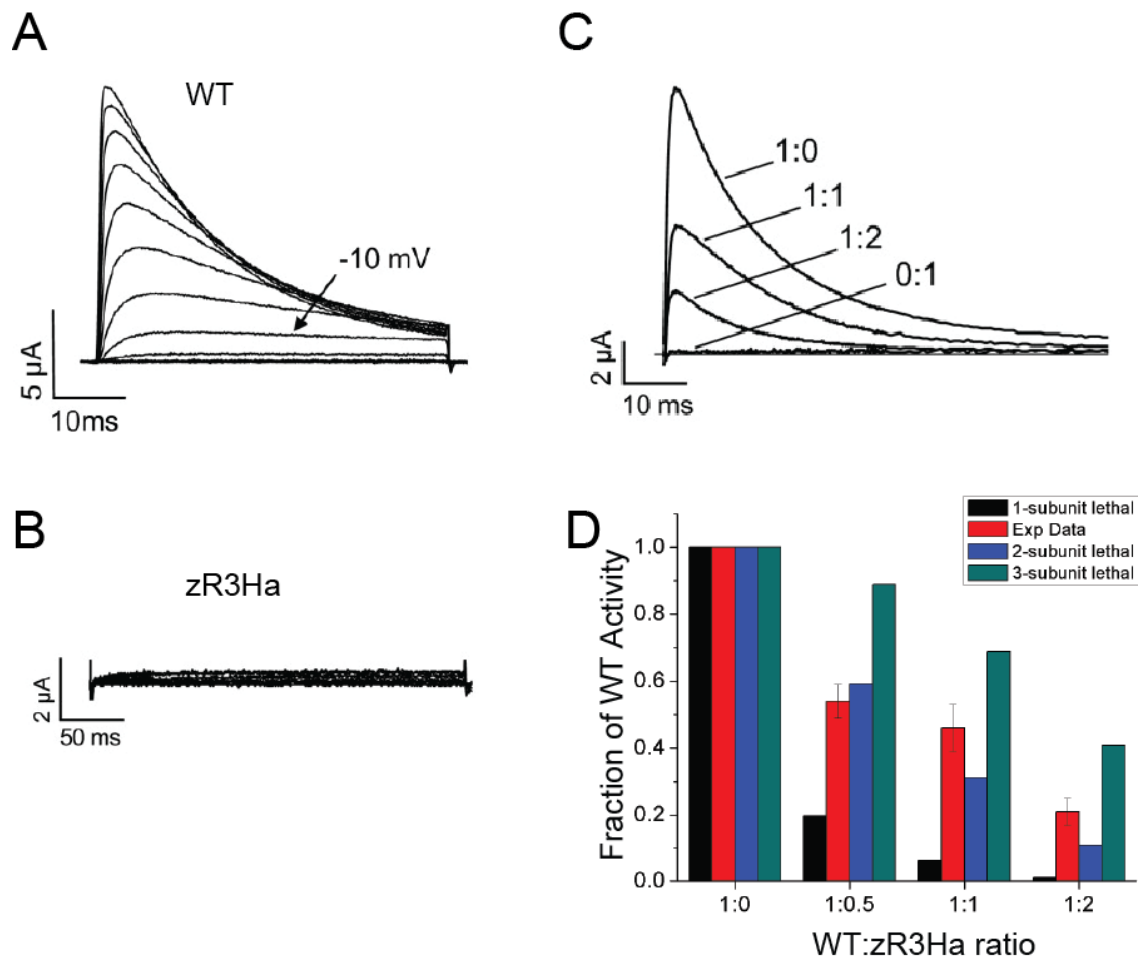


Figure 3.1 zR3Ha shows strong dominant negative effects.

Wildtype (A) and zR3Ha (B) zebrafish $K_v3.3$ were expressed in *Xenopus* oocytes and characterized by two-electrode voltage clamp. Currents were evoked by stepping from -90 mV to voltages ranging from -80 to +60 mV in 10 mV increments. The -10 mV trace in (A) was marked for the comparison to that of zFLi in Fig 3.2A. zR3Ha did not form active channels regardless of the amount of RNA injected. (C) Representative traces from +40 mV at various expression ratios (WT:zR3Ha) were superimposed. (D) Peak current amplitudes at +40 mV were normalized to that of wildtype alone (1:0 ratio). zR3Ha subunits significantly reduced wildtype current amplitude in a dose-dependent manner. (Red bars; $n=7-15$ cells). To investigate the stoichiometry of channels that contribute to the residual currents, the predictions by binomial distribution were also plotted. X-subunit lethal ($x=1$, black bars; $x=2$, blue bars; $x=3$, green bars) shows the theoretical fraction of activity at each ratio in the scenario that incorporating zR3Ha subunits in a channel abolishes its function. Our experimental data (red bars) best fit the 2-subunit lethal hypothesis, suggesting that it requires 2 or more zR3Ha subunits in a channel tetramer to abolish its function.

Figure adapted from Mock et al., 2010.

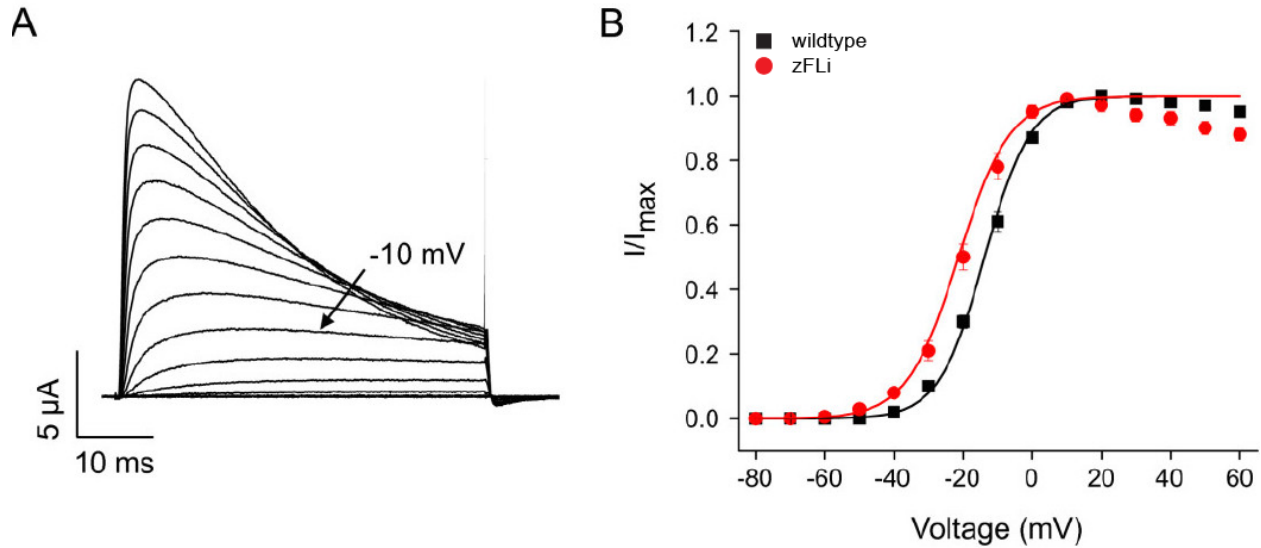


Figure 3.2 zFLi forms functional channels with altered gating properties.

(A) Representative traces recorded from *Xenopus* oocytes expressing zFLi mutant subunits. Currents were elicited by pulsing from -90 mV to voltages from -80 to +60 mV. Trace of -10 mV was marked for comparison to that from wildtype channel (Fig 3.1A). (B) Voltage-dependence of channel activation in wild-type (black) and zFLi (red) channels was calculated from isochronal tail current amplitudes. Test pulses ranged from -80 to +60 mV. Tail currents were recorded by stepping back to -90 mV after a brief 15-ms test pulse. Normalized tail current amplitudes were fitted with single Boltzmann function. The midpoint voltages are -13.8 and -21.4 mV for wildtype and F363L respectively. The slope factors are 6.6 mV for wildtype and 7.4 mV for F363L.

Figure adapted from Mock et al., 2010.

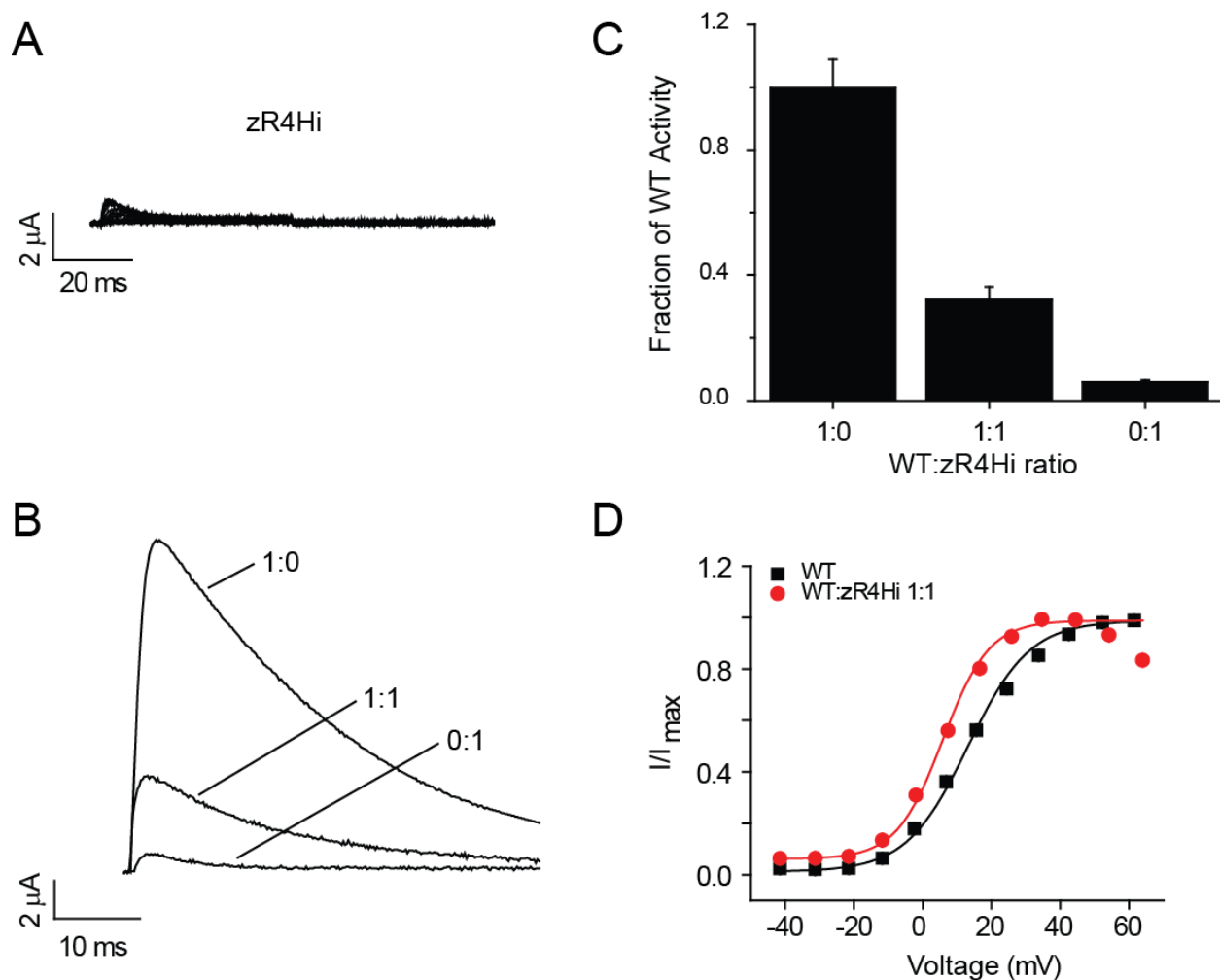


Figure 3.3 zR4Hi causes dominant negative suppression of current amplitude and alters voltage-dependent gating.

(A) Representative traces recorded from *Xenopus* oocytes expressing zR4Hi mutant subunits. Currents were elicited by pulsing from -90 mV to voltages from -80 to +60 mV. The amount of RNA injected in these experiments was 5 ng per oocyte. This was 20 times higher than that used for wild-type or zFLi at 0.25 ng (Fig 3.1A and 3.2A). (B) Representative current traces recorded at +60 mV were shown. Ratios represented the relative RNA amount injected between wild-type and zR4Hi. (C) zR4Hi strongly reduced wild-type current amplitude when co-expressed ($n=3-14$ cells). At 1:1 ratio, the channel activity was 32% of that of wildtype alone (1:0 ratio). (D) Voltage-dependence of activation was determined from the residual current after co-expression of wild-type and zR4Hi at a 1:1 ratio (red circles). Also shown are results from wild-type expressed alone (black squares). Data were fitted with single Boltzmann function. The midpoints were 13 and 7 mV and the slope factors are 11 and 7 mV for wildtype alone and 1:1 ratio respectively ($n=14$ cells for both wildtype and 1:1 ratio).

Experiments and data analysis in this figure were performed by Dr. Meng-Chin Lin.

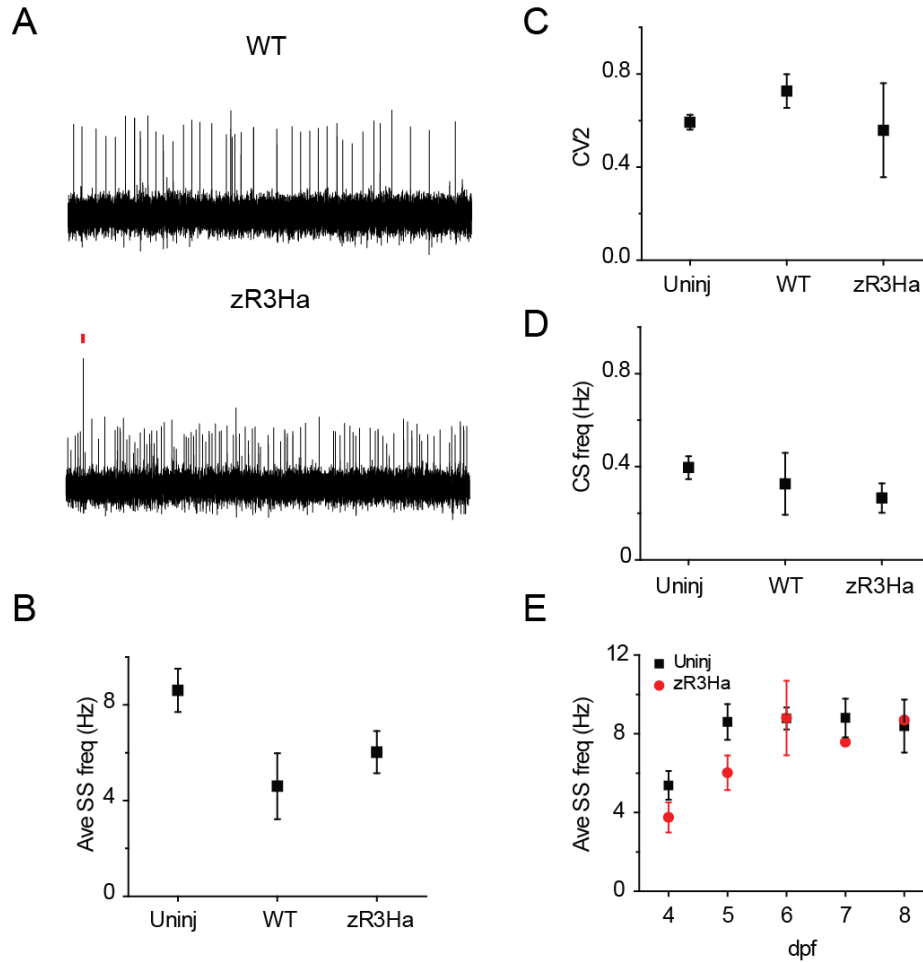


Figure 3.4 zR3Ha has no effect on basal action potential firing in Purkinje cells.

Exogenous zR3Ha and wild-type subunits were expressed in zebrafish cerebellar Purkinje cells through DNA microinjection. “WT” refers to Purkinje cells expressing exogenous wild-type $K_v3.3$ subunits. In these cells, there are both endogenous and exogenous $K_v3.3$ subunits. “Uninj” refer to data recorded from uninjected animals. Purkinje cells in these animals have only endogenous $K_v3.3$ subunits. (A) Representative Purkinje-cell recordings at 5 dpf are shown. Both WT- and zR3Ha-expressing cells generated spontaneous tonic firing pattern. Red mark: complex spike (B) Average tonic firing frequencies at 5 dpf were shown. There was no statistical significance between any of the expression conditions (ANOVA, $p>0.05$, $n=4-29$ cells). (C-D) The regularity of tonic firing (CV2) and the frequency of complex spiking at 5 dpf were analyzed. No significant difference between groups was found (ANOVA, $p>0.05$, $n=3-20$ cells). (E) The average tonic firing frequencies have been plotted against age. Firing frequency in zR3Ha-expressing Purkinje cells increased from 3.8 Hz at 4 dpf to 8.8 Hz at 6 dpf (red circles; $n=4-7$ cells). Firing frequencies measured on 7 and 8 dpf did not differ significantly from 6 dpf (red circles; $n=3$ cells). These values did not differ from that of Purkinje cells from uninjected animals (black squares).

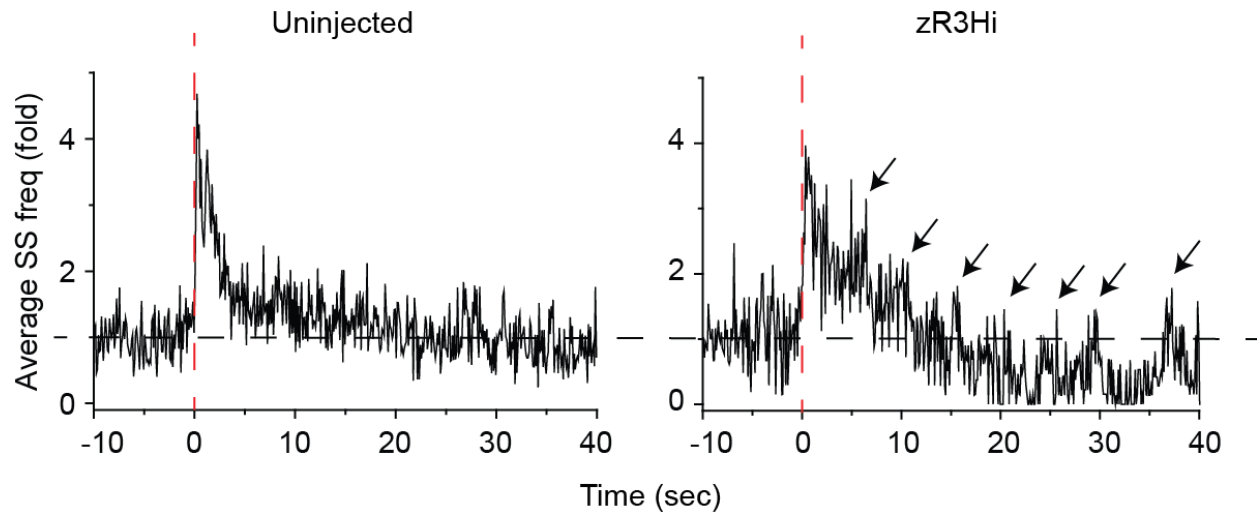


Figure 3.5 zR3Hi induces oscillating firing pattern after sudden-darkness stimulation.

Average responses of Purkinje cells to sudden-darkness were plotted against time (uninjected, $n=8$ trials from 5 cells; R335H $n=8$ trials from 4 cells). The light was turned off at time 0 sec marked with red dashed lines. The baseline activity level was marked with black dashed line. Average simple spike frequency was calculated using 100-ms bin and normalized to the average frequency from -10 to 0 sec. Sudden darkness induced an immediate increase in simple spike frequency that was 4.6-fold in the uninjected animals and 4-fold in the zR3Ha animals. There is no statistical difference between the two. However, after the sudden-darkness stimulation, zR3Ha-expressing cells fired in an oscillating pattern (arrows) during the decay phase that was not present in control cells from uninjected animals. Oscillations were characterized by decreases in firing frequency. In addition, R335H cells showed several periods between time 10 and 40 sec in which the firing frequency was lower than the baseline and close to 0. This was not seen in control Purkinje cells from uninjected animals.

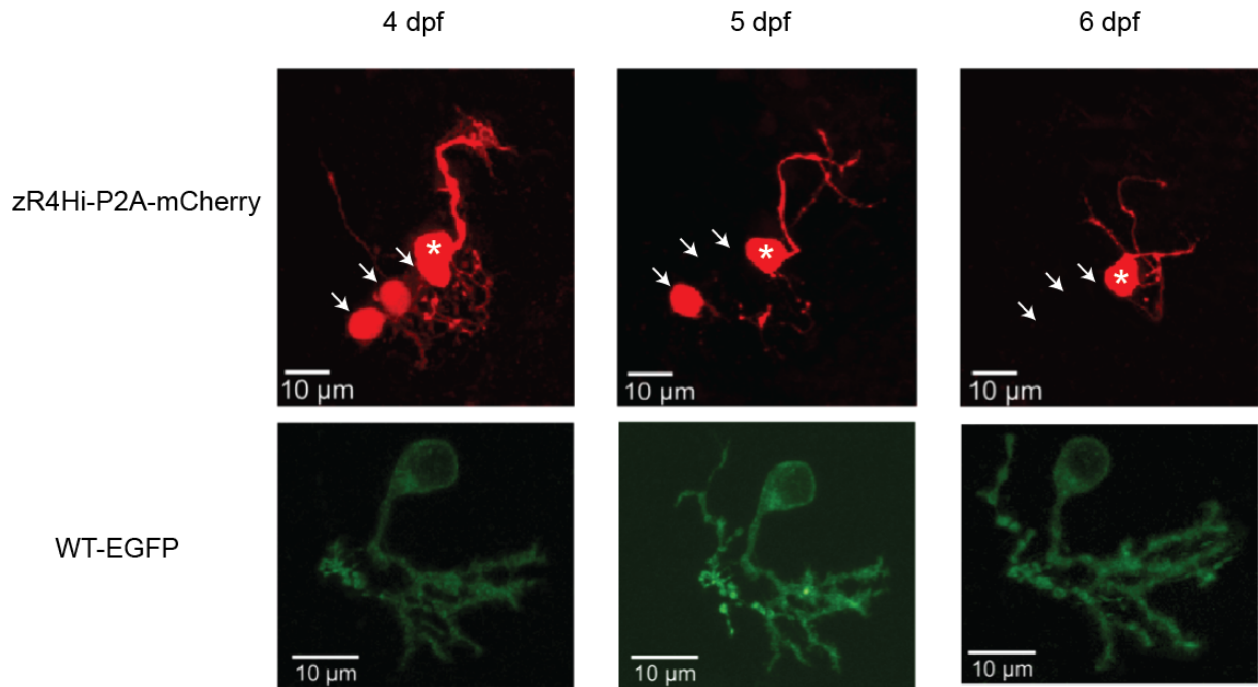


Figure 3.6 zR4Hi triggers rapid dendritic degeneration and cell death in Purkinje cells.

Exogenous zR4Hi (upper panel) and a wildtype Kv3.3-EGFP fusion protein (lower panel) were expressed in Purkinje cells through DNA microinjection. Confocal images in each panel were taken between 4 and 6 dpf from an individual fish. Optical slices were 1 μm . The figure shows a projection of stacked images to encompass the entire cell. Between 4 and 6 dpf, Purkinje cells expressing exogenous WT-EGFP subunit showed significant elaboration of dendritic arbor. In contrast, cells expressing zR4Hi showed dramatic atrophy. Three cells (arrows) expressing zR4Hi were lost within this 48-hour span. The fourth cell (asterisk) showed evident dendritic degeneration.

zR4Hi images were taken by Brittany Ulrich, and WT-EGFP images were by Dr. Fadi Issa.

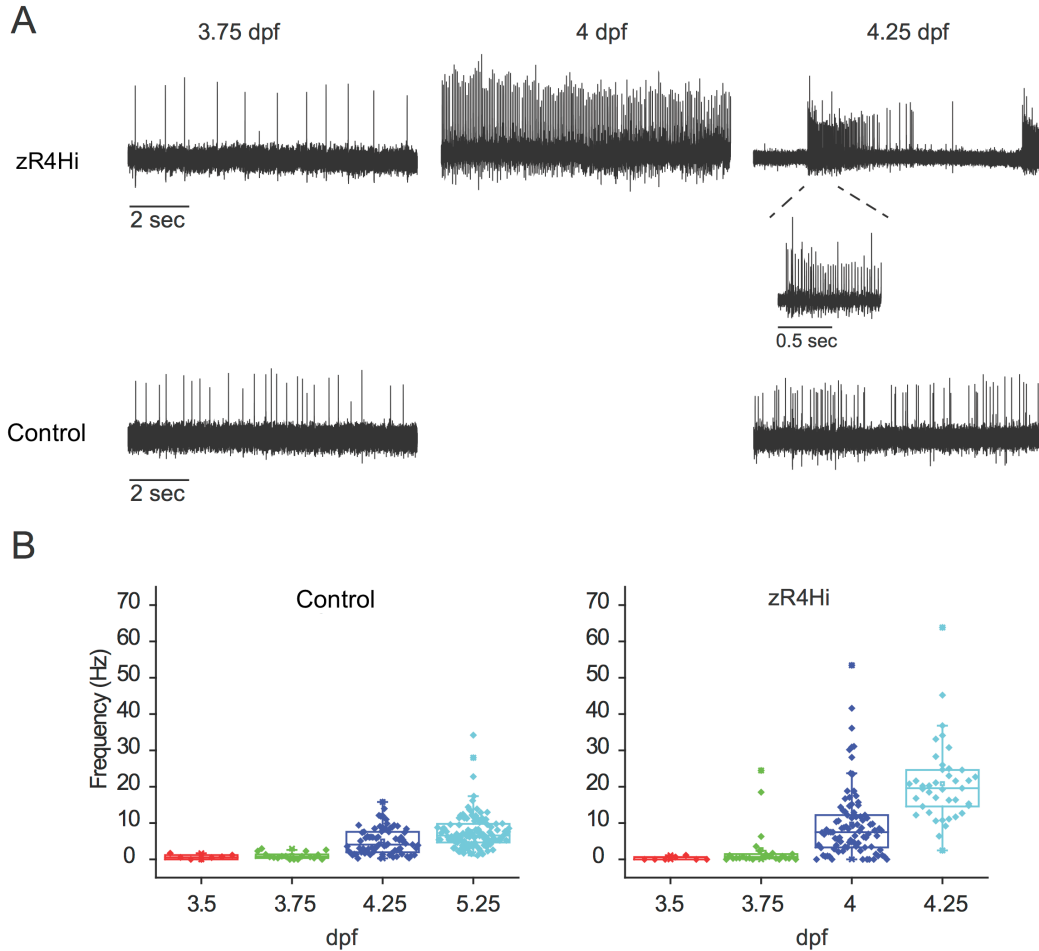


Figure 3.7 zR4Hi induces hyperexcitability in developing Prkinje cells.

(A) Representative *in vivo* loose-patch recordings from Purkinje cells expressing zR4Hi were shown. Traces at different ages were recorded from different animals. The tonic firing frequencies of the shown traces are 1.1 and 17 Hz at 3.75 and 4 dpf respectively. The firing frequency during the first 500 ms of the burst at 4.25 dpf was 48 Hz (expanded trace). (B) Traces recorded from control cells in uninjected animals at the same ages were shown. The tonic frequencies of the shown traces were 2.3 and 6.1 Hz at 3.75 and 4.25 dpf respectively. (C) Average simple spike frequency was calculated from individual 10 s traces and plotted against age. Control Purkinje cells from uninjected animals showed a significant increase in firing frequency from 0.7 Hz at 3.5 dpf to 7.6 Hz at 5.25 dpf (ANOVA, $p < 0.05$, $n = 7-117$ traces from 3-29 cells). A significantly greater increase in firing frequency occurred in zR4Hi-expressing cells, from 0.3 Hz at 3.5 dpf to 20.8 Hz at 4.25 dpf (ANOVA, $p < 0.05$, $n = 7-92$ traces from 3-20 cells). The onset of zR4Hi-induced hyperactivity occurred around 3.75 dpf when the distribution of frequencies started to differ significantly from that of control Purkinje cells from uninjected animals (Student's *t* test, $p < 0.05$). This difference stayed significant at 4.25 dpf. The comparison between normal and mutant expressing cells at later ages was not available because almost all the zR4Hi cells were electrically inactive after 4.25 dpf.

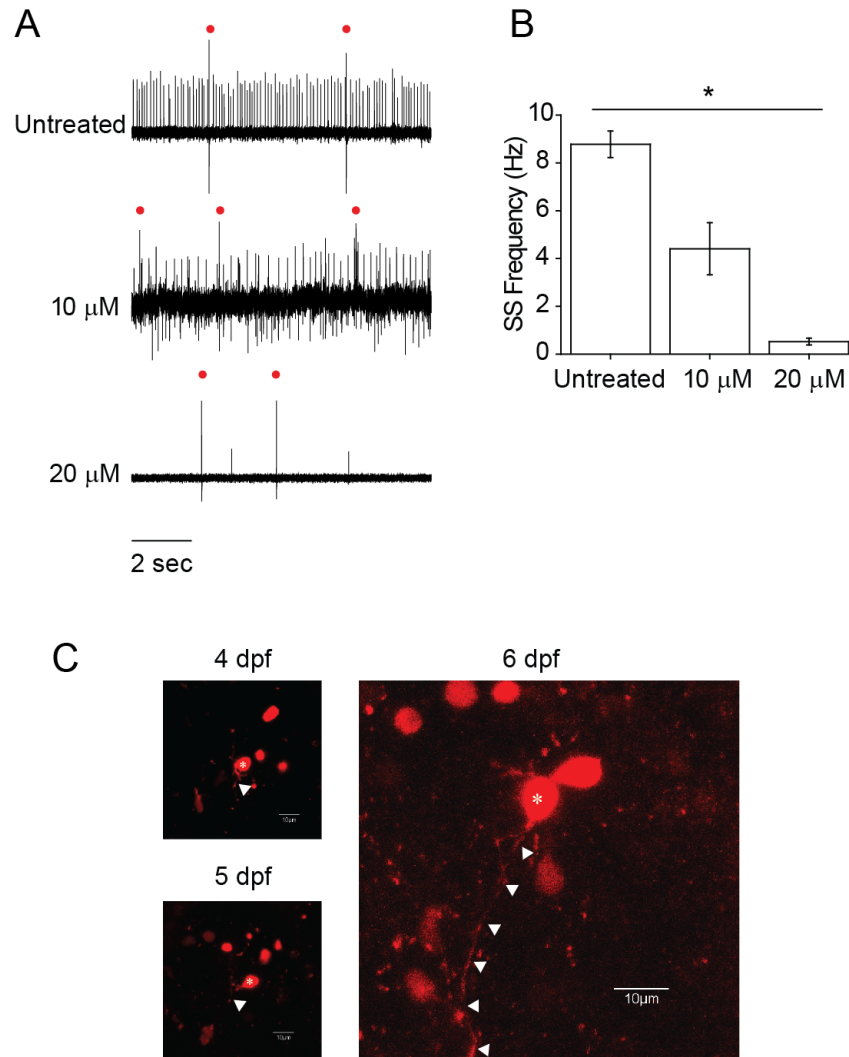


Fig 3.8 SK channel agonist NS13001 reduces tonic firing frequency and provides protective effect against zR4Hi-induced dendritic degeneration.

(A) Representative traces recorded at 6 dpf from three control Purkinje cells are shown. The cell treated with 20 μ M NS13001 showed significantly lower tonic firing frequency than the cell treated with 10 μ M. Complex spikes are labeled with red marks. (B) Average tonic frequencies have been plotted against NS13001 concentration. The frequencies are 8.8 Hz, 4.4 Hz, and 0.5 Hz for untreated, 10 μ M, and 20 μ M respectively ($n=5-31$ cells). NS13001 significantly decreased tonic frequency in Purkinje cells in a dose-dependent manner (ANOVA, $p<0.05$ followed by Tukey's post hoc $p<0.05$) (C) zR4Hi was expressed in Purkinje cells through DNA microinjection of single-celled embryos (see Methods). 20 μ M NS13001 was added to the water in which the animals were incubated starting at 3 dpf. Confocal images were taken from the same animal from 4 to 6 dpf. Optical slices were 1 μ m. Projection stacks of images are shown in the figure. In the presence of NS13001, the dendrites (arrowheads) of a zR4Hi cell (asterisk) continued to grow through 6 dpf. This was not seen in any untreated Purkinje cells.

Confocal images in (B) were taken by Brittany Ulrich.

Chapter 4

Conclusion

Conserved electrical activity and maturation in zebrafish Purkinje cells

Cerebellar Purkinje cells are spontaneously active neurons that show two types of action potentials: simple spikes and complex spikes. The former is intrinsic to the cells and the latter are elicited by climbing fiber inputs originating from the inferior olive in the brain stem. The frequency of simple spikes and the interplay between simple and complex spikes encode the efferent information from Purkinje cell, which is the sole outgoing signal from the mammalian cerebellar cortex. The anatomical conservation between zebrafish and mammalian cerebella has been described in great detail in both mature and developing brain, from the cellular level to the circuit level with a few minor differences (reviewed by Hashimoto and Hibi, 2012). We demonstrated in Chapter 2 that zebrafish Purkinje cell generate both simple spikes and complex spikes as their counterparts in mammalian cerebellum with comparable frequencies and regularity. We also provided evidence suggesting that the same types of ion channel underlie spontaneous repetitive firing behavior in both systems, and that the maturation of cell excitability was conferred by the expression of these ionic conductances. In addition, based on the functional results we obtained from the inferior olive stimulation experiments, I discussed the possibility that the maturation of climbing fiber inputs went through a winnowing process similar to that occurring in mammals, progressing from innervation by multiple climbing fibers to innervation by one climbing fiber input per Purkinje cell. We concluded that, regarding Purkinje cells, zebrafish and mammalian cerebella are highly conserved not only anatomically but also functionally, including the spiking behaviors, synaptic inputs, and maturation processes. Our finding sets the foundation for future studies on cerebellar circuits, cerebellar control of behavior, and neurodegeneration in cerebellum using zebrafish as a biological model system.

Altered cell excitability and neuronal degeneration

Changes in cell excitability are not uncommon in neurodegenerative diseases. However, whether changes in excitability are sufficient to trigger neuronal degeneration has not been shown. SCA13 provides a great opportunity and several advantages to answer this question. It is caused by mutations in a single gene *KCNC3* that encodes a well-studied ion channel, K_v3.3. K_v3.3 regulates membrane excitability, tonic firing, and complex spiking in Purkinje cells. Losing K_v3.3 function leads to broadened spike, spike failure, increased vulnerability to spike adaptation, abnormal muscle twitches, and minor defects in motor performance. Restoring K_v3.3 function in *Kcnc3*-null mice rescues the altered excitability and improves motor coordination (Ruby and Mcbain, 2001; Hurlock et al., 2008; reviewed Joho and Hurlock, 2009). In addition, genetic background plays little role in determining the SCA13 clinical forms. The strong genotype and phenotype correlation suggests the timing of onset, either during infancy or during adulthood, is dependent on the type of mutation (Waters et al., 2006). In other words, the differential effects of mutations on cell function determine the emergence of the disease. These two features make SCA13 more favorable than other diseases of unknown origin or those caused by mutations in multiple genes, by environmental insults, or by poly-glutamine repeats in testing the hypothesis that altered excitability can initiate detrimental pathways that ultimately lead to neuronal degeneration.

As described in Chapter 3, the differential biophysical properties of SCA13 mutations generate distinct phenotypes in firing behavior in zebrafish Purkinje cells. The adult-onset zR3Ha mutation showed frequency-dependent inhibition of cell excitability while not affecting basal firing. In contrast, the infant-onset zR4Hi mutation induced significant hyperexcitability in developing Purkinje cells. While both mutations had dominant negative effects, our findings

suggest it was the altered channel gating of zR4Hi that gave this divergence. In addition, severe, rapid, and early-onset neuronal degeneration was observed in zR4Hi cells but not in zR3Ha cells. Interestingly, the onset of this degeneration was temporally correlated to the emergence of zR4Hi-induced hyperexcitability, and the change in electrical activity preceded the morphological deterioration suggesting a causal relationship between the two phenotypes. Our findings provide preliminary evidence directly linking excitability to neuronal degeneration. We propose that altered excitability is sufficient to trigger pathogenic pathways in vulnerable cell types, and manipulating this alteration might be a potential way to alleviate the progression in diseases like SCA13.

Nonetheless, the exact underlying mechanism tying excitability and degeneration is yet to be investigated. One possible mechanism is through the interactions between excitability and ER stress. This idea has been proposed and explored in amyotrophic lateral sclerosis (ALS). Recently, promising results have been reported by Kiskinis et al (2014) and by Wainger et al (2014) showing the balance between excitability and ER stress is crucial for motor neuron viability. Their findings suggest that aberrant ER stress induced by pathogenic mutations in several ALS genes disrupts this balance and triggers the unfolded protein response, resulting in neurotoxicity. They also showed that blocking unfolded protein response delayed the morphological degeneration and improved the viability of motor neurons. In Chapter 3 of this thesis, we showed that the infant-onset SCA13 mutation, zR4Hi, induces hyperexcitability and rapid neuronal degeneration in Purkinje cells between 4 and 6 dpf in zebrafish. It is interesting that within the same developmental window, a normal Purkinje cell undergoes extensive dendritic elaboration. Because of this intensive outgrowth, it is plausible that Purkinje cells at this stage experience a higher than normal level of ER stress, which makes them more

susceptible to any disturbance to the balance between excitability and ER stress. zR4Hi-induced hyperexcitability may be the critical factor that disrupts the balance and triggers cell death.

Aberrant calcium signaling is a promising mechanism mediating the interaction between hyperexcitability and ER stress. A role for altered calcium signaling has been proposed in many neurodegenerative diseases. Indeed, elevated intracellular Ca^{2+} concentration and abnormal Ca^{2+} signaling have been widely reported in many diseases, including Alzheimer's disease, Parkinson's disease, amyotrophic lateral sclerosis, Huntington's disease and several types of spinocerebellar ataxia caused by polyglutamine repeats (Bezprozvanny, 2009; D'Amelio and Rossini, 2012; Berridge, 2013; Chopra and Shakkottai, 2014; Zaltieri et al., 2015). Aberrant Ca^{2+} activity can induce both acute and long-term alterations in cell functions, such as membrane excitability, protein kinase/phosphatase activity, mitochondrial function and gene expression. The accumulation of these phenotypes is thought to be the trigger to neuronal degeneration. Investigating the roles of Ca^{2+} in the pathogenesis has provided significant insights in the etiology of these diseases. In the case of SCA13, we have shown that zR4Hi, an infant-onset SCA13 mutation, induces hyperexcitability in Purkinje cells, whereas zR3Ha, the adult-onset SCA13 mutation, causes hypoexcitability. These changes in excitability are expected to dysregulate Ca^{2+} signaling in distinct ways, since excitability directly regulates Ca^{2+} entry through voltage-gated calcium channels. Indeed, preliminary results obtained by Dr. Fadi Issa in the Papazian lab suggest that zR4Hi-expressing Purkinje cells have a higher basal level of calcium and larger calcium transients during high frequency firing compared to control cells. In addition, zR4Hi leads to rapid and early-onset neuronal degeneration, while zR3Ha shows no obvious effects on cell morphology. This difference makes them a very good pair to study the effect of Ca^{2+} on neuronal degeneration. Understanding how Ca^{2+} acts under conditions of hyper-

or hypoexcitability is potentially of great therapeutic value. This knowledge may provide insights in developing new approaches that alleviate disease symptoms or delay the progression.

Further detailed investigation is needed to uncover the underlying mechanisms that tie excitability to neuronal degeneration. It is not implausible that this unidentified underlying mechanism may serve as a point of convergence for pathogenic pathways in a variety of neurodegenerative diseases. As described here and earlier in Chapter 1, pathogenic phenotypes such as altered excitability, increased ER stress, and altered Ca^{2+} dynamics seem to be shared by multiple diseases (Bezprozvanny, 2009; D'Amelio and Rossini, 2012; Berridge, 2013; Chopra and Shakkottai, 2014; Zaltieri et al, 2015). We believe that the zebrafish system is a promising model to pursue this investigation because of the various advantages it provides, including ease of genetic modification, rapid development and optical transparency. Combining these advantageous features with tools such as *in vivo* imaging and *in vivo* electrophysiology, we will be able to advance our understanding of brain function and the etiology of neurological diseases.

References

- Akemann, W., and Knöpfel, T. (2006). Interaction of Kv3 potassium channels and resurgent sodium current influences the rate of spontaneous firing of Purkinje neurons. *J. Neurosci.* 26, 4602–12. doi:10.1523/JNEUROSCI.5204-05.2006.
- Altman, J., and Bayer, S. A. (1997). *Development of the cerebellar system: in relation to its evolution, structure, and functions*. CRC Press Available at: <https://books.google.com/books?id=WN1qAAAAMAAJ>.
- Armstrong, D. M., and Rawson, J. A. (1979). Activity patterns of cerebellar cortical neurones and climbing fibre afferents in the awake cat. *J. Physiol.* 289, 425–48. doi:10.1523/JNEUROSCI.6565-10.2011.
- Arrenberg, A. B., and Driever, W. (2013). Integrating anatomy and function for zebrafish circuit analysis. *Front. Neural Circuits* 7, 74. doi:10.3389/fncir.2013.00074.
- Bae, J. S., Simon, N. G., Menon, P., Vucic, S., and Kiernan, M. C. (2013). The puzzling case of hyperexcitability in amyotrophic lateral sclerosis. *J. Clin. Neurol.* 9, 65–74. doi:10.3988/jcn.2013.9.2.65.
- Bae, Y.-K., Kani, S., Shimizu, T., Tanabe, K., Nojima, H., Kimura, Y., Higashijima, S., and Hibi, M. (2009). Anatomy of zebrafish cerebellum and screen for mutations affecting its development. *Dev. Biol.* 330, 406–26. doi:10.1016/j.ydbio.2009.04.013.
- Berridge, M. J. (2013). Dysregulation of neural calcium signaling in Alzheimer disease, bipolar disorder and schizophrenia. *Prion* 7, 2–13. doi:10.4161/pri.21767.

- Bezanilla, F., and Armstrong, C. M. (1977). Inactivation of the sodium channel. I. Sodium current experiments. *J. Gen. Physiol.* 70, 549–566. doi:10.1085/jgp.70.5.549.
- Bezprozvanny, I. (2009). Calcium signaling and neurodegenerative diseases. *Trends Mol. Med.* 15, 89–100. doi:10.1016/j.molmed.2009.01.001.
- Bosman, L. W. J., and Konnerth, a (2009). Activity-dependent plasticity of developing climbing fiber-Purkinje cell synapses. *Neuroscience* 162, 612–23. doi:10.1016/j.neuroscience.2009.01.032.
- Brend, T., and Holley, S. a (2009). Zebrafish whole mount high-resolution double fluorescent in situ hybridization. *J. Vis. Exp.*, 3–5. doi:10.3791/1229.
- Brochu, G., Maler, L., and Hawkes, R. (1990). Zebrin II: a polypeptide antigen expressed selectively by Purkinje cells reveals compartments in rat and fish cerebellum. *J. Comp. Neurol.* 291, 538–552. doi:10.1002/cne.902910405.
- Burgess, H. a, and Granato, M. (2007). Modulation of locomotor activity in larval zebrafish during light adaptation. *J. Exp. Biol.* 210, 2526–39. doi:10.1242/jeb.003939.
- Burrill, J. D., and Easter, S. S. (1994). Development of the retinofugal projections in the embryonic and larval zebrafish (*Brachydanio rerio*). *J. Comp. Neurol.* 346, 583–600. doi:10.1002/cne.903460410.
- Butler, A. B., and Hodos, W. (1996). *Comparative Vertebrate Neuroanatomy: Evolution and Adaptation*. Wiley Available at: <https://books.google.com/books?id=CYFIQgAACAAJ>.

- Chang, S. Y., Zaghera, E., Kwon, E. S., Ozaita, A., Bobik, M., Martone, M. E., Ellisman, M. H., Heintz, N., and Rudy, B. (2007). Distribution of Kv3.3 potassium channel subunits in distinct neuronal populations of mouse brain. *J. Comp. Neurol.* 502, 953–72. doi:10.1002/cne.21353.
- Chhetri, J., Jacobson, G., and Gueven, N. (2014). Zebrafish-on the move towards ophthalmological research. *Eye (Lond).*, 1–14. doi:10.1038/eye.2014.19.
- Chopra, R., and Shakkottai, V. G. (2014). The Role for Alterations in Neuronal Activity in the Pathogenesis of Polyglutamine Repeat Disorders. *Neurotherapeutics* 11, 751–763. doi:10.1007/s13311-014-0289-7.
- Crepel, F. (1982). Regression of functional synapses in the immature mammalian cerebellum. *Trends Neurosci.* 5, 266–269. doi:10.1016/0166-2236(82)90168-0.
- D’Amelio, M., and Rossini, P. M. (2012). Brain excitability and connectivity of neuronal assemblies in Alzheimer’s disease: From animal models to human findings. *Prog. Neurobiol.* 99, 42–60. doi:10.1016/j.pneurobio.2012.07.001.
- D’Angelo, E., Mazzarello, P., Prestori, F., Mapelli, J., Solinas, S., Lombardo, P., Cesana, E., Gandolfi, D., and Congi, L. (2011). The cerebellar network: from structure to function and dynamics. *Brain Res. Rev.* 66, 5–15. doi:10.1016/j.brainresrev.2010.10.002.
- Eisen, A., Kim, S., and Pant, B. (1992). Amyotrophic lateral sclerosis (ALS): a phylogenetic disease of the corticomotoneuron? *Muscle Nerve* 15, 219–224. doi:10.1002/mus.880150215.

- De Felipe, P., Luke, G. a., Hughes, L. E., Gani, D., Halpin, C., and Ryan, M. D. (2006). E unum pluribus: Multiple proteins from a self-processing polyprotein. *Trends Biotechnol.* 24, 68–75. doi:10.1016/j.tibtech.2005.12.006.
- Figuroa, K. P., Minassian, N. A., Stevanin, G., Waters, M., Garibyan, V., Forlani, S., Strzelczyk, A., Bürk, K., Brice, A., Dürr, A., et al. (2010). KCNC3: phenotype, mutations, channel biophysics-a study of 260 familial ataxia patients. *Hum. Mutat.* 31, 191–6. doi:10.1002/humu.21165.
- Figuroa, K. P., Waters, M. F., Garibyan, V., Bird, T. D., Gomez, C. M., Ranum, L. P. W., Minassian, N. A., Papazian, D. M., and Pulst, S. M. (2011). Frequency of KCNC3 DNA variants as causes of spinocerebellar ataxia 13 (SCA13). *PLoS One* 6, 7. doi:10.1371/journal.pone.0017811.
- Fleisch, V. C., and Neuhaus, S. C. F. (2006). Visual behavior in zebrafish. *Zebrafish* 3, 191–201. doi:10.1089/zeb.2006.3.191.
- Goldman-Wohl, D. S., Chan, E., Baird, D., and Heintz, N. (1994). Kv3.3b: a novel Shaw type potassium channel expressed in terminally differentiated cerebellar Purkinje cells and deep cerebellar nuclei. *J. Neurosci.* 14, 511–522.
- Hansen, S. T., Meera, P., Otis, T. S., and Pulst, S. M. (2013). Changes in Purkinje cell firing and gene expression precede behavioral pathology in a mouse model of SCA2. *Hum. Mol. Genet.* 22, 271–283. doi:10.1093/hmg/ddt427.

- Hashimoto, K., and Kano, M. (2013). Synapse elimination in the developing cerebellum. *Cell. Mol. Life Sci.* 70, 4667–80. doi:10.1007/s00018-013-1405-2.
- Hashimoto, M., and Hibi, M. (2012). Development and evolution of cerebellar neural circuits. *Dev. Growth Differ.* 54, 373–89. doi:10.1111/j.1440-169X.2012.01348.x.
- Heap, L. a, Goh, C. C., Kassahn, K. S., and Scott, E. K. (2013). Cerebellar output in zebrafish: an analysis of spatial patterns and topography in eurydendroid cell projections. *Front. Neural Circuits* 7, 53. doi:10.3389/fncir.2013.00053.
- Herman-Bert, a, Stevanin, G., Netter, J. C., Rascol, O., Brassat, D., Calvas, P., Camuzat, a, Yuan, Q., Schalling, M., Dürr, a, et al. (2000). Mapping of spinocerebellar ataxia 13 to chromosome 19q13.3-q13.4 in a family with autosomal dominant cerebellar ataxia and mental retardation. *Am. J. Hum. Genet.* 67, 229–35. Available at: <http://www.pubmedcentral.nih.gov/articlerender.fcgi?artid=1287081&tool=pmcentrez&rendertype=abstract>.
- Hibi, M., and Shimizu, T. (2012). Development of the cerebellum and cerebellar neural circuits. *Dev. Neurobiol.* 72, 282–301. doi:10.1002/dneu.20875.
- Hsieh, J.-Y., Ulrich, B., Issa, F. a., Wan, J., and Papazian, D. M. (2014). Rapid development of Purkinje cell excitability, functional cerebellar circuit, and afferent sensory input to cerebellum in zebrafish. *Front. Neural Circuits* 8, 1–12. doi:10.3389/fncir.2014.00147.

- Hurlock, E. C., McMahon, A., and Joho, R. H. (2008). Purkinje-cell-restricted restoration of Kv3.3 function restores complex spikes and rescues motor coordination in *Kcnc3* mutants. *J. Neurosci.* 28, 4640–8. doi:10.1523/JNEUROSCI.5486-07.2008.
- Ikenaga, T., Yoshida, M., and Uematsu, K. (2006). Cerebellar efferent neurons in teleost fish. *Cerebellum* 5, 268–74. doi:10.1080/14734220600930588.
- Irie, T., Matsuzaki, Y., Sekino, Y., and Hirai, H. (2014). Kv3.3 channels harbouring a mutation of spinocerebellar ataxia type 13 alter excitability and induce cell death in cultured cerebellar Purkinje cells. *J. Physiol.* 592, 229–47. doi:10.1113/jphysiol.2013.264309.
- Issa, F. a, Mazzochi, C., Mock, A. F., and Papazian, D. M. (2011). Spinocerebellar ataxia type 13 mutant potassium channel alters neuronal excitability and causes locomotor deficits in zebrafish. *J. Neurosci.* 31, 6831–41. doi:10.1523/JNEUROSCI.6572-10.2011.
- Ito, M. (2006). Cerebellar circuitry as a neuronal machine. *Prog. Neurobiol.* 78, 272–303. doi:10.1016/j.pneurobio.2006.02.006.
- Ito, M. (2008). Control of mental activities by internal models in the cerebellum. *Nat. Rev. Neurosci.* 9, 304–13. doi:10.1038/nrn2332.
- Ito, M. (2002a). Historical review of the significance of the cerebellum and the role of Purkinje cells in motor learning. *Ann. N. Y. Acad. Sci.* 978, 273–88. Available at: <http://www.ncbi.nlm.nih.gov/pubmed/12582060> [Accessed February 26, 2014].
- Ito, M. (2002b). The molecular organization of cerebellar long-term depression. *Nat. Rev. Neurosci.* 3, 896–902. doi:10.1038/nrn962.

- Ji, Z., and Hawkes, R. (1994). Topography of Purkinje cell compartments and mossy fiber terminal fields in lobules II and III of the rat cerebellar cortex: spinocerebellar and cuneocerebellar projections. *Neuroscience* 61, 935–54. Available at: <http://www.ncbi.nlm.nih.gov/pubmed/7530818> [Accessed September 26, 2014].
- Joho, R. H., and Hurlock, E. C. (2009). The role of Kv3-type potassium channels in cerebellar physiology and behavior. *Cerebellum* 8, 323–33. doi:10.1007/s12311-009-0098-4.
- Kani, S., Bae, Y.-K., Shimizu, T., Tanabe, K., Satou, C., Parsons, M. J., Scott, E., Higashijima, S., and Hibi, M. (2010). Proneural gene-linked neurogenesis in zebrafish cerebellum. *Dev. Biol.* 343, 1–17. doi:10.1016/j.ydbio.2010.03.024.
- Kasumu, A. W., Hougaard, C., Rode, F., Jacobsen, T. A., Sabatier, J. M., Eriksen, B. L., Strøbæk, D., Liang, X., Egorova, P., Vorontsova, D., et al. (2012). Selective Positive Modulator of Calcium-Activated Potassium Channels Exerts Beneficial Effects in a Mouse Model of Spinocerebellar Ataxia Type 2. *Chem. Biol.* 19, 1340–1353. doi:10.1016/j.chembiol.2012.07.013.
- Kawakami, K., Takeda, H., Kawakami, N., Kobayashi, M., Matsuda, N., and Mishina, M. (2004). A transposon-mediated gene trap approach identifies developmentally regulated genes in zebrafish. *Dev. Cell* 7, 133–44. doi:10.1016/j.devcel.2004.06.005.
- Khaliq, Z. M., Gouwens, N. W., and Raman, I. M. (2003). The contribution of resurgent sodium current to high-frequency firing in Purkinje neurons: an experimental and modeling study. *J. Neurosci.* 23, 4899–912. Available at: <http://www.ncbi.nlm.nih.gov/pubmed/12832512> [Accessed December 9, 2014].

- Kim, J. H., Lee, S.-R., Li, L.-H., Park, H.-J., Park, J.-H., Lee, K. Y., Kim, M.-K., Shin, B. A., and Choi, S.-Y. (2011). High cleavage efficiency of a 2A peptide derived from porcine teschovirus-1 in human cell lines, zebrafish and mice. *PLoS One* 6, e18556. doi:10.1371/journal.pone.0018556.
- Kiskinis, E., Sandoe, J., Williams, L. a, Boulting, G. L., Moccia, R., Wainger, B. J., Han, S., Peng, T., Thams, S., Mikkilineni, S., et al. (2014). Pathways disrupted in human ALS motor neurons identified through genetic correction of mutant SOD1. *Cell Stem Cell* 14, 781–95. doi:10.1016/j.stem.2014.03.004.
- Koziol, L. F., Budding, D., Andreasen, N., D’Arrigo, S., Bulgheroni, S., Imamizu, H., Ito, M., Manto, M., Marvel, C., Parker, K., et al. (2014). Consensus Paper: The Cerebellum’s Role in Movement and Cognition. *Cerebellum* 13, 151–77. doi:10.1007/s12311-013-0511-x.
- Loewenstein, Y., Mahon, S., Chadderton, P., Kitamura, K., Sompolinsky, H., Yarom, Y., and Häusser, M. (2005). Bistability of cerebellar Purkinje cells modulated by sensory stimulation. *Nat. Neurosci.* 8, 202–11. doi:10.1038/nn1393.
- Martina, M., Yao, G. L., and Bean, B. P. (2003). Properties and functional role of voltage-dependent potassium channels in dendrites of rat cerebellar Purkinje neurons. *J. Neurosci.* 23, 5698–707. Available at: <http://www.ncbi.nlm.nih.gov/pubmed/12843273> [Accessed December 9, 2014].
- McKay, B. E., and Turner, R. W. (2004). Kv3 K⁺ channels enable burst output in rat cerebellar Purkinje cells. *Eur. J. Neurosci.* 20, 729–739. doi:10.1111/j.1460-9568.2004.03539.x.

- McKay, B. E., and Turner, R. W. (2005). Physiological and morphological development of the rat cerebellar Purkinje cell. *J. Physiol.* 567, 829–50. doi:10.1113/jphysiol.2005.089383.
- Meyer, M. P., and Smith, S. J. (2006). Evidence from in vivo imaging that synaptogenesis guides the growth and branching of axonal arbors by two distinct mechanisms. *J. Neurosci.* 26, 3604–14. doi:10.1523/JNEUROSCI.0223-06.2006.
- Minassian, N. A., Lin, M.-C. A., and Papazian, D. M. (2012). Altered Kv3.3 Channel Gating in Early Onset Spinocerebellar Ataxia Type 13. *J. Physiol.* 7, 1599–1614. doi:10.1113/jphysiol.2012.228205.
- Mock, A. F., Richardson, J. L., Hsieh, J.-Y., Rinetti, G., and Papazian, D. M. (2010). Functional effects of spinocerebellar ataxia type 13 mutations are conserved in zebrafish Kv3.3 channels. *BMC Neurosci.* 11, 99. doi:10.1186/1471-2202-11-99.
- Niell, C. M., Meyer, M. P., and Smith, S. J. (2004). In vivo imaging of synapse formation on a growing dendritic arbor. *Nat. Neurosci.* 7, 254–60. doi:10.1038/nn1191.
- Papazian, D. M., Timpe, L. C., Jan, Y. N., and Jan, L. Y. (1991). Alteration of voltage-dependence of Shaker potassium channel by mutations in the S4 sequence. *Nature* 349, 305–310. doi:10.1038/349305a0.
- Raman, I. M., Sprunger, L. K., Meisler, M. H., and Bean, B. P. (1997). Altered subthreshold sodium currents and disrupted firing patterns in Purkinje neurons of Scn8a mutant mice. *Neuron* 19, 881–91. Available at: <http://www.ncbi.nlm.nih.gov/pubmed/9354334>.

- Rudy, B., Chow, A., Lau, D., Amarillo, Y., Ozaita, A., Saganich, M., Moreno, H., Nadal, M. S., Hernandez-Pineda, R., Hernandez-Cruz, A., et al. (1999). Contributions of Kv3 channels to neuronal excitability. *Ann. N. Y. Acad. Sci.* 868, 304–343. doi:10.1111/j.1749-6632.1999.tb11295.x.
- Rudy, B., and McBain, C. J. (2001). Kv3 channels: voltage-gated K⁺ channels designed for high-frequency repetitive firing. *Trends Neurosci.* 24, 517–26. Available at: <http://www.ncbi.nlm.nih.gov/pubmed/11506885>.
- Ryan, M. D., King, a. M. Q., and Thomas, G. P. (1991). Cleavage of foot-and-mouth disease virus polyprotein is mediated by residues located within a 19 amino acid sequence. *J. Gen. Virol.* 72, 2727–2732. doi:10.1099/0022-1317-72-11-2727.
- Schonewille, M., Khosrovani, S., Winkelman, B. H. J., Hoebeek, F. E., De Jeu, M. T. G., Larsen, I. M., Van der Burg, J., Schmolesky, M. T., Frens, M. A., and De Zeeuw, C. I. (2006). Purkinje cells in awake behaving animals operate at the upstate membrane potential. *Nat. Neurosci.* 9, 459–461; author reply 461. doi:10.1038/nn0406-461.
- Schoonheim, P. J., Arrenberg, A. B., Del Bene, F., and Baier, H. (2010). Optogenetic localization and genetic perturbation of saccade-generating neurons in zebrafish. *J. Neurosci.* 30, 7111–20. doi:10.1523/JNEUROSCI.5193-09.2010.
- Sreedharan, J., and Brown, R. H. (2013). Amyotrophic lateral sclerosis: Problems and prospects. *Ann. Neurol.* 74, 309–316. doi:10.1002/ana.24012.

- Swenson, R. P., and Armstrong, C. M. (1981). K⁺ channels close more slowly in the presence of external K⁺ and Rb⁺. *Nature* 291, 427–429. doi:10.1038/291427a0.
- Szymczak, A. L., and Vignali, D. A. A. (2005). Development of 2A peptide-based strategies in the design of multicistronic vectors. *Expert Opin. Biol. Ther.* 5, 627–638. doi:10.1517/14712598.5.5.627.
- Tanabe, K., Kani, S., Shimizu, T., Bae, Y.-K., Abe, T., and Hibi, M. (2010). Atypical protein kinase C regulates primary dendrite specification of cerebellar Purkinje cells by localizing Golgi apparatus. *J. Neurosci.* 30, 16983–92. doi:10.1523/JNEUROSCI.3352-10.2010.
- Thisse, C., and Thisse, B. (2008). High-resolution in situ hybridization to whole-mount zebrafish embryos. *Nat. Protoc.* 3, 59–69. doi:10.1038/nprot.2007.514.
- Timpe, L. C., Schwarz, T. L., Tempel, B. L., Papazian, D. M., Jan, Y. N., and Jan, L. Y. (1988). Expression of functional potassium channels from Shaker cDNA in *Xenopus* oocytes. *Nature* 331, 143–145. doi:10.1038/331143a0.
- Tsai, C. W., Tseng, J. J., Lin, S. C., Chang, C. Y., Wu, J. L., Horng, J. F., and Tsay, H. J. (2001). Primary structure and developmental expression of zebrafish sodium channel Na(v)1.6 during neurogenesis. *DNA Cell Biol.* 20, 249–55. doi:10.1089/104454901750232445.
- Veys, K., Snyders, D., and De Schutter, E. (2013). Kv3.3b expression defines the shape of the complex spike in the Purkinje cell. *Front. Cell. Neurosci.* 7, 205. doi:10.3389/fncel.2013.00205.

- Wainger, B. J., Kiskinis, E., Mellin, C., Wiskow, O., Han, S. S. W., Sandoe, J., Perez, N. P., Williams, L. a, Lee, S., Boulting, G., et al. (2014). Intrinsic membrane hyperexcitability of amyotrophic lateral sclerosis patient-derived motor neurons. *Cell Rep.* 7, 1–11. doi:10.1016/j.celrep.2014.03.019.
- Walter, J. T., Alviña, K., Womack, M. D., Chevez, C., and Khodakhah, K. (2006). Decreases in the precision of Purkinje cell pacemaking cause cerebellar dysfunction and ataxia. *Nat. Neurosci.* 9, 389–97. doi:10.1038/nn1648.
- Waters, M. F., Minassian, N. a, Stevanin, G., Figueroa, K. P., Bannister, J. P. a, Nolte, D., Mock, A. F., Evidente, V. G. H., Fee, D. B., Müller, U., et al. (2006). Mutations in voltage-gated potassium channel KCNC3 cause degenerative and developmental central nervous system phenotypes. *Nat. Genet.* 38, 447–51. doi:10.1038/ng1758.
- Westphal, R. E., and O'Malley, D. M. (2013). Fusion of locomotor maneuvers, and improving sensory capabilities, give rise to the flexible homing strikes of juvenile zebrafish. *Front. Neural Circuits* 7, 108. doi:10.3389/fncir.2013.00108.
- Womack, M. D., and Khodakhah, K. (2003). Somatic and dendritic small-conductance calcium-activated potassium channels regulate the output of cerebellar Purkinje neurons. *J. Neurosci.* 23, 2600–2607.
- Wulff, P., Schonewille, M., Renzi, M., Viltono, L., Sassoè-Pognetto, M., Badura, A., Gao, Z., Hoebeek, F. E., van Dorp, S., Wisden, W., et al. (2009). Synaptic inhibition of Purkinje cells mediates consolidation of vestibulo-cerebellar motor learning. *Nat. Neurosci.* 12, 1042–9. doi:10.1038/nn.2348.

Wullimann, M. F., and Rupp, B. (1996). *Neuranatomy of the Zebrafish Brain*. doi:10.1007/978-3-0348-8979-7.

Zagha, E., Lang, E. J., and Rudy, B. (2008). Kv3.3 channels at the Purkinje cell soma are necessary for generation of the classical complex spike waveform. *J. Neurosci.* 28, 1291–300. doi:10.1523/JNEUROSCI.4358-07.2008.

Zaltieri, M., Longhena, F., Pizzi, M., Missale, C., Spano, P., and Bellucci, A. (2015). Mitochondrial Dysfunction and α -Synuclein Synaptic Pathology in Parkinson's Disease: Who's on First? *Parkinsons. Dis.* 2015, 1–10. doi:10.1155/2015/108029.

Zhou, H., Lin, Z., Voges, K., Ju, C., Gao, Z., Bosman, L. W., Ruigrok, T. J., Hoebeek, F. E., De Zeeuw, C. I., and Schonewille, M. (2014). Cerebellar modules operate at different frequencies. *Elife* 3, e02536. doi:10.7554/eLife.02536.